WEC PROPRIETARY CLASS 3

Westinghouse Energy Systems

WEC PROPRIETARY CLASS 3

Westinghouse Energy Systems

WESTINGHOUSE CLASS 3

WCAP-12845

ANALYSIS OF CAPSULE U FROM THE COMMONWEALTH EDISON COMPANY BRAIDWOOD UNIT 2 REACTOR VESSEL RADIATION SURVEILLANCE PROGRAM

E. Terek
S. L. Anderson
L. Albertin

March 1991

Work Performed Under Shop Order BMVP-106

Prepared by Westinghouse Electric Corporation
for the Commonwealth Edison Company

Approved by: T. A. Meyer
T. A. Meyer, Manager
Structural Reliability and
Plant Life Optimization

WESTINGHOUSE ELECTRIC CORPORATION
Nuclear and Advanced Technology Division
P.O. Box 2728
Pittsburgh, Pennsylvania 15230-2728

PREFACE

This report has been technically reviewed and verified.

	Reviewer
Sections 1 through 5, 7, 8 and Appendix B	J. M. Chicots J. M. Chicots
Section 6	E. P. Lippincott

TABLE OF CONTENTS

LIST OF ILLUSTRATIONS

LIST OF ILLUSTRATIONS (Cont)

LIST OF ILLUSTRATIONS (Cont)

LIST OF TABLES

LIST OF TABLES (Cont)

LIST OF TABLES (Cont)

SECTION 1.0
SUMMARY OF RESULTS

The analysis of the reactor vessel materials contained in surveillance Capsule U, the first capsule to be removed from the Commonwealth Edison Company Braidwood Unit 2 reactor pressure vessel, led to the following conclusions:

- The capsule received an average fast neutron fluence (E > 1.0 MeV) of 3.91×10^{18} n/cm^2 after 1.15 EFPY of plant operation.

- Irradiation of the reactor vessel lower shell forging 50D102-1/50C97-1 Charpy specimens to 3.91×10^{18} n/cm^2 (E > 1.0 MeV) resulted in no 30 and 50 ft-lb transition temperature increases for specimens oriented parallel to the major working direction (tangential orientation). This results in a 30 ft-lb transition temperature of -10°F and a 50 ft-lb transition temperature of 15°F (tangential orientation).

- Irradiation of the reactor vessel lower shell forging 50D102-1/50C97-1 Charpy specimens to 3.91×10^{18} n/cm^2 (E > 1.0 MeV) resulted in 30 and 50 ft-lb transition temperature increases of 5 and 10°F, respectively, for specimens oriented normal to the major working direction (axial orientation). This results in a 30 ft-lb transition temperature of -20°F and a 50 ft-lb transition temperature of 10°F (axial orientation).

- The weld metal Charpy specimens irradiated to 3.91×10^{18} n/cm^2 (E > 1.0 MeV) resulted in no 30 ft-lb transition temperature increase and a 50 ft-lb transition temperature increase of 5°F. This results in a 30 ft-lb transition temperature of -20°F and a 50 ft-lb transition temperature of 45°F for the weld metal.

- Irradiation of the reactor vessel weld HAZ metal Charpy specimens to 3.91 x 10^{18} n/cm^2 (E > 1.0 MeV) resulted no 30 ft-lb and 50 ft-lb transition temperature increases and no USE decrease. This results in a 30 ft-lb transition temperature of -135°F and a 50 ft-lb transition temperature of -105°F for the weld HAZ metal.

- The average upper shelf energy of lower shell forging 50D102-1/50C97-1 (tangential orientation) resulted in no energy decrease after irradiation to 3.91 x 10^{18} n/cm^2 (E > 1.0 MeV). This results in an upper shelf energy of 168 ft-lb (tangential orientation).

- The average upper shelf energy of lower shell forging 50D102-1/50C97-1 (axial orientation) resulted in a decrease in energy of 16 ft-lb after irradiation to 3.91 x 10^{18} n/cm^2 (E > 1.0 MeV). This results in an upper shelf energy of 137 ft-lb (axial orientation).

- The average upper shelf energy of the weld metal resulted in a decrease 9 ft-lb after irradiation to 3.91 x 10^{18} n/cm^2 (E > 1.0 MeV). This results in an upper shelf energy of 62 ft-lb.

- The surveillance capsule U test results do not indicate any significant changes in the RT_{NDT} values of the reactor vessel surveillance materials.

- The surveillance capsule materials exhibit a more than adequate upper shelf energy level for continued safe plant operation and are expected to maintain an upper shelf energy of no less than 50 ft-lb throughout the life (32 EFPY) of the vessel as required by 10CFR50, Appendix G.

- The calculated end-of-life (32 EFPY) maximum neutron fluence (E > 1.0 MeV) for the Braidwood Unit 2 reactor vessel is as follows:

  Vessel inner radius * - 3.03×10^{19} n/cm^2
  Vessel 1/4 thickness - 1.66×10^{19} n/cm^2
  Vessel 3/4 thickness - 3.57×10^{18} n/cm^2

  * Clad/base metal interface

- The above calculated 32 EFPY fluences are based on the original core and are expected to decrease with the implementation of a low leakage fuel management program.

SECTION 2.0
INTRODUCTION

This report presents the results of the examination of Capsule U, the first capsule to be removed from the reactor in the continuing surveillance program which monitors the effects of neutron irradiation on the Commonwealth Edison Company Braidwood Unit 2 reactor pressure vessel materials under actual operating conditions.

The surveillance program for the Braidwood Unit 2 reactor pressure vessel materials was designed and recommended by the Westinghouse Electric Corporation. A description of the surveillance program and the preirradiation mechanical properties of the reactor vessel materials is presented in WCAP-11188 "Commonwealth Edison Company Braidwood Station Unit No. 2 Reactor Vessel Radiation Surveillance Program" by L. R. Singer [1]. The surveillance program was planned to cover the 40-year design life of the reactor pressure vessel and was based on ASTM E185-82, "Standard Practice for Conducting Surveillance Tests for Light-Water Cooled Nuclear Power Reactor Vessels"[6]. Westinghouse Power Systems personnel were contracted to aid in the preparation of procedures for removing capsule "U" from the reactor and its shipment to the Westinghouse Science and Technology Center Hot Cell Facility, where, the postirradiation mechanical testing of the Charpy V-notch impact and tensile surveillance specimens was performed.

This report summarizes the testing of and the postirradiation data obtained from surveillance Capsule "U" removed from the Braidwood Unit 2 reactor vessel and discusses the analysis of these data.

SECTION 3.0
BACKGROUND

The ability of the large steel pressure vessel containing the reactor core and its primary coolant to resist fracture constitutes an important factor in ensuring safety in the nuclear industry. The beltline region of the reactor pressure vessel is the most critical region of the vessel because it is subjected to significant fast neutron bombardment. The overall effects of fast neutron irradiation on the mechanical properties of low alloy, ferritic pressure vessel steels such as SA508 Class 3 (base material of the Commonwealth Edison Company Station Braidwood Unit 2 reactor pressure vessel lower shell forging) are well documented in the literature. Generally, low alloy ferritic materials show an increase in hardness and tensile properties and a decrease in ductility and toughness under certain conditions of irradiation.

A method for performing analyses to guard against fast fracture in reactor pressure vessels has been presented in "Protection Against Nonductile Failure," Appendix G to Section III of the ASME Boiler and Pressure Vessel Code[4]. The method uses fracture mechanics concepts and is based on the reference nil-ductility temperature (RT_{NDT}).

RT_{NDT} is defined as the greater of either the drop weight nil-ductility transition temperature (NDTT per ASTM E-208) or the temperature 60°F less than the 50 ft-lb (and 35-mil lateral expansion) temperature as determined from Charpy specimens oriented normal (axial) to the major working direction of the material. The RT_{NDT} of a given material is used to index that material to a reference stress intensity factor curve (K_{IR} curve) which appears in Appendix G of the ASME Code. The K_{IR} curve is a lower bound of dynamic, crack arrest, and static fracture toughness results obtained from several heats of pressure vessel steel. When a given material is indexed to the K_{IR} curve, allowable stress intensity factors can be obtained for this material as a function of temperature. Allowable operating limits can then be determined using these allowable stress intensity factors.

RT_{NDT} and, in turn, the operating limits of nuclear power plants can be adjusted to account for the effects of radiation on the reactor vessel material properties. The radiation embrittlement changes in mechanical properties of a given reactor pressure vessel steel can be monitored by a reactor surveillance program such as the Braidwood Unit 2 Reactor Vessel Radiation Surveillance Program,[1] in which a surveillance capsule is periodically removed from the operating nuclear reactor and the encapsulated specimens are tested. The increase in the average Charpy V-notch 30 ft-lb temperature (ΔRT_{NDT}) due to irradiation is added to the original RT_{NDT} to adjust the RT_{NDT} for radiation embrittlement. This adjusted RT_{NDT} (RT_{NDT} initial + ΔRT_{NDT}) is used to index the material to the K_{IR} curve and, in turn, to set operating limits for the nuclear power plant which take into account the effects of irradiation on the reactor vessel materials.

SECTION 4.0
DESCRIPTION OF PROGRAM

Six surveillance capsules for monitoring the effects of neutron exposure on the Braidwood Unit 2 reactor pressure vessel core region material were inserted in the reactor vessel prior to initial plant start-up. The six capsules were positioned in the reactor vessel between the neutron shield pads and the vessel wall as shown in Figure 4-1. The vertical center of the capsules is opposite the vertical center of the core.

Capsule U was removed after 1.15 effective full power years (EFPY) of plant operation. This capsule contained Charpy V-notch, tensile, and 1/2 T compact tension (CT) specimens (Figure 4-2) from the lower shell forging 50D102-1/50C97-1 and weld metal representative of the intermediate to lower shell beltline weld seam of the reactor vessel and Charpy V-notch specimens from weld heat-affected-zone (HAZ) material. All heat-affected zone specimens were obtained from within the HAZ of forging 50D102-1/50C97-1 of the representative weld.

The chemical composition and heat treatment of the surveillance material is presented in Tables 4-1 through 4-4. The chemical analysis reported in Tables 4-1 through 4-3 were obtained from unirradiated beltline material. In addition, a chemical analysis using Inductively Coupled Plasma Spectrometry (ICPS) was performed on irradiated specimens from forging 50D102-1/50C97-1 and weld metal and is reported in Table 4-5, also, reported in Table 4-6 are the chemistry results from the NBS certified reference standards.

All test specimens were machined from the 1/4 thickness location of the forging. Test specimens represent material taken at least one forging thickness from the quenched end of the forging. Base metal Charpy V-notch impact and tension specimens were oriented with the longitudinal axis of the specimen parallel to the major working direction of the forging (tangential orientation) and also normal to the major working direction (axial orientation). Charpy V-notch and tensile specimens from the weld metal were oriented such that the long dimension of the specimen was normal to the welding direction.

The 1/2T CT test specimens in Capsule U are from the lower shell course forging 50D102-1/50C97-1 and were machined in both the axial and tangential orientations. Thus, the simulated crack in the specimen will propagate normal and parallel to the major working direction of forging 50D102-1/50C97-1. The 1/2T CT Test specimens from the weld metal were machined with the notch oriented in the direction of welding. Thus, the simulated crack in the specimen will propagate parallel to the weld direction. All CT specimens were fatigue precracked according to ASTM E399.

Capsule U contained dosimeter wires of pure copper, iron, nickel, and aluminum-0.15 weight percent cobalt (cadmium-shielded and unshielded). In addition, cadmium shielded dosimeters of neptunium (Np^{237}) and uranium (U^{238}) were placed in the capsule to measure the integrated flux at specific neutron energy levels.

Thermal monitors made from the two low-melting eutectic alloys and sealed in Pyrex tubes were included in the capsule. The composition of the two alloys and their melting points are as follows:

2.5% Ag, 97.5% Pb	Melting Point: 579°F (304°C)
1.5% Ag, 1.0% Sn, 97.5% Pb	Melting Point: 590°F (310°C)

The arrangement of the various mechanical specimens, dosimeters and thermal monitors contained in Capsule U are shown in Figure 4-2.

TABLE 4-1

CHEMICAL COMPOSITION OF THE BRAIDWOOD UNIT 2 REACTOR VESSEL INTERMEDIATE SHELL FORGING [b]

Element	Chemical Compositon (weight %) Upper Shell Forging 49D963 / 49C904 -1-1 MK24-2
C	.20[a]
Mn	1.33
P	.007
S	.007
Si	.25
Ni	.71
Mo	.53
Cr	.08
Cu	.03
Al	.024
Co	.012
Pb	.0003 max.
W	.005 max.
Ti	.001 max
Zr	.005 max
V	.01 max.
Sn	.003
As	.006
Cb	.005 max.
N_2	.0097
B	Not Reported

a. Chemical Analyses by Japan Steel Works, Ltd.

b. Data reported here is the unirradiated chemistry results reported in WCAP-11188 [1]

TABLE 4-2

CHEMICAL COMPOSITION OF THE BRAIDWOOD UNIT 2 REACTOR VESSEL LOWER SHELL FORGING [c]

Element	Chemical Compositon (weight %)	
	Lower Shell Forging 50D102 / 50C97 -1-1 MK24-3	
C	.22[a]	.24[b]
Mn	1.30	1.38
P	.006	.013
S	.004	.009
Si	.28	.30
Ni	.75	.77
Mo	.49	.56
Cr	.08	.095
Cu	.06	.057
Al	.025	.024
Co	.011	.008
Pb	.0003 max.	< .001
W	.005 max.	< .01
Ti	.005 max.	.004
Zr	.005 max.	< .002
V	.01 max.	< .002
Sn	.007	.004
As	.008	.007
Cb	.005 max.	< .002
N_2	.0084	.009
B	Not Reported	< .001

a. Chemical Analyses by Japan Steel Works, Ltd.

b. Westinghouse Analyses from the Surveillance Program Test Plate.

c. Data reported here is the unirradiated chemistry results reported in WCAP-11188 [1]

TABLE 4-3

CHEMICAL COMPOSITION OF THE BRAIDWOOD UNIT 2 REACTOR VESSEL WELD METAL USED FOR THE UPPER TO LOWER SHELL CLOSING GIRTH SEAM [c]

Element	Chemical Compositon (weight %)	
	Weld Filler Wire Heat Number 442011 Linde No. 80 flux, Lot Number 0344	
C	.066[a]	.069[b]
Mn	1.44	1.45
P	.015	.011
S	.012	.013
Si	.48	.53
Ni	.67	.64
Mo	.44	.46
Cr	.10	.082
Cu	.04	.040
Al	.004	.007
Co	.011	.004
Pb	.0006	< .001
W	.010	< .01
Ti	.007	.003
Zr	.003	< .002
V	.005	< .002
Sn	.005	.004
As	.004	.004
Cb	.004	< .002
N_2	.013	.012
B	.0007	< .001

a. Chemical Analysis of "Filler Wire Qualification Test" by Babcock and Wilcox, Company, Test No. WF-562

b. Westinghouse Analyses from the Surveillance Program Test Weldment.

c. Data reported here is the unirradiated chemistry results reported in WCAP-11188 [1]

TABLE 4-4

HEAT TREATMENT HISTORY OF THE BRAIDWOOD UNIT NO. 2
REACTOR VESSEL BELTLINE MATERIAL [1]

Material	Temperature (°F)	Time[a] (hr)	Cooling
Upper Shell Forging 49D963} 49C904} -1-1 (MK24-2)	Austenitizing: 1600 ± 25 (871°C)	6.75[a]	Water-quenched
	Tempered: 1225 ± 25 (663°C)	12.25[a]	Air-cooled
	Stress Relief: 1150 ± 50 (621°C)	11.75[b]	Furnace-cooled
Lower Shell Forging 50D102} 50C97} -1-1 (MK24-3)	Austenitizing: 1600 ± 25 (871°C)	6.5 [a]	Water-quenched
	Tempered: 1225 ± 25 (663°C)	12.25[a]	Air-cooled
	Stress Relief: 1150 ± 50 (621°C)	11.75[b]	Furnace-cooled
Upper Shell To Lower Shell Closing Girth Weld Seam (Heat 442011, Flux Linde 80, Lot No. 0344)	Stress Relief: 1150 ± 50 (621°C)	11.75[b]	Furnace-cooled
Surveillance Program Test Material			
Surveillance Program Test Forging 50D102-1 50C97-1	Post Weld Stress Relief: 1150 ± 50 (621°C)	14.25[b][c]	Furnace-cooled
Surveillance Program Test Weldment	Post Weld Stress Relief: 1150 ± 50 (621°C)	12.5 [b][c]	Furnace-cooled

a. Data obtained from Japan Steel Works, Ltd. Material Test Reports.
b. Data from Babcock and Wilcox, Co.
c. The Stress Relief Heat Treatment received by the Surveillance Test Forging and Weldment have been simulated.

TABLE 4-5

CHEMICAL COMPOSITION OF BRAIDWOOD UNIT 2 CAPSULE U

IRRADIATED CHARPY IMPACT SPECIMENS

Specimen No.	Chemical Composition (wt.%)										
	Cu	Ni	C	Mn	P	S	Si	Cr	Mo	V	Co
FL-6	0.049	0.745	0.229	1.261	<.005	<.003	0.294	0.083	0.483	<.002	<.002
FW-1	0.032	0.704	0.070	1.628	0.011		0.467	0.090	0.466	0.006	<.002
FW-7	0.034	0.754		1.687	0.013	0.009	0.450	0.092	0.503	0.007	<.002
FW-14	0.032	0.698	0.068	1.583	0.009	0.009		0.088	0.458	0.006	<.002
FW-2	0.026	0.623									
FW-2*	0.028	0.635									
FW-3	0.031	0.679									
FW-4	0.029	0.644									
FW-5	0.032	0.699									
FW-6	0.034	0.765									
FW-8	0.031	0.673	0.038								
FW-9	0.034	0.724				0.010					
FW-10	0.035	0.747									
FW-11	0.033	0.711									
FW-12	0.031	0.688									
FW-13	0.035	0.750					0.010				
FW-15	0.031	0.685									

Analyses	Method of Analysis
Metals	ICPS, Inductively Coupled Plasma Spectrometry
Carbon	EC-12, LECO Carbon Analyzer
Sulfur	Combustion/titration
Silicon	Dissolution/gravimetric
Iron	(Matrix Element: Remainder by Difference)

* Second run to show duplication of results

TABLE 4-6
CHEMISTRY RESULTS FROM THE NBS
CERTIFIED REFERENCE STANDARDS

Material ID		Low Alloy Steel: NBS Certified Reference Standards			
		NBS 361		NBS 362	
		Certified	Measured(a)	Certified	Measured(a)
Metals		Concentration in Weight Percent			
Fe	*	95.60	(matrix)	95.30	(matrix)
Co		0.032	0.033	0.300	0.318
Cu		0.042	0.043	0.500	0.514
Cr		0.694	0.663	0.300	0.297
Mn		0.660	0.644	1.040	1.050
Mo		0.190	0.193	0.068	0.054
Ni		2.000	2.072	0.590	0.610
P		0.014	0.0144	0.041	0.0417
V		0.011	0.011	0.040	0.040
C		0.383	0.386	0.160	0.162/0.161
S		0.014	N. A.	0.036	0.0354
Si		0.222	0.208/0.219	0.390	0.383

Material ID		Low Alloy Steel: NBS Certified Reference Standards			
		NBS 363		NBS 364	
		Certified	Measured(a)	Certified	Measured(a)
Metals		Concentration in Weight Percent			
Fe	*	94.40	(matrix)	96.7	(matrix)
Co		0.048	0.051	0.15	0.149
Cu		0.100	0.102	0.249	0.252
Cr		1.310	1.315	0.063	0.058
Ni		0.300	0.314	0.144	0.139
Mn		1.500	1.539	0.255	0.250
Mo		0.028	0.025	0.490	0.491
P		0.029	0.0285	0.010	0.0096
V		0.310	N. A.	0.105	0.100
C		0.620	N. A.	0.87	N. A.
S		0.0068	N. A.	0.0250	0.0247
Si		0.740	0.710	0.065	N. A.

* Matrix element calculated as difference for material balance.
Tentative value, certified ± 100% of value.
N. A. - Not analyzed

(a) Method of analysis -- Inductively Coupled Plasma Spectrometry (ICPS) for all elements except C, S and Si.

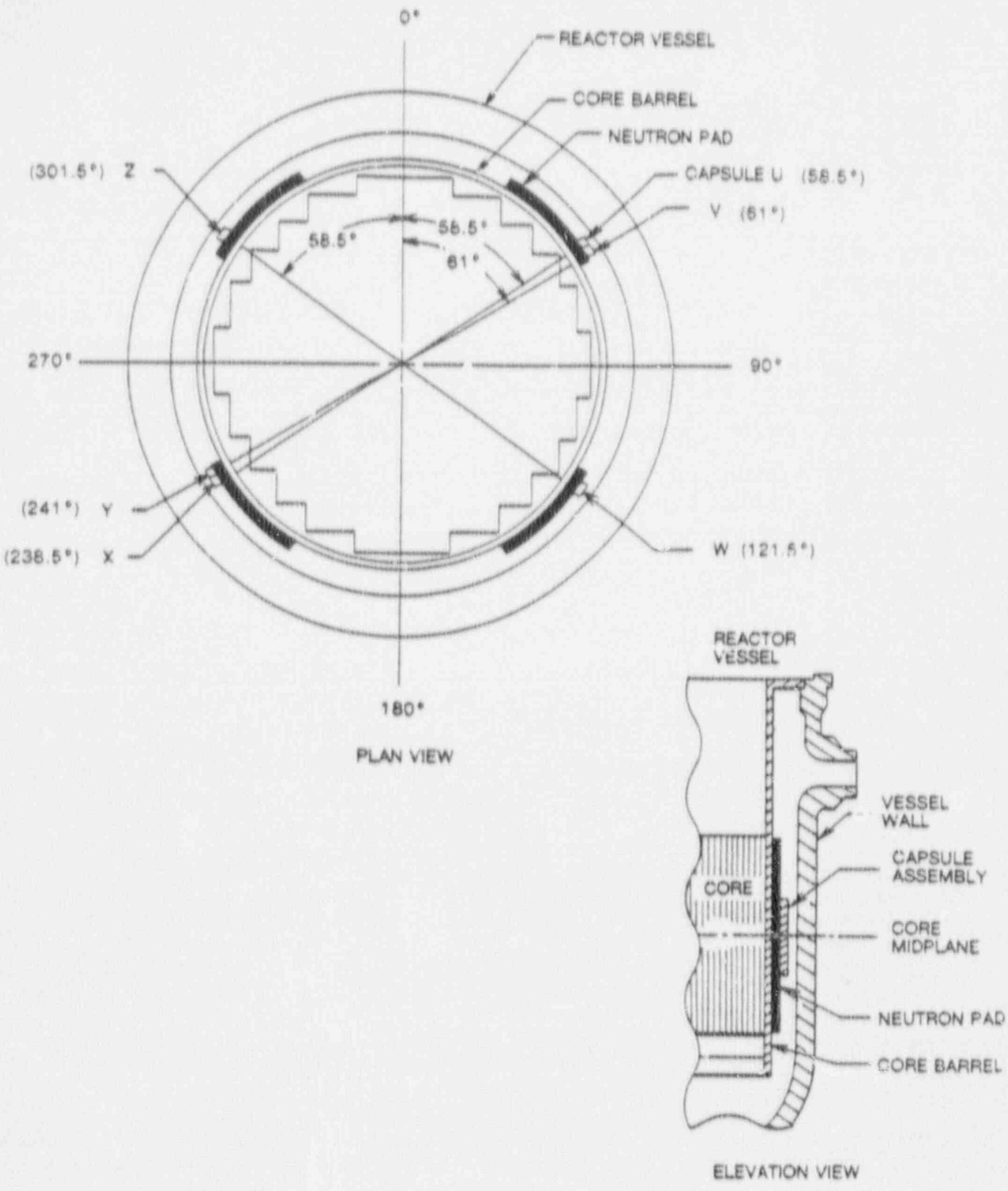

Figure 4-1. Arrangement of Surveillance Capsules in the Braidwood Unit 2 Reactor Vessel

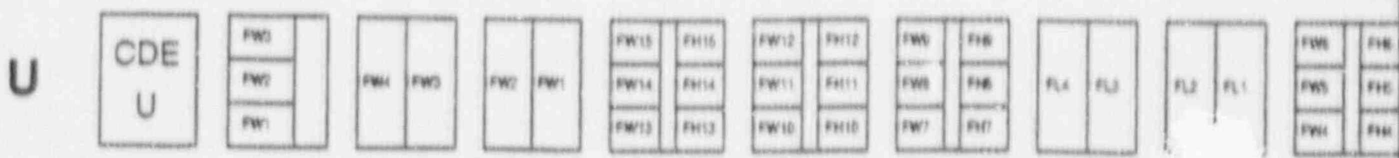

LEGEND: FL - LOWER SHELL FORGING 50D102-1/50C97-1 (TANGENTIAL)
FT - LOWER SHELL FORGING 50D102-1/50C97-1 (AXIAL)
FW - WELD METAL
FH - HEAT-AFFECTED-ZONE MATERIAL

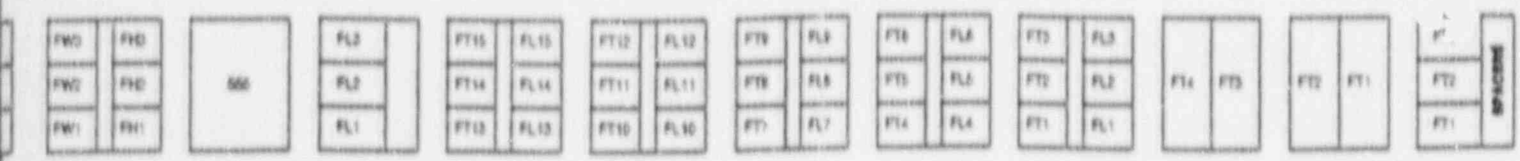

Figure 4-2 Capsule U Diagram Showing Location of Specimens, Thermal Monitors and Dosimeters

9104120295-01

SECTION 5.0
TESTING OF SPECIMENS FROM CAPSULE U

5.1 Overview

The post-irradiation mechanical testing of the Charpy V-notch and tensile specimens was performed at the Westinghouse Science and Technology Center hot cell with consultation by Westinghouse Power Systems personnel. Testing was performed in accordance with 10CFR50, Appendices G and H[2], ASTM Specification E185-82[6], and Westinghouse Procedure MHL 8402, Revision 1 as modified by RMF Procedures 8102, Revision 1 and 8103, Revision 1.

Upon receipt of the capsule at the hot cell laboratory, the specimens and spacer blocks were carefully removed, inspected for identification number, and checked against the master list in WCAP-11188[1]. No discrepancies were found.

Examination of the two low-melting point 304°C (579°F) and 310°C (590°F) eutectic alloys indicated no melting of either type of thermal monitor. Based on this examination, the maximum temperature to which the test specimens were exposed was less than 304°C (579°F).

The Charpy impact tests were performed per ASTM Specification E23-88[7] and RMF Procedure 8103, Revision 1 on a Tinius-Olsen Model 74, 358J machine. The tup (striker) of the Charpy machine is instrumented with an Effects Technology Model 500 instrumentation system. With this system, load-time and energy-time signals can be recorded in addition to the standard measurement of Charpy energy (E_D). From the load-time curve (Appendix B), the load of general yielding (P_{GY}), the time to general yielding (t_{GY}), the maximum load (P_M), and the time to maximum load (t_M) can be determined. Under some test conditions, a sharp drop in load indicative of fast fracture was observed. The load at which fast fracture was initiated is identified as the fast fracture load (P_F), and the load at which fast fracture terminated is identified as the arrest load (P_A).

The energy at maximum load (E_M) was determined by comparing the energy-time record and the load-time record. The energy at maximum load is roughly equivalent to the energy required to initiate a crack in the specimen. Therefore, the propagation energy for the crack (E_p) is the difference between the total energy to fracture (E_D) and the energy at maximum load.

The yield stress (σ_Y) was calculated from the three-point bend formula having the following expression:

$$\sigma_Y = P_{GY} * (L/[B*(W-a)^2*C]) \tag{1}$$

where the constant C is dependent on the notch flank angle (ϕ), notch root radius (ρ), and the type of loading (i.e., pure bending or three-point bending). In three-point bending a Charpy specimen in which ϕ = 45° and ρ = 0.010", Equation 1 is valid with with C = 1.21. Therefore (for L = 4W),

$$\sigma_Y = P_{GY} * (L/[B*(W-a)^2*1.21]) = [3.3P_{GY}W]/[B(W-a)^2] \tag{2}$$

For the Charpy specimens, B = 0.394 in., W = 0.394 in., and a = 0.079 in. Equation 2 then reduces to:

$$\sigma_Y = 33.3 \times P_{GY} \tag{3}$$

where σ_Y is in units of psi and P_{gy} is in units of lbs. The flow stress was calculated from the average of the yield and maximum loads, also using the three-point bend formula.

Percent shear was determined from post-fracture photographs using the ratio-of-areas methods in compliance with ASTM Specification A370-89[8]. The lateral expansion was measured using a dial gage rig similar to that shown in the same specification.

Tension tests were performed on a 20,000-pound Instron, split-console test machine (Model 1115) per ASTM Specification E8-89b[9] and E21-79 (1988)[10], and RMF Procedure 8102, Revision 1. All pull rods, grips, and pins were made of Inconel 718 hardened to HRC45. The upper pull rod was connected through a universal joint to improve axiality of loading. The tests were conducted at a constant crosshead speed of 0.05 inches per minute throughout the test.

Deflection measurements were made with a linear variable displacement transducer (LVDT) extensometer. The extensometer knife edges were spring-loaded to the specimen and operated through specimen failure. The extensometer gage length is 1.00 inch. The extensometer is rated as Class B-2 per ASTM E83-85[11].

Elevated test temperatures were obtained with a three-zone electric resistance split-tube furnace with a 9-inch hot zone. All tests were conducted in air.

Because of the difficulty in remotely attaching a thermocouple directly to the specimen, the following procedure was used to monitor specimen temperature. Chromel-alumel thermocouples were inserted in shallow holes in the center and each end of the gage section of a dummy specimen and in each grip. In the test configuration, with a slight load on the specimen, a plot of specimen temperature versus upper and lower grip and controller temperatures was developed over the range of room temperature to 550°F (288°C). The upper grip was used to control the furnace temperature. During the actual testing the grip temperatures were used to obtained desired specimen temperatures. Experiments indicated that this method is accurate to ±2°F.

The yield load, ultimate load, fracture load, total elongation, and uniform elongation were determined directly from the load-extension curve. The yield strength, ultimate strength, and fracture strength were calculated using the original cross-sectional area. The final diameter and final gage length were determined from post-fracture photographs. The fracture area used to calculate the fracture stress (true stress at fracture) and percent reduction in area was computed using the final diameter measurement.

5.2 Charpy V-Notch Impact Test Results

The results of Charpy V-notch impact tests performed on the various materials contained in Capsule U irradiated to 3.91 x 10^{18} n/cm^2 (E > 1.0 MeV) are presented in Tables 5-1 through 5-4 and are compared with unirradiated results[1] as shown in Figures 5-1 through 5-4. The transition temperature increases and upper shelf energy decreases for the Capsule U materials are summarized in Table 5-5.

Irradiation of the reactor vessel lower shell forging 50D102-1/50C97-1 Charpy specimens to 3.91 x 10^{18} n/cm^2 (E > 1.0 MeV) at 550°F (Figure 5-1) resulted no 30 and 50 ft-lb transition temperature increases for specimens oriented perpendicular to the major working direction (tangential orientation). This resulted in a 30 ft-lb transition temperature of -10°F and a 50 ft-lb transition temperature of 15°F for specimens oriented perpendicular to the major working direction (tangential orientation).

The average upper shelf energy (USE) of the lower shell forging 50D102-1/50C97-1 Charpy specimens (tangential orientation) resulted in no energy decrease after irradiation to 3.91 x 10^{18} n/cm^2 (E > 1.0 MeV) at 550°F. This resulted in an average USE of 168 ft-lb (Figure 5-1).

Irradiation of the reactor vessel lower shell forging 50D102-1/50C97-1 Charpy specimens to 3.91 x 10^{18} n/cm^2 (E > 1.0 MeV) at 550°F (Figure 5-2) resulted in a 30 ft-lb transion temperature increase of 5°F and a 50 ft-lb transition temperature increase of 10°F for specimens oriented parallel to the major working direction (axial orientation). This resulted in a 30 ft-lb transition temperature of -20°F and a 50 ft-lb transition temperature of 10°F for specimens oriented perpendicular to the major working direction (axial orientation).

The average upper shelf energy (USE) of the lower shell forging 50D102-1/50C97-1 Charpy specimens (axial orientation) resulted in a decrease of 16 ft-lb in energy after irradiation to 3.91×10^{18} n/cm^2 (E > 1.0 MeV) at 550°F. This resulted in an average USE of 137 ft-lb (Figure 5-2).

Irradiation of the reactor vessel core region weld metal Charpy specimens to 3.91×10^{18} n/cm^2 (E > 1.0 MeV) at 550°F (Figure 5-3) resulted in no 30 ft-lb transition temperature increase and a 50 ft-lb transition temperature increase of 5°F. This resulted in a 30 ft-lb transition temperature of -20°F and a 50 ft-lb transition temperature of 45°F

The average upper shelf energy (USE) of the reactor vessel core region weld metal resulted in a decrease of 9 ft-lb in energy after irradiation to 3.91×10^{18} n/cm^2 (E > 1.0 MeV) at 550°F. This resulted in an average USE of 62 ft-lb.

Irradiation of the reactor vessel weld metal Heat-Affected Zone (HAZ) specimens to 3.91×10^{18} n/cm^2 (E > 1.0 MeV) at 550°F (Figure 5-4) resulted in no 30 and 50 ft-lb transition temperature increases. This resulted in a 30 ft-lb transition temperature of -135°F and a 50 ft-lb transition temperature of -105°F

The average upper shelf energy (USE) of the reactor vessel HAZ metal resulted in an increase of 45 ft-lb after irradiation to 3.91×10^{18} n/cm^2 (E > 1.0 MeV) at 550°F, however this is not unexpected due to the large scatter of data points. This resulted in an average USE of 200 ft-lb.

The fracture appearance of each irradiated Charpy specimen from the various materials is shown in Figures 5-5 through 5-8 and show an increasingly ductile or tougher appearance with increasing test temperature.

A comparison of the 30 ft-lb transition temperature increases for the various Braidwood Unit 2 surveillance materials with predicted increases using the methods of NRC Regulatory Guide 1.99, Revision 2[3] is presented in Table 5-6. This comparison indicates that the transition temperature increases and the USE decreases resulting from irradiation to 3.91 x 10^{18} n/cm^2 (E > 1.0 MeV) are less than the Guide predictions.

Unusual energy and fracture behavior was shown by tangential base metal specimens FL13 and FL14. The impact energy value of 76.0 ft-lb at -35°F for specimen FL13 is close to the impact energy value of 74.0 ft-lb for specimen FL11 which was tested at +20°F, yet our test records indicate that specimen FL13 was tested at the prescribed temperature. The fracture appearances of specimens FL13 and FL11 are also similar (Figure 5-5), and examination of the irregular facture path and brinelling of the notched face of specimen FL13 (Figure 5-9) suggest that the high energy value is correct and that the specimen was tested properly. The impact energy value of 19.0 ft-lb for specimen FL4 tested at -25°F seems to be low. It should be more like 30 ft-lb. The fracture appearance of this specimen (Figure 5-5) suggests a low impact energy value, and the more brittle fracture path of this specimen seen in Figure 5-10 is also in line with a low fracture toughness behavior.

HAZ metal Charpy specimen FH2 showed an unusually high impact energy value (243 ft-lb) at 250 °F. The specimens fracture path was examined and compared to the fracture path of another HAZ specimen (FH1) which showed a considerably lower impact energy value (162 ft-lb) at 225°F. The results are shown in Figure 5-11. The comparison showed that fracture in specimen FH2 was more irregular than in specimen FH1. Fracture in specimen FH2 appeared to have started in a very tough microstructure of the Heat-Affect-Zone, with some fracture actually initiating outside the notch root. The specimen, in effect, behaved like a blunt notch type specimen, thus accounting for the high energy value during fracture.

The load-time records for the individual instrumented Charpy specimens are contained in Appendix A.

5.3 Tension Test Results

The results of tension tests performed on shell forging 50D102-1/50C97-1 (tangential and axial orientation) and the weld metal irradiated to 3.91 x 10^{18} n/cm^2 (E > 1.0 MeV) are shown in Table 5-7 and are compared with unirradiated results[1] as shown in Figures 5-12 through 5-14. The tension test results for forging 50D102-1/50C97-1 are shown in Figures 5-12 and 5-13 and indicated that irradiation to 3.91 x 10^{18} n/cm^2 (E > 1.0 MeV) caused a less than 6 ksi increase in the 0.2 percent offset yield strength and ultimate tensile strength. The weld metal tension tests results are shown in Figure 5-14 and show that the ultimate tensile strength and the 0.2 percent offset yield strength increased by less than 5 ksi with irradiation to 3.91 x 10^{18} n/cm^2 (E > 1.0 MeV). The small increases in 0.2% yield strength and tensile strength exhibited by the forging material and weld metal indicate that these materials are not highly sensitive to irradiation to 3.91 x 10^{18} n/cm^2 (E > 1.0 MeV), as is also indicated by the Charpy impact test results. The fractured tension specimens for the forging material are shown in Figures 5-15 and 5-16, while the fractured specimens for the weld metal are shown in Figure 5-17. The engineering stress-strain curves for the tension tests are shown in Figures 5-18 through 5-22.

5.4 Compact Tension Tests

Per the surveillance capsule testing program with the Commonwealth Edison Company, 1/2 T-compact tension fracture mechanics specimens will not be tested and will be stored at the Westinghouse Science and Technology Center Hot Cell.

TABLE 5-1

CHARPY V-NOTCH IMPACT DATA FOR THE BRAIDWOOD UNIT 2

FORGING 50D102-1/50C97-1 IRRADIATED AT 550°F,

FLUENCE 3.91×10^{18} n/cm^2 (E > 1.0 MeV)

Sample No.	Temperature (°F)	(°C)	Impact Energy (ft-lb)	(J)	Lateral Expansion (mils)	(mm)	Shear (%)
			Tangential Orientation				
FL12	- 75	(-59)	5.0	(7.5)	4.0	(0.10)	0
FL13	- 35	(-37)	76.0	(103.0)	46.0	(1.17)	70
FL4	- 25	(-32)	19.0	(26.0)	14.0	(0.36)	15
FL9	0	(-18)	33.0	(44.5)	23.0	(0.58)	25
FL5	15	(- 9)	47.0	(63.5)	35.0	(0.89)	45
FL11	20	(- 7)	74.0	(100.5)	52.0	(1.32)	70
FL10	40	(4)	89.0	(120.5)	58.0	(1.47)	75
FL6	75	(24)	138.0	(187.0)	80.0	(2.03)	90
FL7	100	(38)	140.0	(190.0)	83.0	(2.11)	90
FL3	125	(52)	136.0	(184.5)	84.0	(2.13)	95
FL2	150	(66)	175.0	(237.5)	93.0	(2.36)	100
FL15	200	(93)	172.0	(233.0)	86.0	(2.18)	100
FL1	250	(121)	184.0	(249.0)	81.0	(2.06)	100
FL8	300	(149)	173.0	(234.5)	84.0	(2.13)	100
			Axial Orientation				
FT3	- 75	(-57)	8.0	(11.0)	4.0	(0.10)	5
FT14	- 50	(-46)	10.0	(13.5)	6.0	(0.15)	10
FT6	- 20	(-29)	40.0	(54.0)	24.0	(0.61)	25
FT4	0	(-18)	35.0	(47.5)	24.0	(0.61)	30
FT8	20	(- 7)	82.0	(111.0)	57.0	(1.45)	70
FT1	25	(- 4)	63.0	(85.5)	40.0	(1.02)	55
FT2	40	(4)	71.0	(96.5)	50.0	(1.27)	65
FT11	60	(16)	74.0	(100.5)	55.0	(1.40)	70
FT15	80	(27)	100.0	(135.5)	68.0	(1.73)	80
FT13	105	(41)	116.0	(157.5)	78.0	(1.98)	90
FT10	105	(66)	128.0	(174.0)	82.0	(2.08)	100
FT5	200	(93)	125.0	(169.5)	81.0	(2.06)	100
FT9	200	(93)	139.0	(188.5)	83.0	(2.11)	100
FT12	250	(121)	149.0	(202.0)	86.0	(2.18)	100
FT7	300	(149)	145.0	(196.5)	82.0	(2.08)	100

TABLE 5-2

CHARPY V-NOTCH IMPACT DATA FOR THE BRAIDWOOD UNIT 2 REACTOR VESSEL WELD METAL AND HAZ METAL IRRADIATED AT 550°F, FLUENCE 3.91 x 10^{18} n/cm^2 (E > 1.0 MeV)

Sample No.	Temperature (°F)	(°C)	Impact Energy (ft-lb)	(J)	Lateral Expansion (mils)	(mm)	Shear (%)
			Weld Metal				
FW11	-110	(-79)	18.0	(24.5)	12.0	(0.30)	10
FW8	- 80	(-62)	7.0	(9.5)	5.0	(0.13)	5
FW7	- 70	(-57)	18.0	(24.5)	16.0	(0.41)	15
FW5	- 45	(-43)	25.0	(34.0)	19.0	(0.48)	20
FW1	- 20	(-29)	31.0	(42.0)	23.0	(0.58)	25
FW3	0	(-18)	33.0	(44.5)	28.0	(0.71)	30
FW12	20	(- 7)	44.0	(59.5)	35.0	(0.89)	45
FW14	35	(2)	43.0	(58.5)	36.0	(0.91)	45
FW9	60	(16)	46.0	(62.5)	38.0	(0.97)	50
FW6	90	(32)	59.0	(80.0)	54.0	(1.37)	100
FW4	120	(49)	63.0	(85.5)	60.0	(1.52)	100
FW10	150	(66)	59.0	(80.0)	54.0	(1.37)	100
FW2	200	(93)	60.0	(81.5)	49.0	(1.24)	100
FW1[illegible]	250	(121)	68.0	(92.0)	63.0	(1.60)	100
FW1[illegible]	300	(149)	63.0	(85.5)	61.0	(1.55)	100
			HAZ Metal				
FH3	-170	(-112)	7.0	(9.5)	10.0	(0.25)	5
FH8	-150	(-101)	19.0	(26.0)	17.0	(0.43)	15
FH4	-125	(- 87)	82.0	(111.0)	47.0	(1.19)	75
FH6	-115	(- 82)	29.0	(39.5)	15.0	(0.38)	20
FH15	- 95	(- 71)	68.0	(92.0)	38.0	(0.97)	60
FH7	- 75	(- 59)	76.0	(103.0)	41.0	(1.04)	65
FH9	- 25	(- 32)	97.0	(131.5)	58.0	(1.47)	85
FH11	5	(- 15)	111.0	(150.5)	59.0	(1.50)	95
FH14	30	(- 1)	174.0	(236.0)	85.0	(2.16)	100
FH12	60	(16)	155.0	(210.0)	80.0	(2.03)	95
FH10	100	(38)	56.0	(76.0)	43.0	(1.09)	60
FH13	150	(66)	204.0	(276.5)	82.0	(2.08)	100
FH5	200	(93)	191.0	(259.0)	83.0	(2.11)	100
FH1	225	(107)	162.0	(219.5)	55.0	(1.40)	100
FH2	250	(121)	243.0	(329.0)	69.0	(1.75)	100

TABLE 5-3

INSTRUMENTED CHARPY IMPACT TEST RESULTS FOR THE BRAIDWOOD UNIT 2 SHELL FORGING

50D102-1/50C97-1 IRRADIATED AT 550°F, FLUENCE 3.91 x 10^{18} n/cm^2 (E > 1.0 MeV)

Sample Number	Test Temp (°F)	Charpy Energy (ft-lb)	Normalized Energies (ft-lb/in²) Charpy Ed/A	Maximum Em/A	Prop Ep/A	Yield Load (kips)	Time to Yield (μsec)	Maximum Load (kips)	Time to Maximum (μsec)	Fracture Load (kips)	Arrest Load (kips)	Yield Stress (ksi)	Flow Stress (ksi)
						Tangential Orientation							
FL12	-75	5.0	40	30	10	3.30	95	3.35	110	3.35	0.01	109	110
FL13	-35	76.0	612	315	297	3.45	90	4.65	655	4.25	0.60	115	134
FL4	-25	19.0	153	116	37	3.55	95	4.05	280	4.05	0.01	118	126
FL9	0	33.0	266	217	49	3.2	105	4.10	520	4.10	0.01	108	121
FL5	15	47.0	378	338	41	3.25	85	4.40	730	4.40	0.01	107	127
FL11	20	74.0	596	360	235	3.05	90	4.20	825	3.90	0.01	101	120
FL10	40	89.0	717	318	399	2.95	95	4.10	755	3.65	0.55	97	116
FL6	50	93.0	749	243	405	3.15	100	4.40	765	3.95	1.10	104	125
FL14	75	138.0	1111	316	795	3.2	100	4.70	670	3.00	1.80	105	130
FL7	100	140.0	1127	312	816	3.00	115	4.70	690	3.05	1.60	99	127
FL3	125	136.0	1095	358	737	2.95	90	4.60	770	2.80	1.80	98	125
FL2	150	175.0	1409	286	1123	2.80	105	4.20	685	--*	--*	93	116
FL15	200	172.0	1385	325	1060	2.35	65	3.90	790	--*	--*	78	104
FL1	250	184.0	1482	189	1292	1.70	40	3.00	600	--*	--*	56	78
FL8	300	173.0	1393	232	1161	1.75	20	3.20	685	--*	--*	57	82
						Axial Orientation							
FT3	-75	8.0	64	42	23	3.45	90	3.65	130	3.65	0.01	114	117
FT14	-50	10.0	81	56	24	3.40	110	3.50	175	3.45	0.01	112	114
FT6	-20	40.0	312	257	66	3.30	125	4.40	605	4.25	0.01	109	127
FT4	0	35.0	282	221	61	3.15	90	4.20	510	4.20	0.20	104	122
FT8	20	82.0	660	272	389	2.45	110	4.00	690	2.40	1.30	81	107
FT1	25	63.0	507	304	204	3.10	80	4.50	655	4.35	0.15	102	126
FT2	40	71.0	572	337	235	3.05	80	4.45	730	4.3	0.65	101	124
FT11	60	74.0	596	299	297	3.05	90	4.35	670	4.10	1.20	101	123
FT15	80	100.0	805	360	445	3.05	95	4.65	765	3.90	1.60	101	127
FT13	105	116.0	934	354	580	2.95	95	4.50	775	3.2	1.85	98	123
FT10	150	128.0	1032	COMPUTER MALFUNCTION			-	-	-	-	-	-	-
FT5	200	125.0	1007	267	739	2.80	115	4.00	680	--*	--*	92	112
FT9	200	139.0	1119	329	790	2.75	100	4.30	755	--*	--*	92	117
FT12	250	149.0	1202	COMPUTER MALFUNCTION			-	-	-	-	-	-	-
FT7	300	145.0	1166	271	897	2.00	60	3.45	745	--*	--*	66	90

*Fully ductile fracture; no arrest load

TABLE 5-4

INSTRUMENTED CHARPY IMPACT TEST RESULTS FOR THE BRAIDWOOD UNIT 2

WELD METAL AND HAZ METAL IRRADIATED AT 550°F, FLUENCE 3.91 x 10^{18} n/cm^2 (E > 1.0 MeV)

Sample Number	Test Temp (°F)	Charpy Energy (ft-lb)	Normalized Energies (ft-lb/in²) Charpy Ed/A	Maximum Em/A	Prop Ep/A	Yield Load (kips)	Time to Yield (μsec)	Maximum Load (kips)	Time to Maximum (μsec)	Fracture Load (kips)	Arrest Load (kips)	Yield Stress (ksi)	Flow Stress (ksi)
Weld Metal													
FW11	-110	18.0	145	101	44	3.00	130	3.90	300	3.80	0.01	99	114
FW8	-80	7.0	56	38	18	3.60	140	3.70	150	3.60	0.01	119	120
FW7	-70	18.0	145	108	37	3.40	105	3.80	285	3.55	0.01	113	120
FW5	-45	25.0	201	175	26	3.30	90	4.05	410	4.00	0.01	110	122
FW1	-20	31.0	250	158	93	3.05	45	3.85	370	3.70	0.01	101	114
FW3	0	33.0	266	206	60	3.00	90	3.75	510	3.75	0.20	99	112
FW12	20	44.0	354	209	145	3.10	90	3.90	500	3.70	1.70	103	116
FW14	35	43.0	346	159	187	2.95	110	3.70	430	3.60	1.55	98	110
FW9	60	46.0	370	220	151	2.95	105	4.20	520	4.10	2.60	97	118
FW6	90	59.0	475	207	268	2.85	95	3.95	505	—*	—*	94	113
FW4	120	63.0	507	204	303	2.85	95	3.95	500	—*	—*	94	113
FW10	150	59.0	475	185	290	2.75	145	3.50	530	—*	—*	90	103
FW2	200	60.0	483	180	304	2.55	115	3.4[illegible]	520	—*	—*	85	99
FW15	250	68.0	548	177	370	2.45	60	3.55	470	—*	—*	81	99
FW13	300	63.0	507	205	302	2.45	140	3.30	605	—*	—*	81	95
HAZ Metal													
FH3	-170	7.0	56	46	10	3.85	90	4.20	130	4.20	0.01	128	134
FH8	-150	19.0	153	211	-58	3.95	105	4.95	425	4.95	0.01	131	147
FH4	-125	82.0	660	371	290	4.15	115	5.40	670	4.80	0.15	138	158
FH6	-115	29.0	234	190	44	3.75	50	4.80	360	4.80	0.01	124	142
FH15	- 95	68.0	548	274	274	3.45	95	4.50	585	4.15	0.25	115	132
FH7	- 75	76.0	612	312	300	3.40	80	4.50	655	4.10	0.50	113	131
FH9	- 25	97.0	781	364	417	3.35	95	4.85	730	4.05	1.60	111	136
FH11	5	111.0	894	368	525	3.50	125	4.85	770	3.70	0.35	116	138
FH14	30	174.0	1401	327	1074	3.45	100	4.00	670	—*	—*	115	137
FH12	60	155.0	1248	359	889	3.15	100	4.60	770	[illegible].10	1.45	104	128
FH10	100	56.0	451	198	253	2.95	95	3.75	505	3.45	2.80	98	111
FH13	150	20[illegible].0	1643	279	1364	2.60	90	4.05	684	—*	—*	86	110
FH5	200	191.0	1538	277	1261	2.75	150	4.00	720	—*	—*	92	112
FH1	225	162.0	1304	331	974	2.7	45	4.04	765	—*	—*	89	112
FH2	250	243.0	1957	329	1627	2.35	70	3.80	820	—*	—*	78	102

*Fully ductile fracture; no arrest load

TABLE 5-5

EFFECT OF 550°F IRRADIATION TO 3.91 x 10^{18} n/cm^2 (E > 1.0 MeV)

ON NOTCH TOUGHNESS PROPERTIES OF BRAIDWOOD UNIT 2 REACTOR VESSEL SURVEILLANCE MATERIALS

Material	Average 30 ft-lb Transition Temperature (°F)			Average 35 mil Lateral Expansion Temperature (°F)			Average 50 ft-lb Transition Temperature (°F)			Average Energy Absorption at Full Shear (ft-lb)		
	Unirradiated	Irradiated	ΔT	Unirradiated	Irradiated	ΔT	Unirradiated	Irradiated	ΔT	Unirradiated	Irradiated	Δ(ft-lb)
Forging 50D102-1/50C97-1 (Tangential)	- 10	- 10	0	10	10	0	15	15	0	168	176	+ 8*
Forging 50D102-1/50C97-1 (Axial)	- 25	- 20	5	- 5	5	10	0	10	10	153	137	-16
Weld Metal	- 20	- 20	0	5	15	10	40	45	5	71	62	- 9
HAZ Metal	-135	-135	0	-80	-75	5	-105	-105	0	155	200	+45*

* These values reflect scatter in the data and not real increases. Thus, the values will be reported as 168 ft-lb for the plate (tangential orientation) and 155 ft-lb for the HAZ metal.

TABLE 5-6

COMPARISON OF BRAIDWOOD UNIT 2 SURVEILLANCE MATERIAL 30 FT-LB TRANSITION TEMPERATURE SHIFTS AND UPPER SHELF ENERGY DECREASES WITH REGULATORY GUIDE 1.99 REVISION 2 PREDICTIONS

		30 ft-lb Transition Temp. Shift		Upper Shelf Energy Decrease	
Material	Fluence 10^{18} n/cm^2	R.G. 1.99 Rev. 2 (Predicted)[a] (°F)	Capsule U (°F)	R.G. 1.99 Rev. 2 (Predicted) (%)	Capsule U (%)
Forging 50D102-1/50C97-1 (Tangential)	3.91	25.2	0	15.5	0
Forging 50D102-1/50C97-1 (Axial)	3.91	25.2	5	15.5	10.5
Weld Metal	3.91	33.3	0	15.5	12.7
HAZ Metal	3.91	--	0	--	0

a) Mean wt. % values of Cu and Ni from Reference 1 and Table 4-5 were used to calculate the chemistry factors for the forging and weld metal.

TABLE 5-7

TENSILE PROPERTIES FOR BRAIDWOOD UNIT 2 REACTOR VESSEL SURVEILLANCE MATERIAL IRRADIATED AT 550°F TO 3.91 x 10^{18} n/cm^2 (E > 1.0 MeV)

Material	Sample Number	Test Temp. (°F)	0.2% Yield Strength (ksi)	Ultimate Strength (ksi)	Fracture Load (kip)	Fracture Stress (ksi)	Fracture Strength (ksi)	Uniform Elongation (%)	Total Elongation (%)	Reduction in Area (%)
Forging	FL1	75	70.3	91.7	2.70	203.4	55.0	11.4	25.2	69
50D102-1/	FL2	300	63.2	83.5	2.50	158.8	50.9	9.0	21.9	63
50C97-1	FL3	550	60.6	87.6	2.70	220.0	55.0	9.9	22.2	68
(Tangent. Orient.)										
Forging	FT1	75	70.8	94.7	2.88	234.7	58.7	11.1	24.2	69
50D102-1/	FT2	300	65.2	84.5	2.70	211.5	55.0	9.0	21.9	67
50C97-1	FT3	550	62.6	90.7	3.20	250.6	65.2	9.9	19.7	64
(Axial Orient.)										
Weld	FW1	75	74.9	89.6	3.10	181.4	63.2	9.9	21.0	61
Weld	FW2	300	68.8	82.5	2.95	166.9	60.1	8.4	18.9	59
Weld	FW3	550	67.7	85.6	3.15	172.5	64.2	7.5	17.3	55

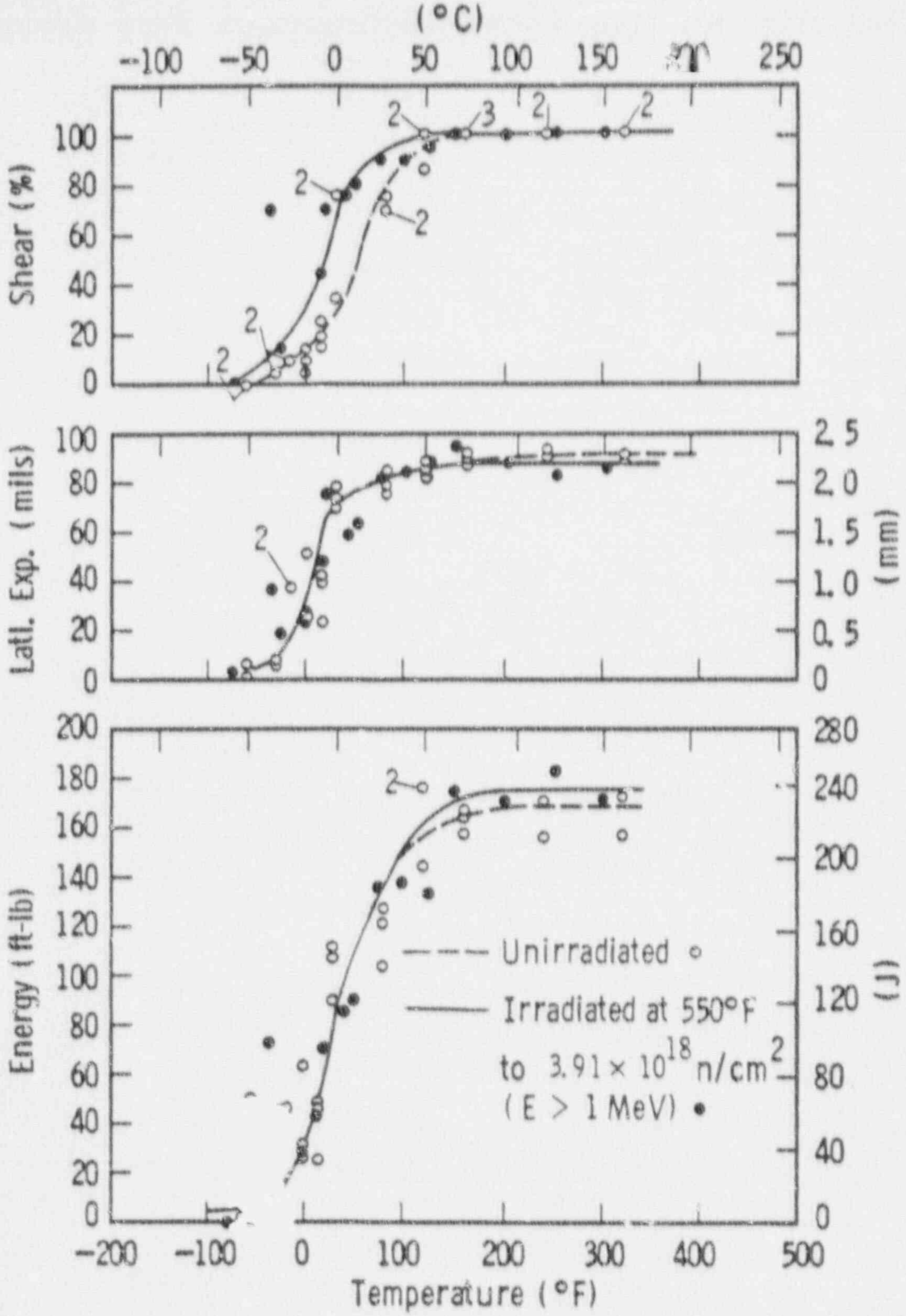

Figure 5-1. Charpy V-Notch Impact Properties for Braidwood Unit 2 Reactor Vessel Shell Forging 50D102-1/50C97-1 (Tangential Orientation)

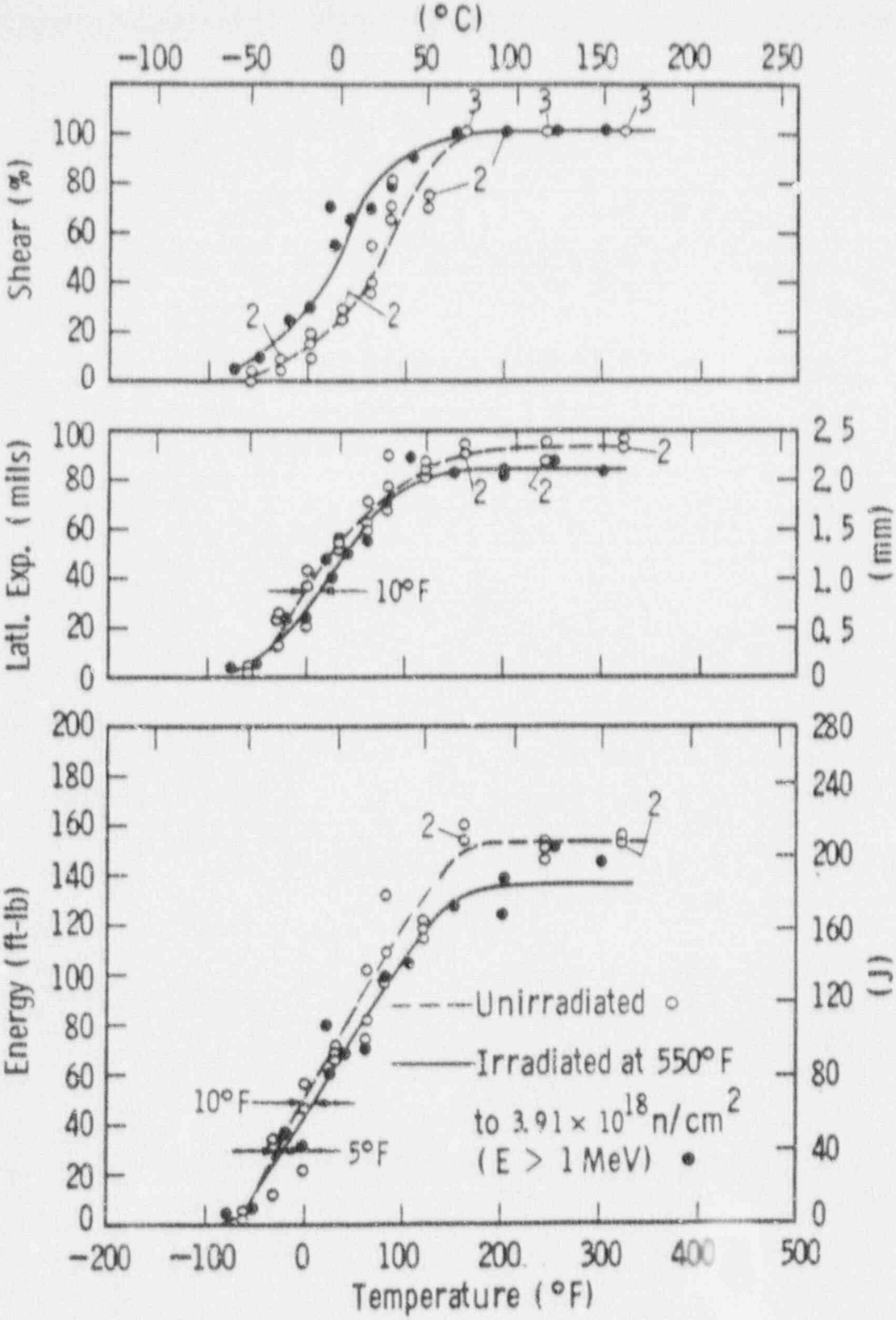

Figure 5-2. Charpy V-Notch Impact Properties for Braidwood Unit 2 Reactor Vessel Shell Forging 50D102-1/50C97-1 (Axial Orientation)

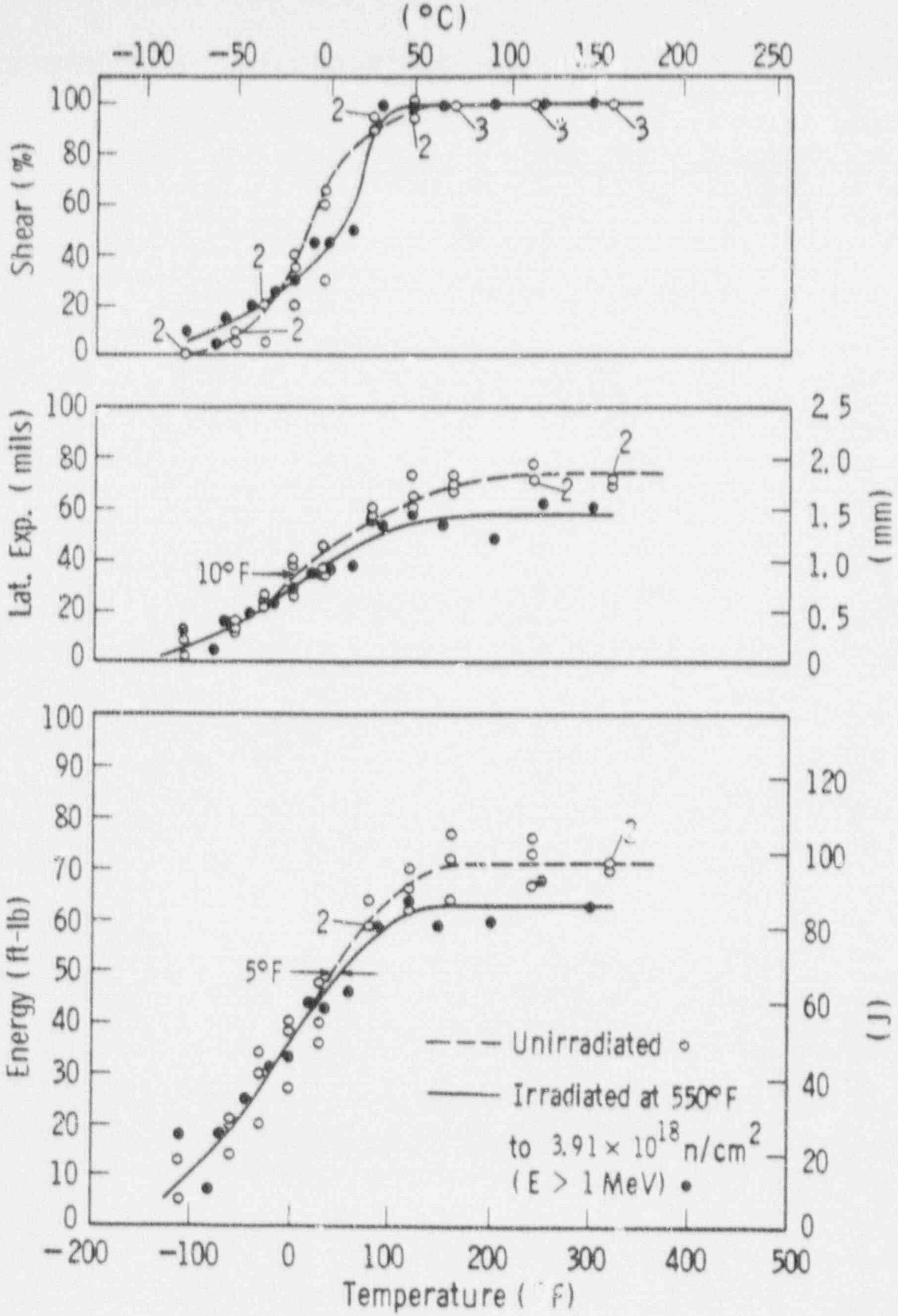

Figure 5-3. Charpy V-Notch Impact Properties for Braidwood Unit 2 Reactor Vessel Weld Metal

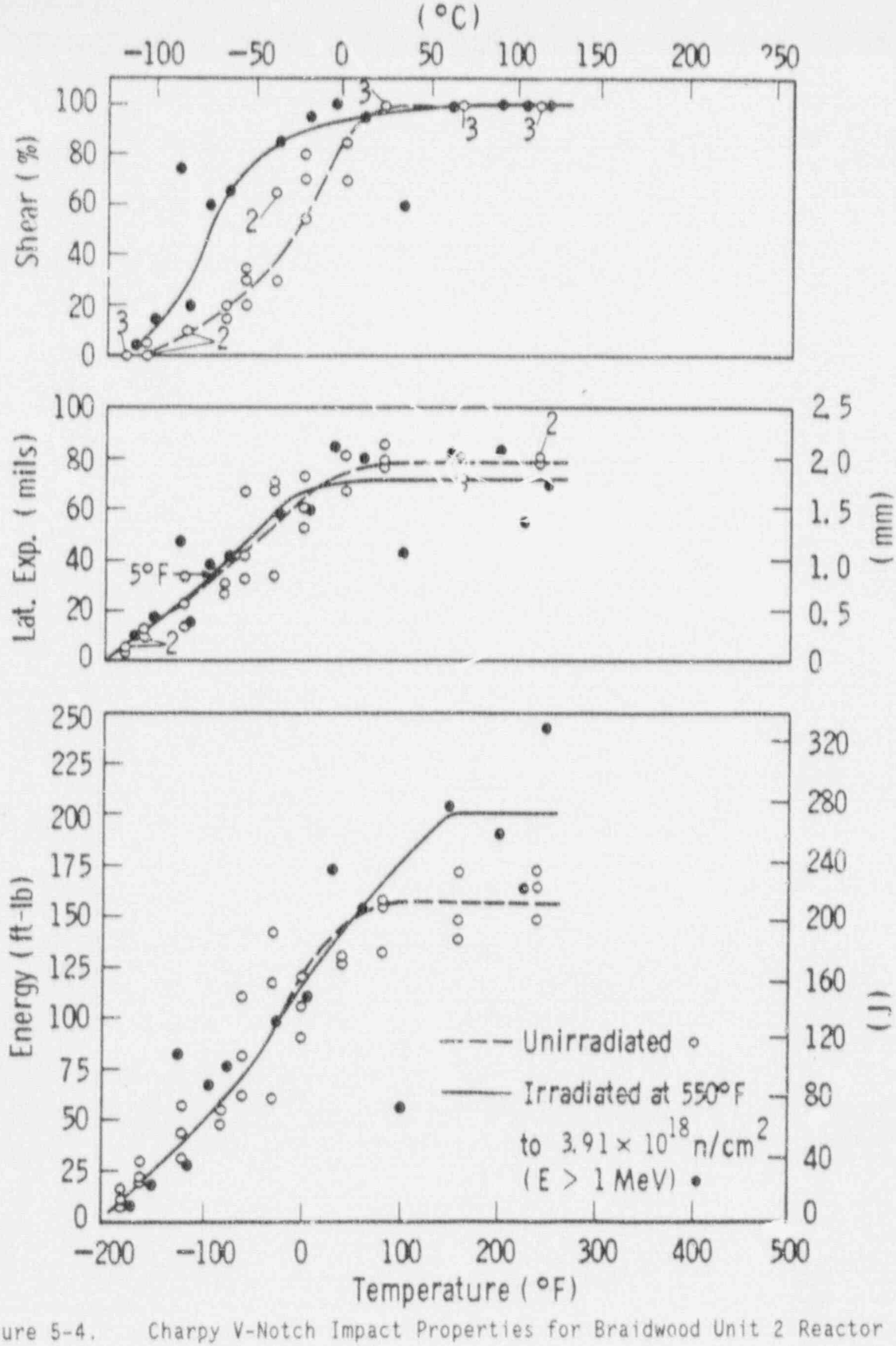

Figure 5-4. Charpy V-Notch Impact Properties for Braidwood Unit 2 Reactor Vessel Weld Heat Affected Zone Metal

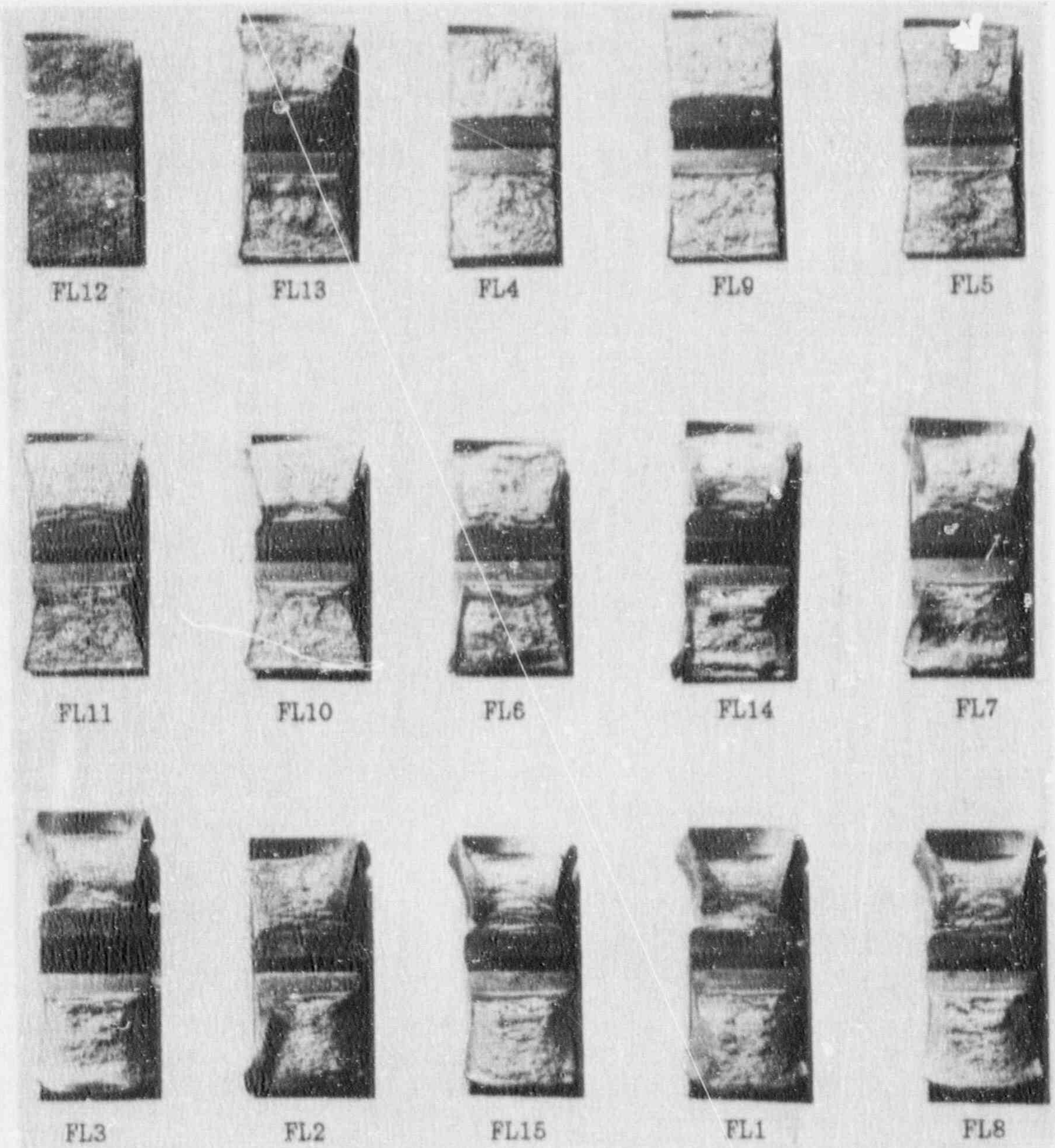

Figure 5-5. Charpy Impact Specimen Fracture Surfaces for Braidwood Unit 2 Reactor Vessel Shell Forging 50D102-1/50C97-1 (Tangential Orientation)

Figure 5-6. Charpy Impact Specimen Fracture Surfaces for Braidwood Unit 2 Reactor Vessel Shell Forging 50D102-1/50C97-1 (Axial Orientation)

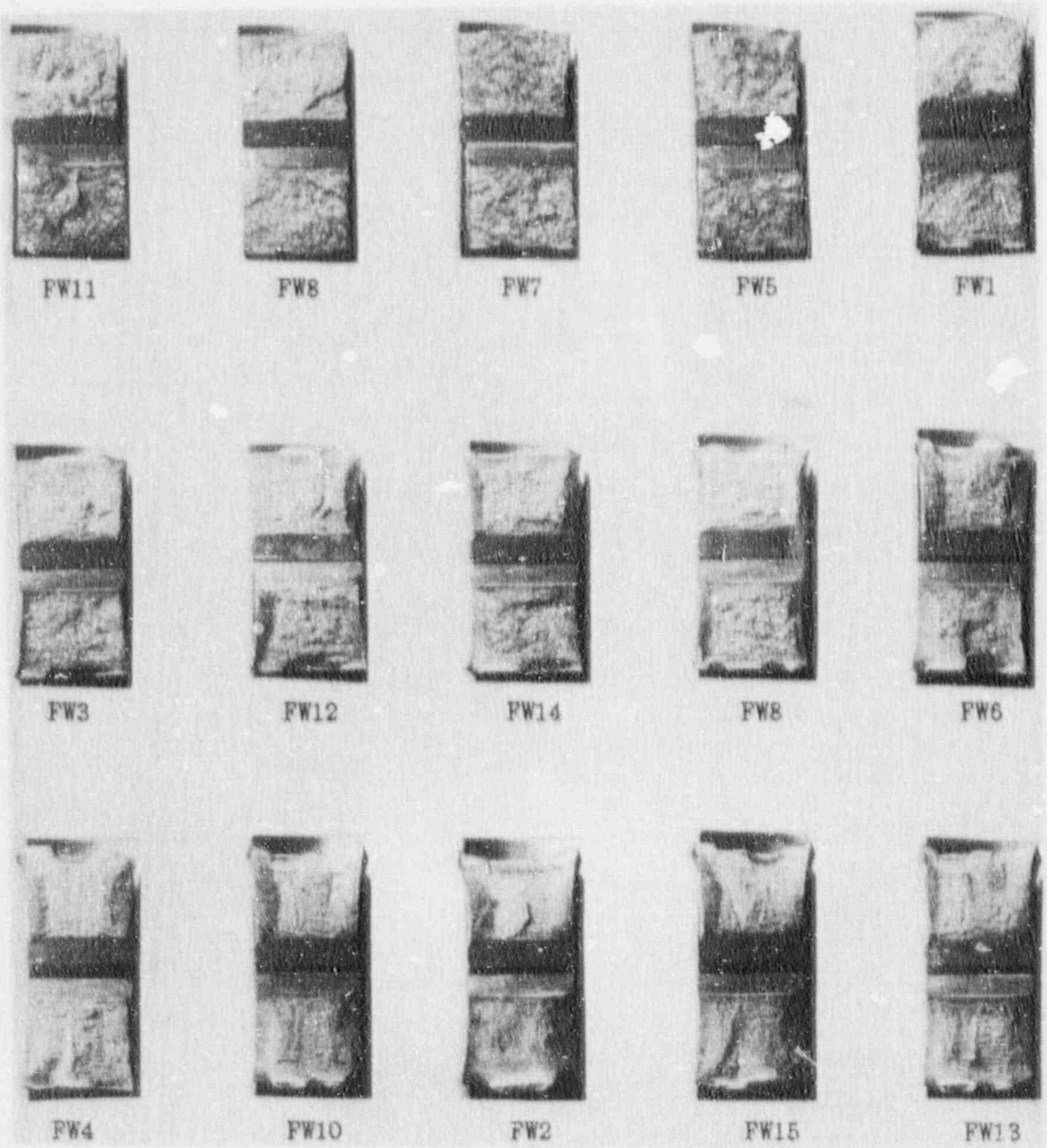

Figure 5-7. Charpy Impact Specimen Fracture Surfaces for Braidwood Unit 2 Reactor Vessel Weld Metal

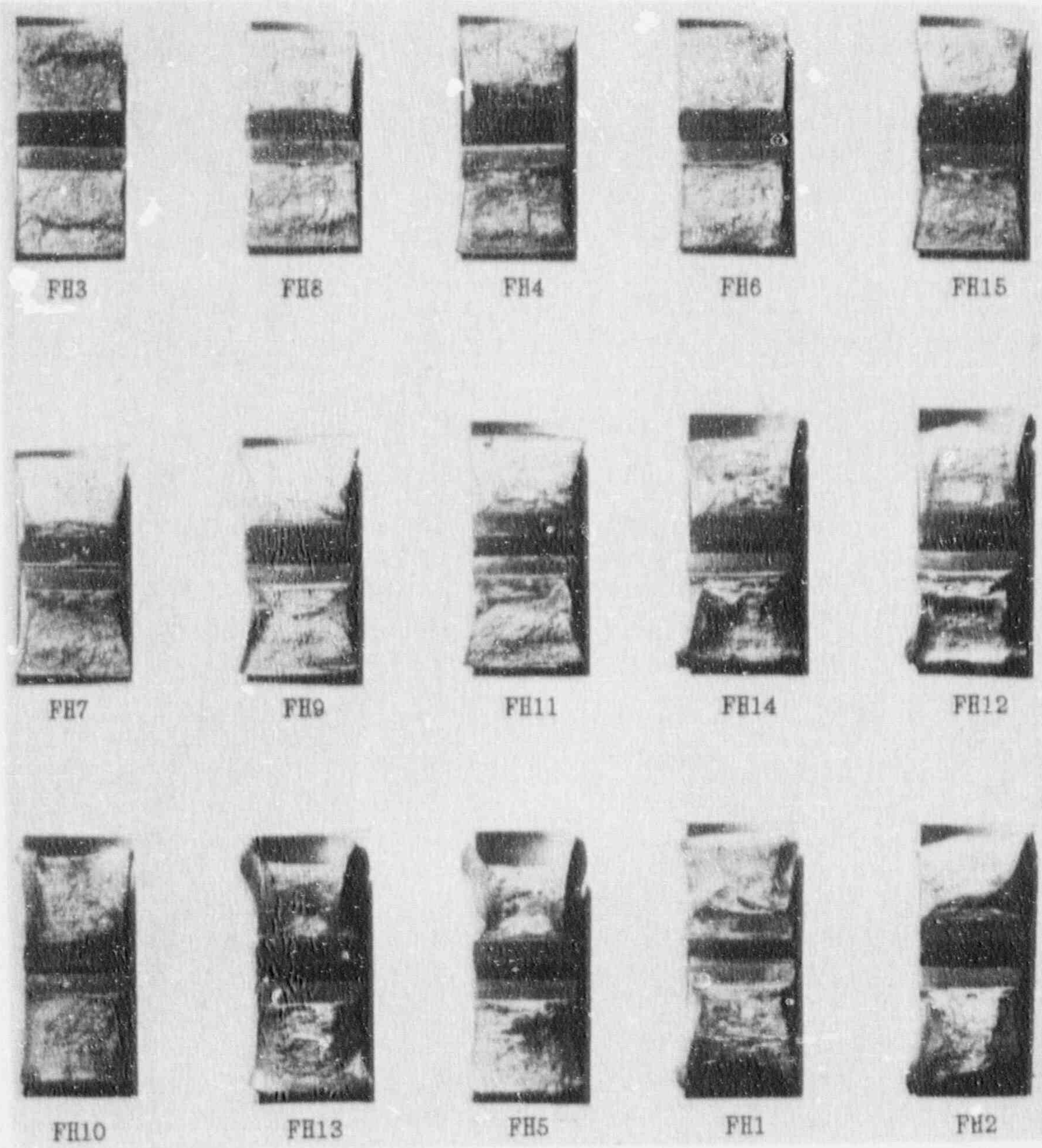

Figure 5-8. Charpy Impact Specimen Fracture Surfaces for Braidwood Unit 2 Reactor Vessel Weld Heat Affected Zone Metal

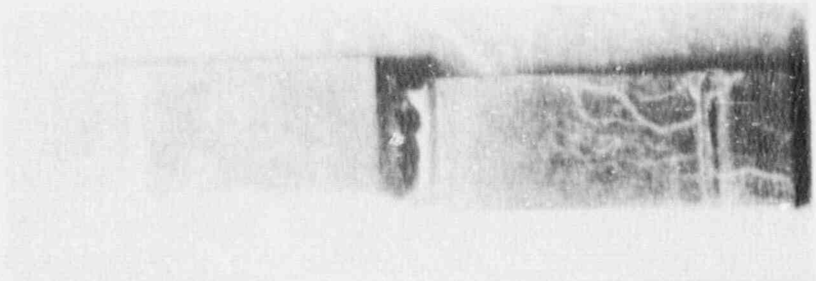

Top

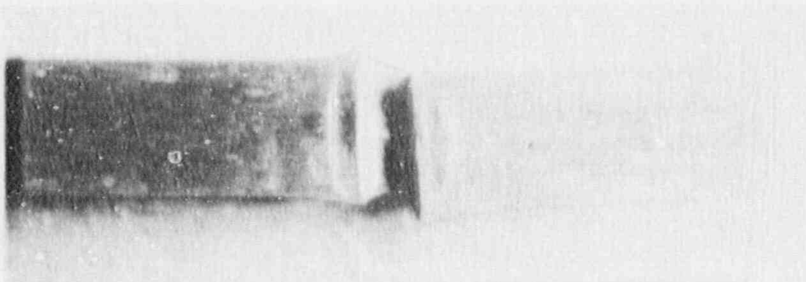

Bottom

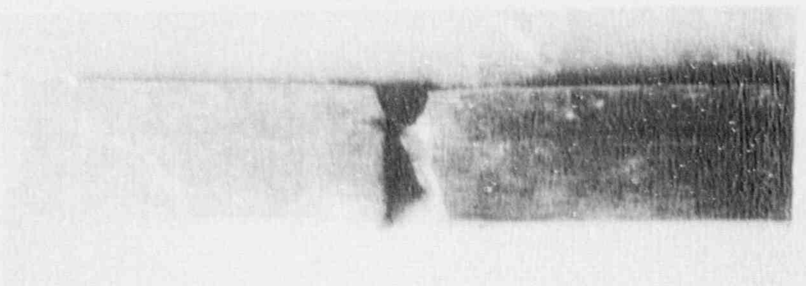

Side 1

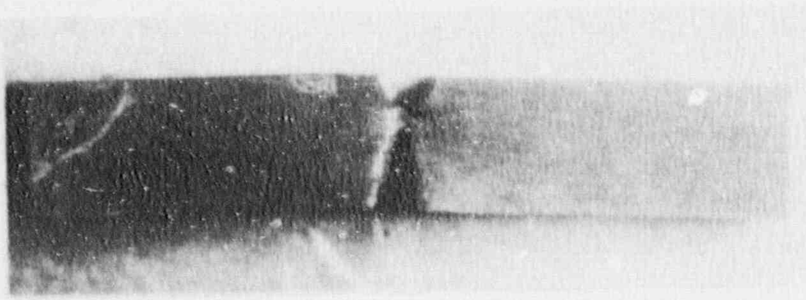

Side 2

Figure 5-9. Fracture Appearance of Specimen FL13

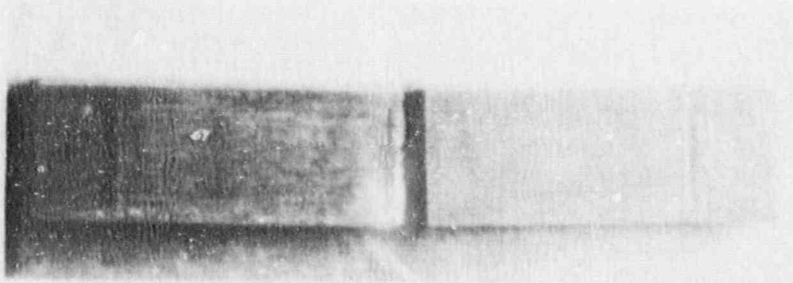

Top

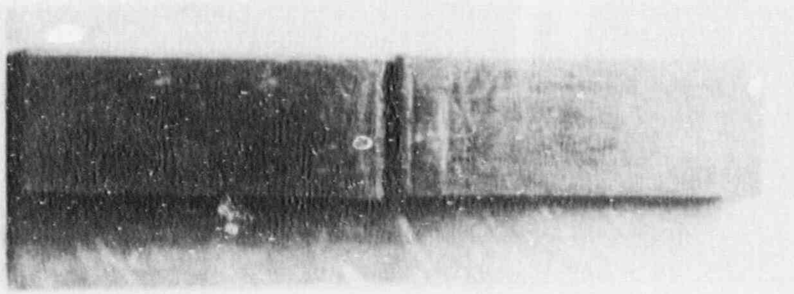

Bottom

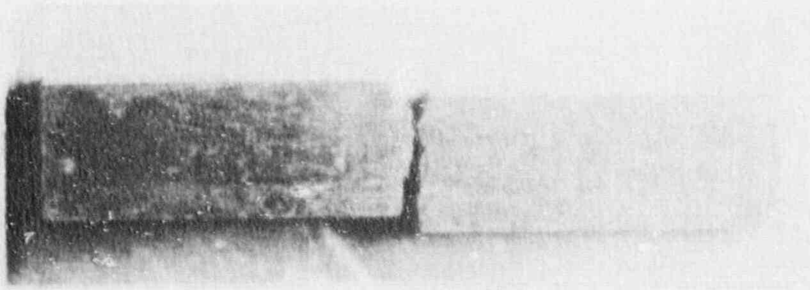

Side 1

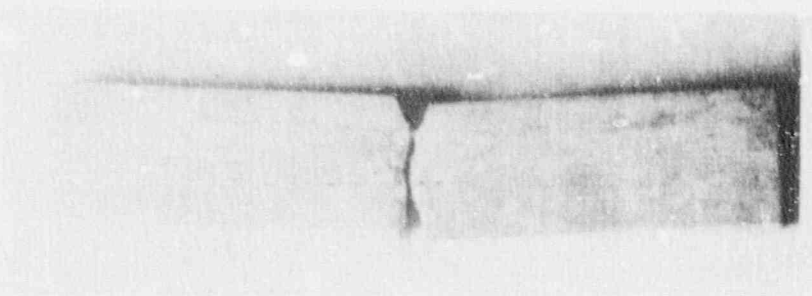

Side 2

Figure 5-10. Fracture Appearance of Specimen FL4

Fracture of Charpy Specimen FH1

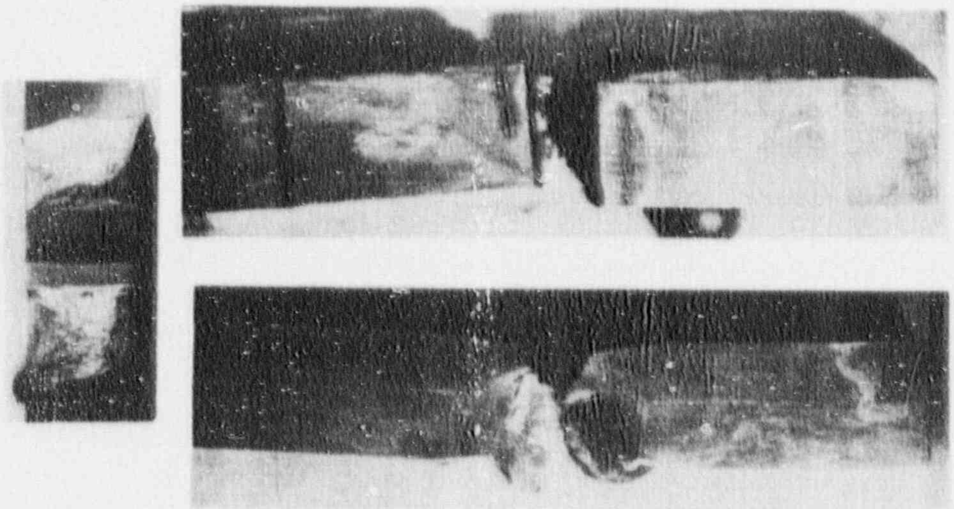

Fracture of Charpy Specimen FH2

Figure 5-11. Fracture Paths in Heat-Affected-Zone Charpy Specimens FH1 and FH2

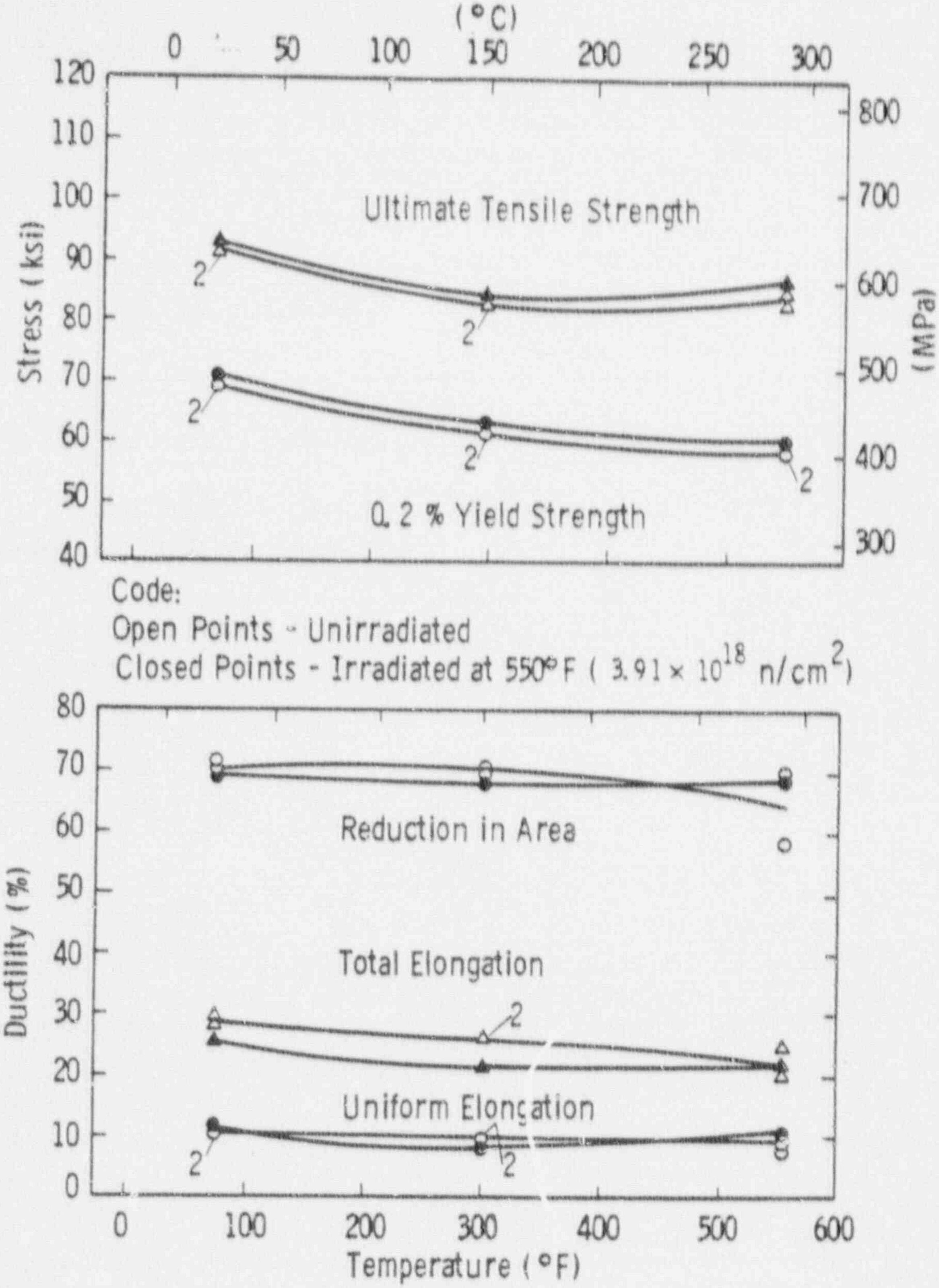

Figure 5-12. Tensile Properties for Braidwood Unit 2 Reactor Vessel Shell Forging 50D102-1/50C97-1 (Tangential Orientation)

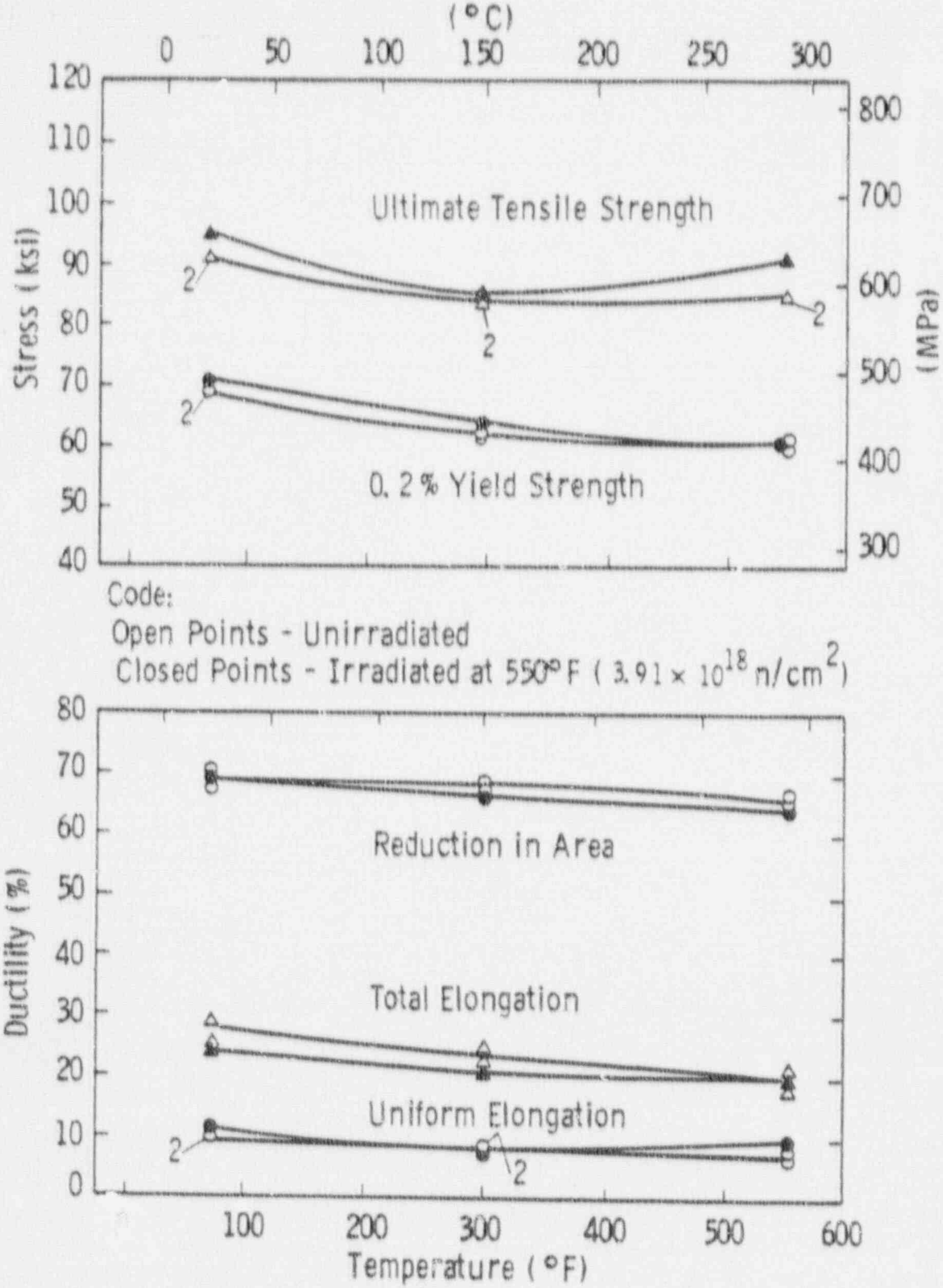

Figure 5-13. Tensile Properties for Braidwood Unit 2 Reactor Vessel Shell Forging 50D102-1/50C97-1 (Axial Orientation)

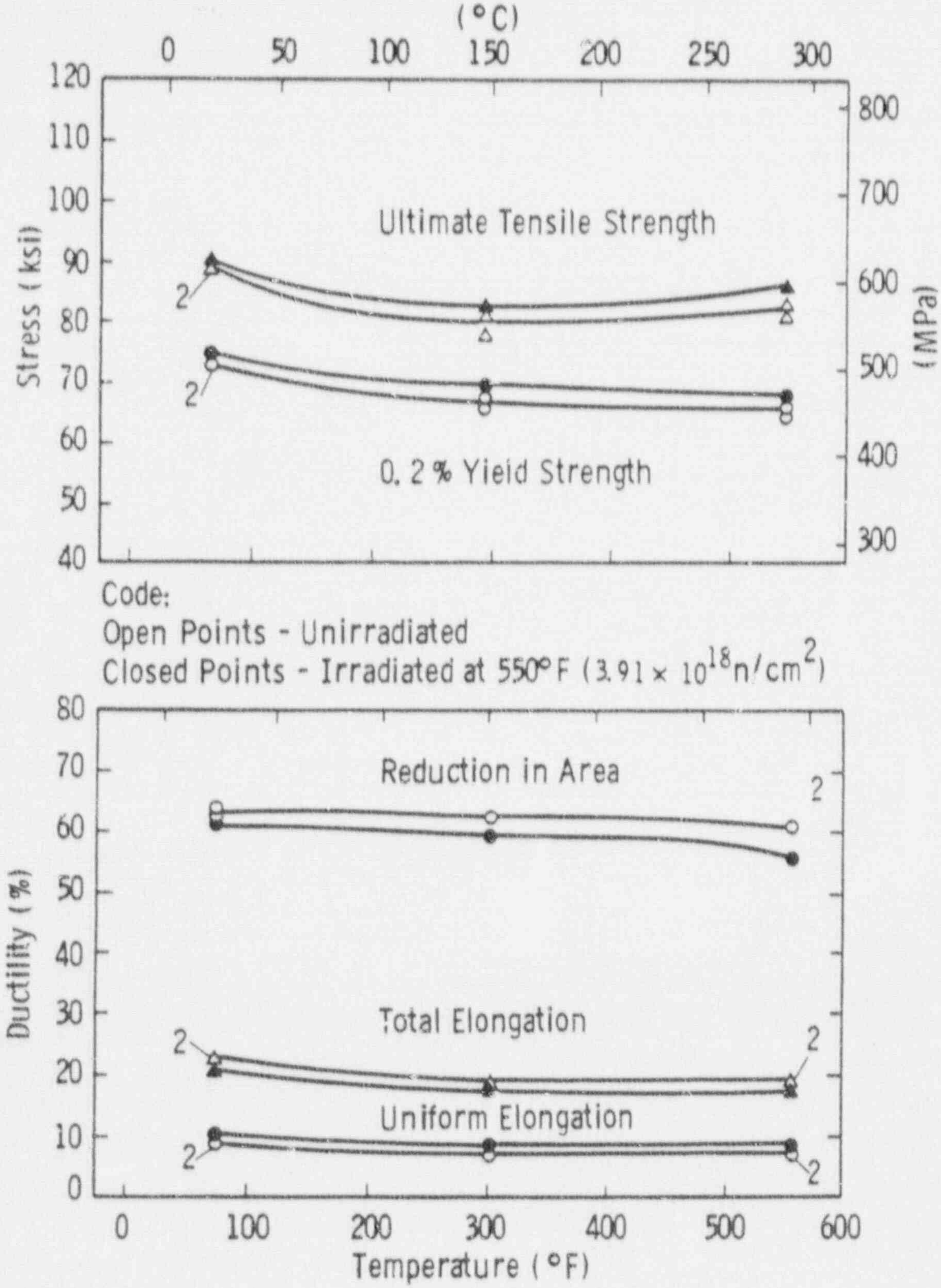

Figure 5-14. Tensile Properties for Braidwood Unit 2 Reactor Vessel Weld Metal

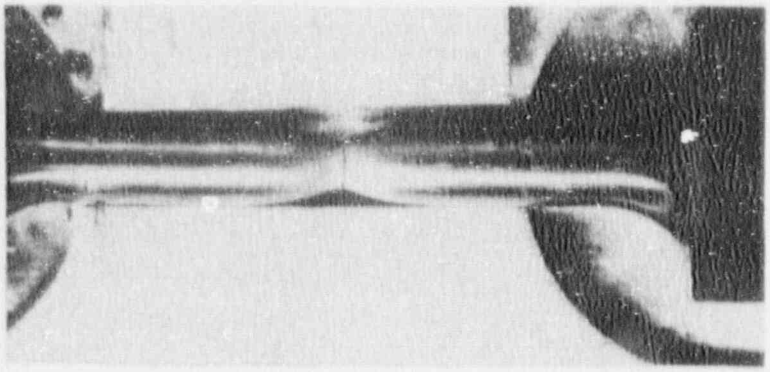

Specimen FL1 75°F

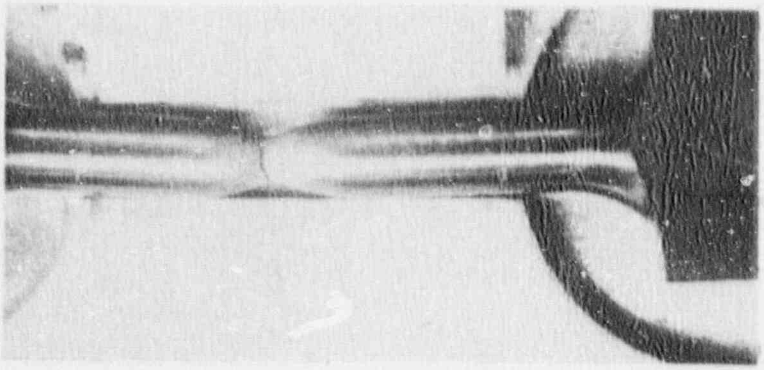

Specimen FL2 300°F

Specimen FL3 550°F

Figure 5-15. Fractured Tensile Specimens from Braidwood Unit 2 Reactor Vessel Shell Forging 50D102-1/50C97-1 (Tangential Orientation)

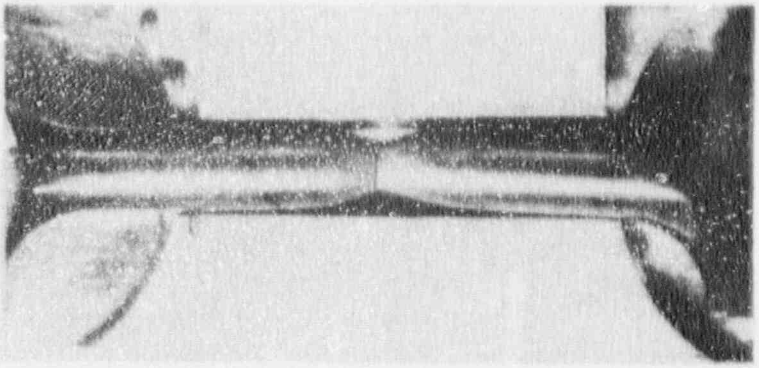

Specimen FT1 75°F

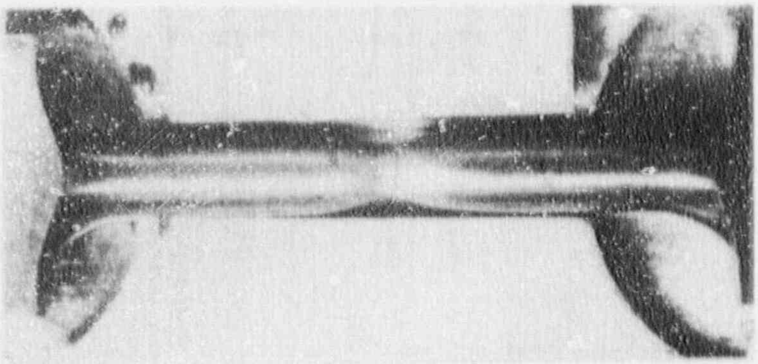

Specimen FT2 300°F

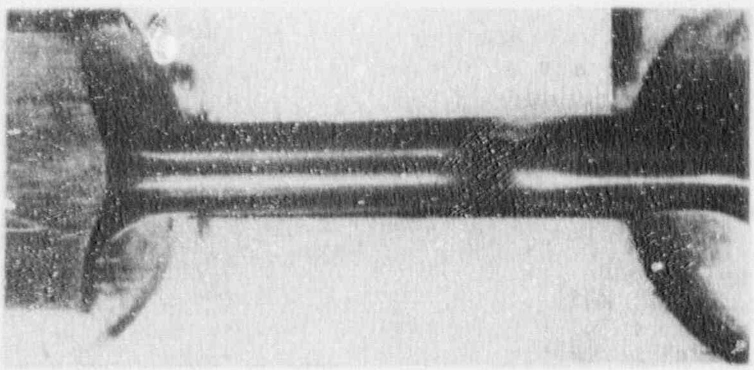

Specimen FT3 550°F

Figure 5-16. Fractured Tensile Specimens from Braidwood Unit 2 Reactor Vessel Shell Forging 50D102-1/50C97-1 (Axial Orientation)

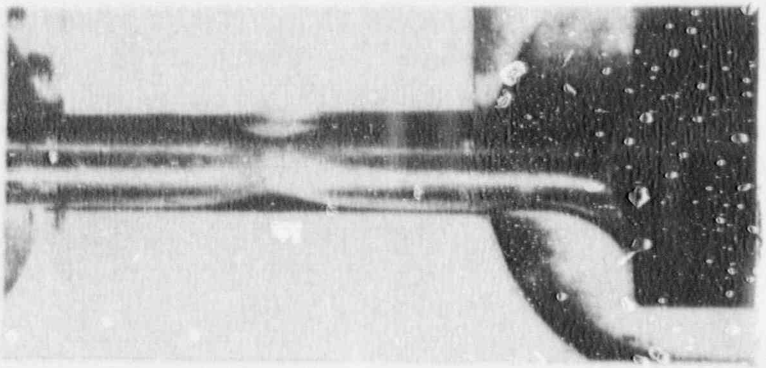

Specimen FW1 75°F

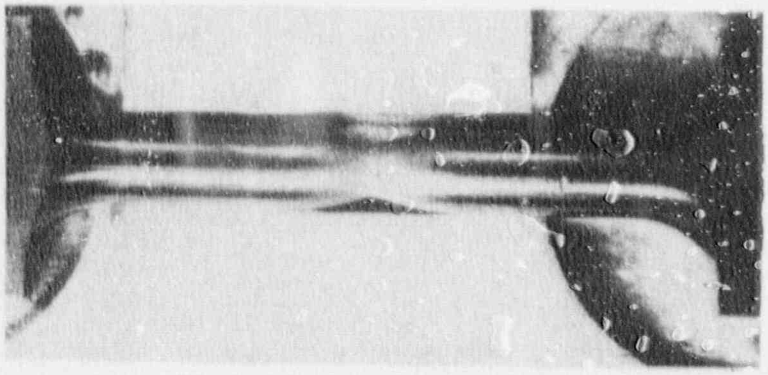

Specimen FW2 300°F

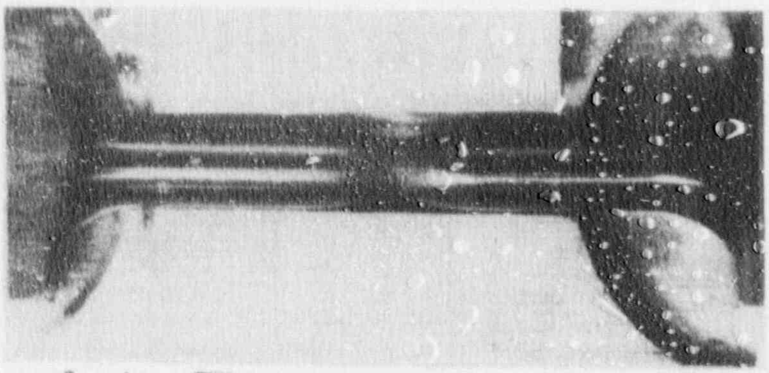

Specimen FW3 550°F

Figure 5-17. Fractured Tensile Specimens from Braidwood Unit 2 Reactor Vessel Weld Metal

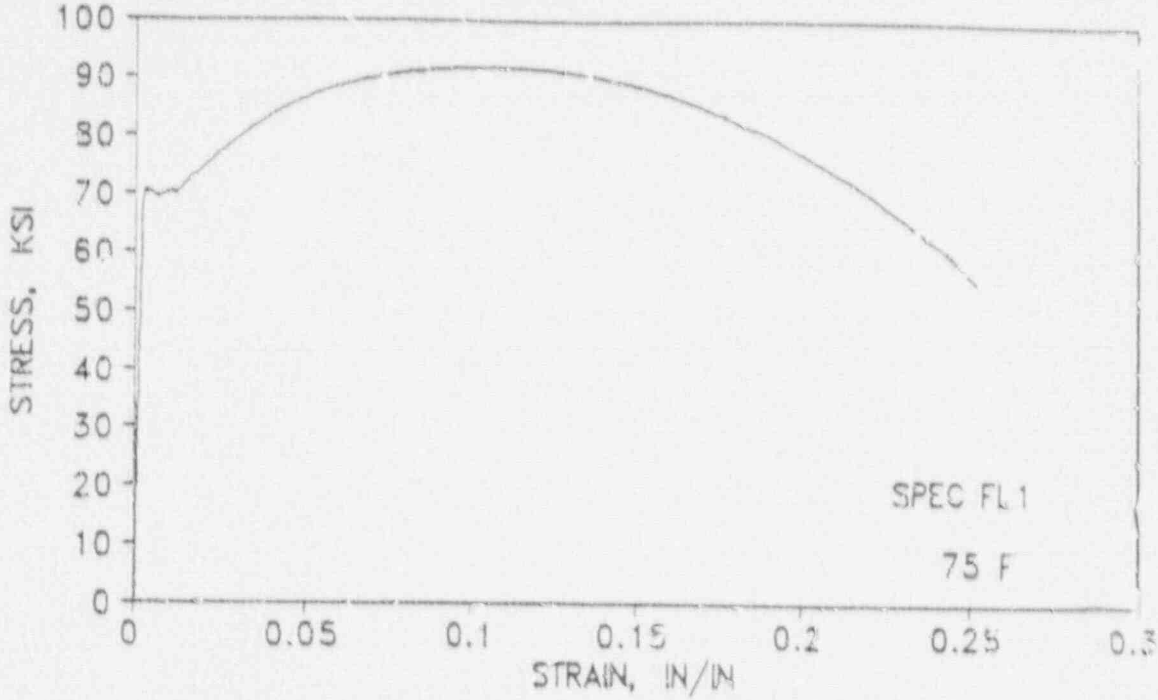

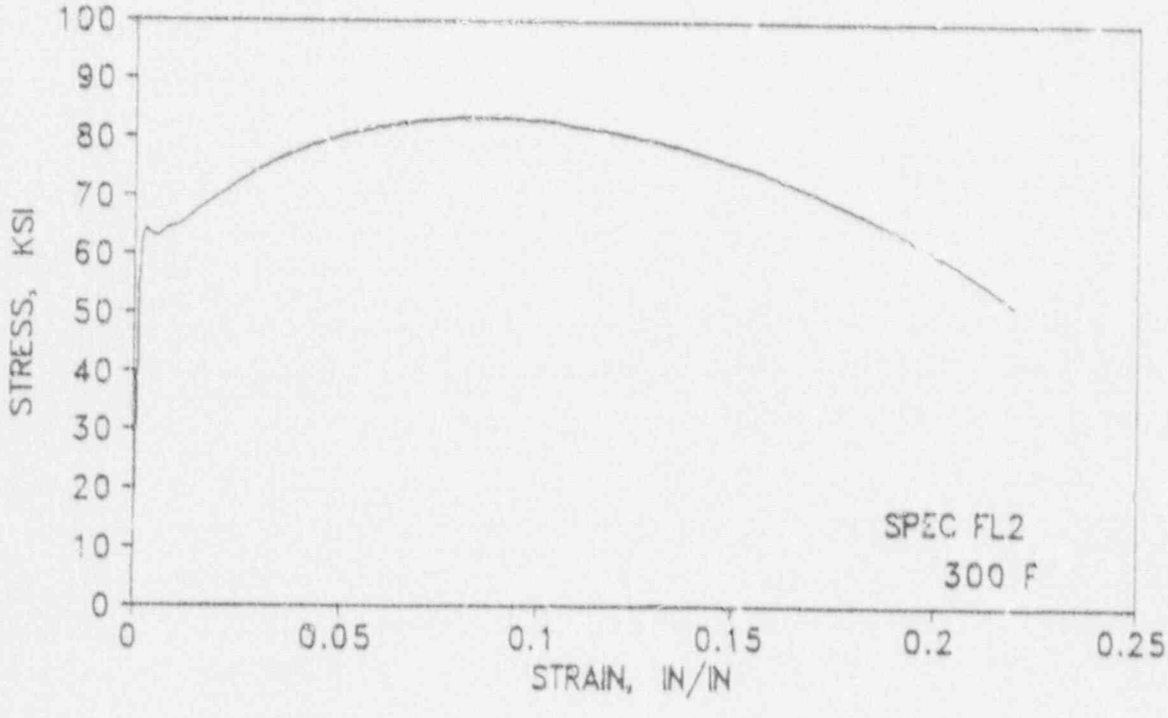

Figure 5-18. Stress-Strain Curves for Tension Specimens FL1 and FL2

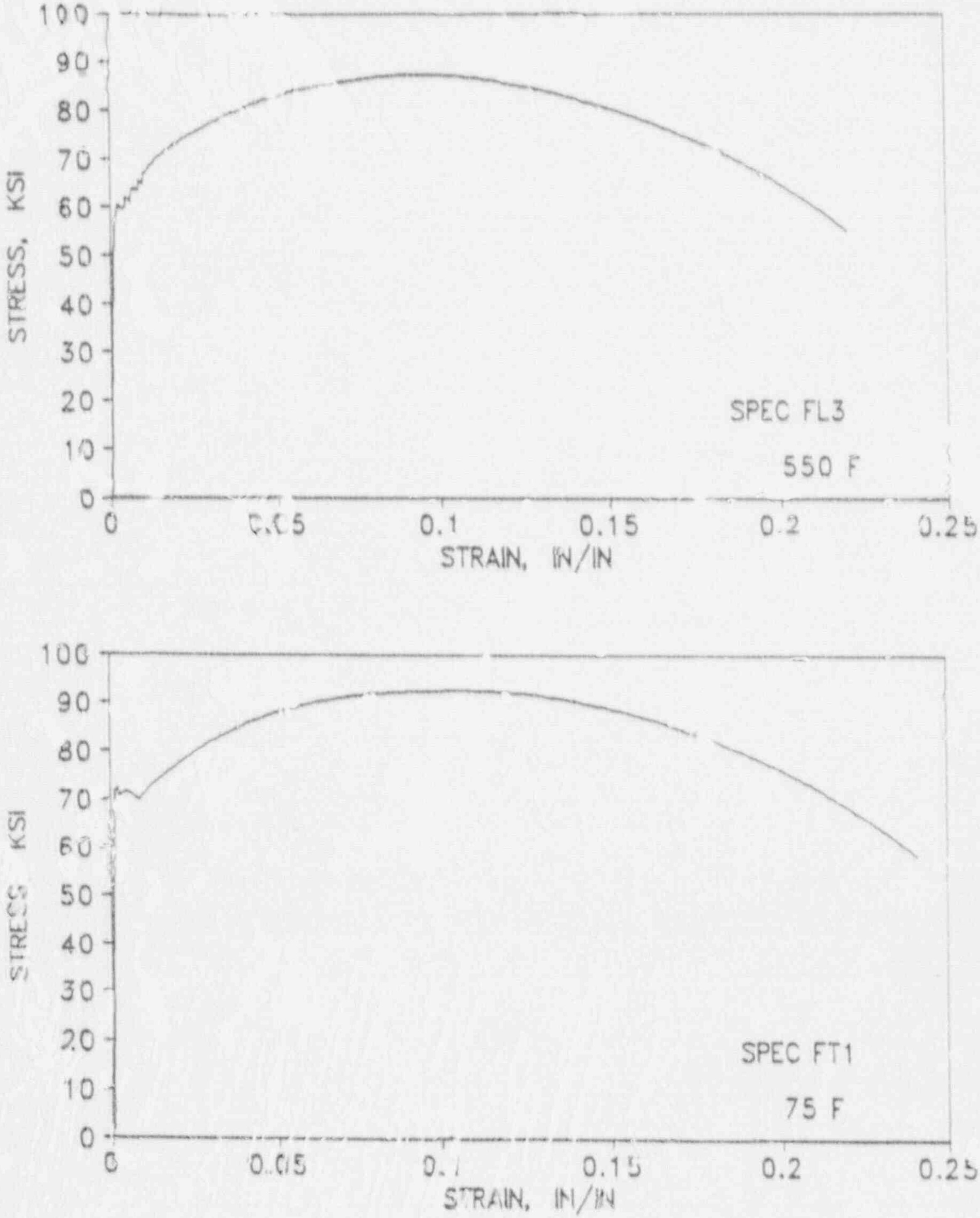

Figure 5-19. Stress-Strain curves for Tension Specimens FL3 and FT1

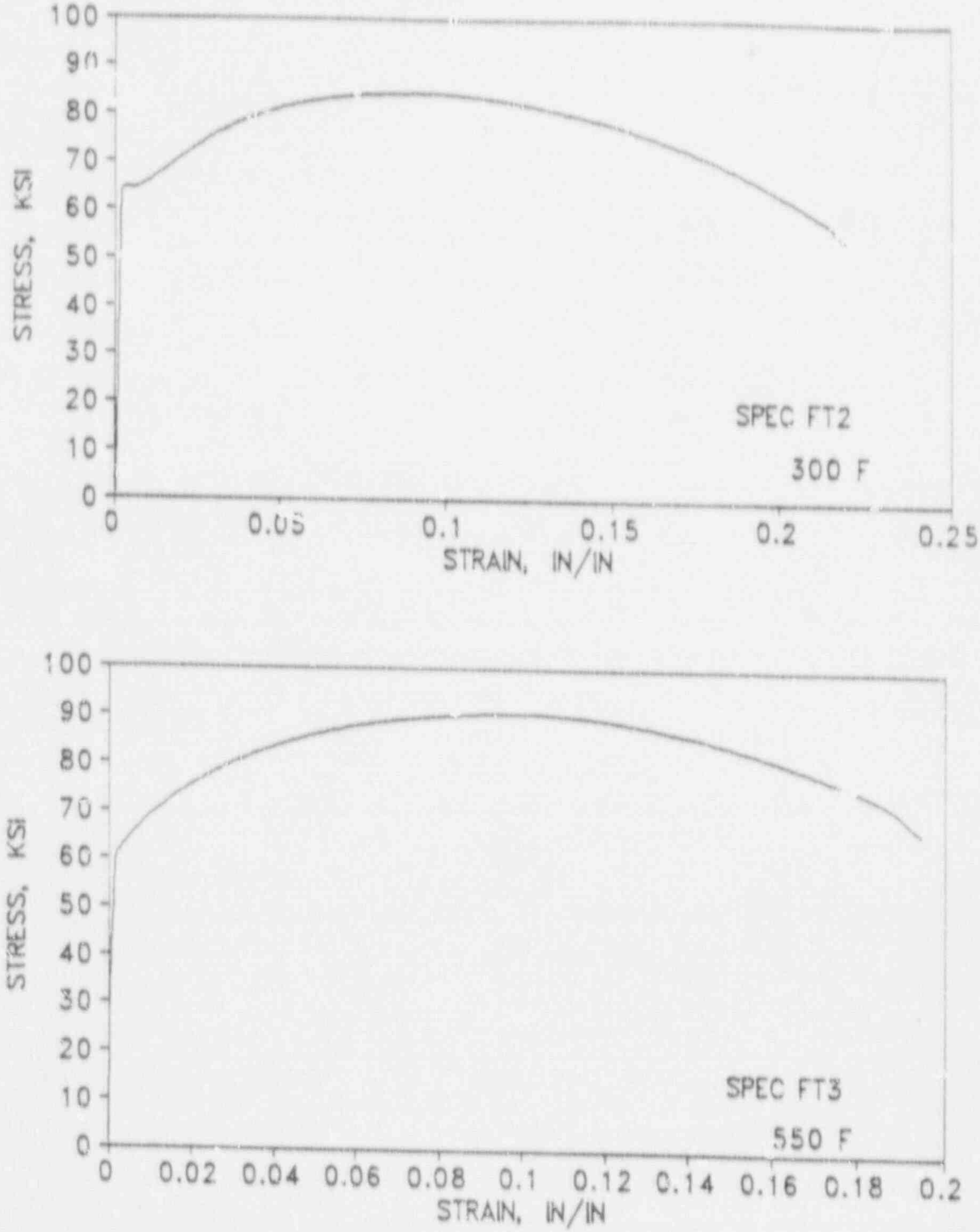

Figure 5-20. Stress-Strain Curves for Tension Specimens FT2 and FT3

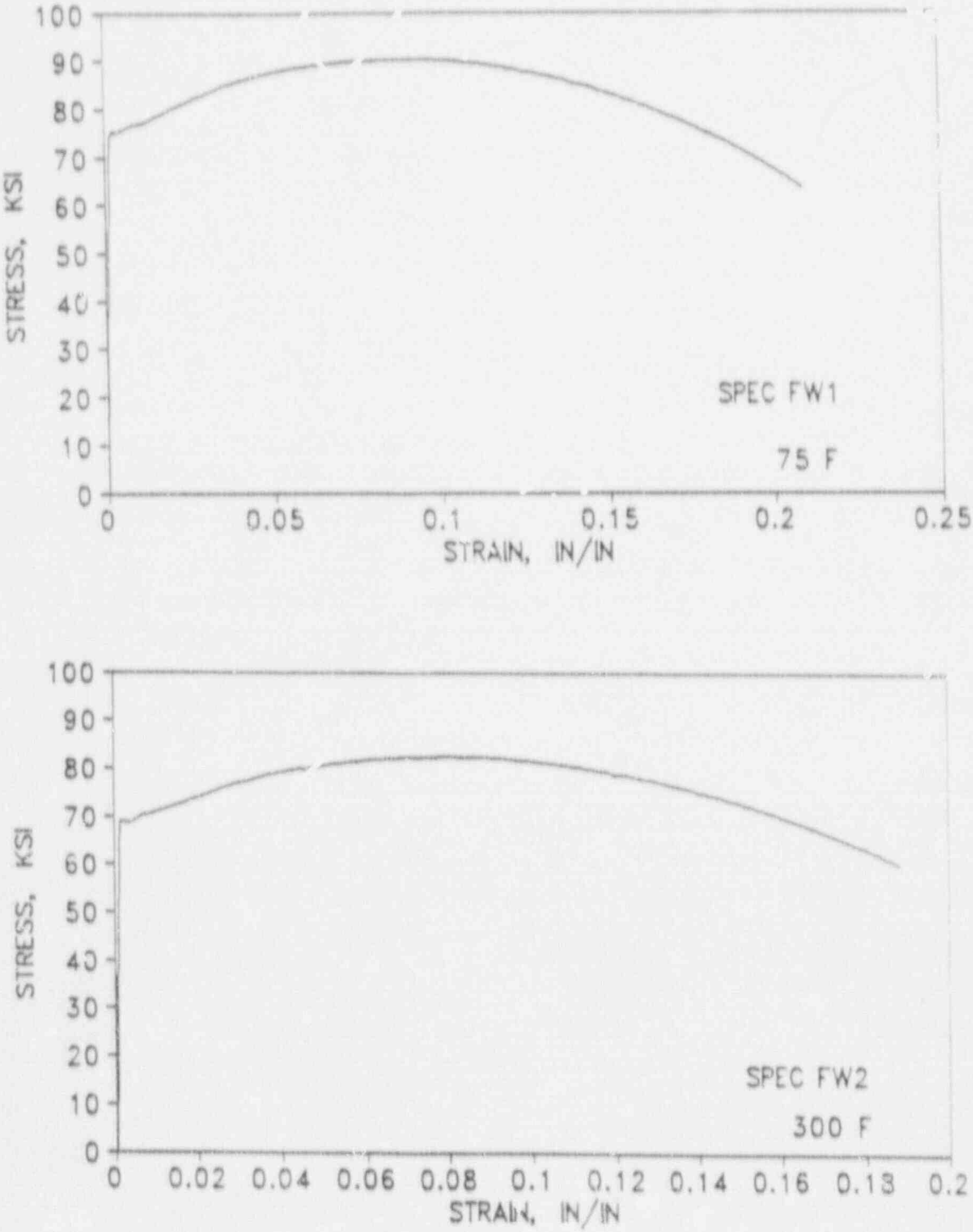

Figure 5-21. Stress-Strain Curves for Tension Specimens FW1 and FW2

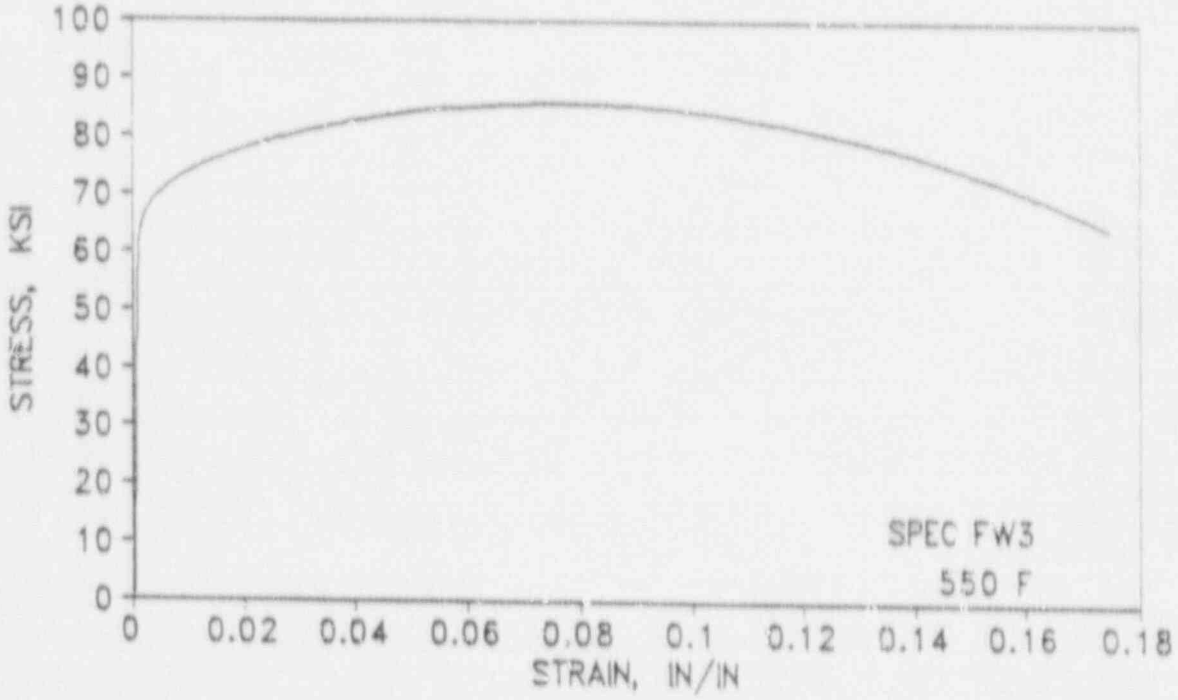

Figure 5-22. Stress-Strain Curve for Tension Specimen FW3

SECTION 6.0

RADIATION ANALYSIS AND NEUTRON DOSIMETRY

6.1 Introduction

Knowledge of the neutron environment within the reactor pressure vessel and surveillance capsule geometry is required as an integral part of LWR reactor pressure vessel surveillance programs for two reasons. First, in order to interpret the neutron radiation-induced material property changes observed in the test specimens, the neutron environment (energy spectrum, flux, fluence) to which the test specimens were exposed must be known. Second, in order to relate the changes observed in the test specimens to the present and future condition of the reactor vessel, a relationship must be established between the neutron environment at various positions within the reactor vessel and that experienced by the test specimens. The former requirement is normally met by employing a combination of rigorous analytical techniques and measurements obtained with passive neutron flux monitors contained in each of the surveillance capsules. The latter information is derived solely from analysis.

The use of fast neutron fluence (E > 1.0 MeV) to correlate measured materials properties changes to the neutron exposure of the material for light water reactor applications has traditionally been accepted for development of damage trend curves as well as for the implementation of trend curve data to assess vessel condition. In recent years, however, it has been suggested that an exposure model that accounts for differences in neutron energy spectra between surveillance capsule locations and positions within the vessel wall could lead to an improvement in the uncertainties associated with damage trend curves as well as to a more accurate evaluation of damage gradients through the pressure vessel wall.

Because of this potential shift away from a threshold fluence toward an energy dependent damage function for data correlation, ASTM Standard Practice E853, "Analysis and Interpretation of Light Water Reactor Surveillance Results," recommends reporting displacements per iron atom (dpa) along with fluence (E > 1.0 MeV) to provide a data base for future reference. The energy dependent dpa function to be used for this evaluation is specified in ASTM Standard Practice E693, "Characterizing Neutron Exposures in Ferritic Steels in Terms of Displacements per Atom." The application of the dpa parameter to the assessment of embrittlement gradients through the thickness of the pressure vessel wall has already been promulgated in Revision 2 to the Regulatory Guide 1.99, "Radiation Embrittlement of Reactor Vessel Materials."

This section provides the results of the neutron dosimetry evaluations performed in conjunction with the analysis of test specimens contained in surveillance capsule U. Fast neutron exposure parameters in terms of fast neutron fluence (E > 1.0 MeV), fast neutron fluence (E > 0.1 MeV), and iron atom displacements (dpa) are established for the capsule irradiation history. The analytical formalism relating the measured capsule exposure to the exposure of the vessel wall is described and used to project the integrated exposure of the vessel itself. Also uncertainties associated with the derived exposure parameters at the surveillance capsule and with the projected exposure of the pressure vessel are provided.

6.2 Discrete Ordinates Analysis

A plan view of the reactor geometry at the core midplane is shown in Figure 4-1. Six irradiation capsules attached to the neutron pads are included in the reactor design to constitute the reactor vessel surveillance program. The capsules are located at azimuthal angles of 58.5, 61.0, 121.5, 238.5, 241.0, and 301.5° relative to the core cardinal axes as shown in Figure 4-1.

A plan view of a dual surveillance capsule holder attached to the neutron pad is shown in Figure 6-1. The stainless steel specimen containers are 1.182 by 1-inch and approximately 56 inches in height. The containers are positioned axially such that the specimens are centered on the core midplane, thus spanning the central 5 feet of the 12-foot high reactor core.

From a neutron transport standpoint, the surveillance capsule structures are significant. They have a marked effect on both the distribution of neutron flux and the neutron energy spectrum in the water annulus between the neutron pad and the reactor vessel. In order to properly determine the neutron environment at the test specimen locations, the capsules themselves must be included in the analytical model.

In performing the fast neutron exposure evaluations for the surveillance capsules and reactor vessel, two distinct sets of transport calculations were carried out. The first, a single computation in the conventional forward mode, was used primarily to obtain relative neutron energy distributions throughout the reactor geometry as well as to establish relative radial distributions of exposure parameters (ϕ(E > 1.0 MeV), ϕ(E > 0.1 MeV), and dpa) through the vessel wall. The neutron spectral information was required for the interpretation of neutron dosimetry withdrawn from the surveillance capsule as well as for the determination of exposure parameter ratios; i.e., dpa/ϕ(E > 1.0 MeV), within the pressure vessel geometry. The relative radial gradient information was required to permit the projection of measured exposure parameters to locations interior to the pressure vessel wall; i.e., the 1/4T, 1/2T, and 3/4T locations.

The second set of calculations consisted of a series of adjoint analyses relating the fast neutron flux (E > 1.0 MeV) at surveillance capsule positions, and several azimuthal locations on the pressure vessel inner radius to neutron source distributions within the reactor core. The importance functions generated from these adjoint analyses provided the basis for all absolute exposure projections and comparison with measurement. These importance functions, when combined with cycle specific neutron source distributions, yielded absolute predictions of neutron exposure at the locations of interest for the cycle 1 irradiation; and established the means to perform similar predictions and dosimetry evaluations for all subsequent fuel cycles. It is important to note that the cycle specific neutron source distributions utilized in these analyses included not only spatial variations of fission rates within the reactor core; but, also accounted for the effects of varying neutron yield per fission and fission spectrum introduced by the build-up of plutonium as the burnup of individual fuel assemblies increased.

The absolute cycle specific data from the adjoint evaluations together with relative neutron energy spectra and radial distribution information from the forward calculation provided the means to:

1. Evaluate neutron dosimetry obtained from surveillance capsule locations.

2. Extrapolate dosimetry results to key locations at the inner radius and through the thickness of the pressure vessel wall.

3. Enable a direct comparison of analytical prediction with measurement.

4. Establish a mechanism for projection of pressure vessel exposure as the design of each new fuel cycle evolves.

The forward transport calculation for the reactor model summarized in Figures 4-1 and 6-1 was carried out in R, θ geometry using the DOT two-dimensional discrete ordinates code[12] and the SAILOR cross-section library[13]. The SAILOR library is a 47 group ENDFB-IV based data set produced specifically for light water reactor applications. In these analyses anisotropic scattering was treated with a P_3 expansion of the cross-sections and the angular discretization was modeled with an S_8 order of angular quadrature.

The reference core power distribution utilized in the forward analysis was derived from statistical studies of long-term operation of Westinghouse 4-loop plants. Inherent in the development of this reference core power distribution is the use of an out-in fuel management strategy; i.e., fresh fuel on the core periphery. Furthermore, for the peripheral fuel assemblies, a 2σ uncertainty derived from the statistical evaluation of plant to plant and cycle to cycle variations in peripheral power was used. Since it is unlikely that a single reactor would have a power distribution at the nominal $+2\sigma$

level for a large number of fuel cycles, the use of this reference distribution is expected to yield somewhat conservative results.

All adjoint analyses were also carried out using an S_8 order of angular quadrature and the P_3 cross-section approximation from the SAILOR library. Adjoint source locations were chosen at several azimuthal locations along the pressure vessel inner radius as well as the geometric center of each surveillance capsule. Again, these calculations were run in R, θ geometry to provide neutron source distribution importance functions for the exposure parameter of interest; in this case, ϕ (E > 1.0 MeV). Having the importance functions and appropriate core source distributions, the response of interest could be calculated as:

$$R\ (r, \theta) = \int_r \int_\theta \int_E I(r, \theta, E)\ S\ (r, \theta, E)\ r\ dr\ d\theta\ dE$$

where: $R\ (r, \theta)$ = ϕ (E > 1.0 MeV) at radius r and azimuthal angle θ

$I\ (r, \theta, E)$ = Adjoint importance function at radius, r, azimuthal angle θ, and neutron source energy E.

$S\ (r, \theta, E)$ = Neutron source strength at core location r, θ and energy E.

Although the adjoint importance functions used in the Braidwood Unit 2 analysis were based on a response function defined by the threshold neutron flux (E > 1.0 MeV), prior calculations have shown that, while the implementation of low leakage loading patterns significantly impact the magnitude and the spatial distribution of the neutron field, changes in the relative neutron energy spectrum are of second order. Thus, for a given location the ratio of dpa/ϕ (E > 1.0 MeV) is insensitive to changing core source distributions. In the application of these adjoint important functions to the Braidwood Unit 2 reactor, therefore, the iron displacement rates (dpa) and the neutron flux (E > 0.1 MeV) were computed on a cycle specific basis by using dpa/ϕ (E > 1.0 MeV) and ϕ (E > 0.1 MeV)/ϕ (E > 1.0 MeV) ratios from the forward analysis in conjunction with the cycle specific ϕ (E > 1.0 MeV) solutions from the individual adjoint evaluations.

The reactor core power distribution used in the plant specific adjoint calculations was taken from the fuel cycle design report for the first operating cycle of Braidwood Unit 2[14]. The relative power levels in fuel assemblies that are significant contributors to the neutron exposure of the pressure vessel and surveillance capsules are summarized in Figure 6-2. For comparison purposes, the core power distribution (design basis) used in the reference forward calculation is also illustrated in Figure 6-2.

Selected results from the neutron transport analyses performed for the Braidwood Unit 2 reactor are provided in Tables 6-1 through 6-5. The data listed in these tables establish the means for absolute comparisons of analysis and measurement for the capsule irradiation period and provide the means to correlate dosimetry results with the corresponding neutron exposure of the pressure vessel wall.

In Table 6-1, the calculated exposure parameters [ϕ (E > 1.0 MeV), ϕ(E > 0.1 MeV), and dpa] are given at the geometric center of the two surveillance capsule positions for both the design basis and the plant specific core power distributions. The plant specific data, based on the adjoint transport analysis, are meant to establish the absolute comparison of measurement with analysis. The design basis data derived from the forward calculation are provided as a point of reference against which plant specific fluence evaluations can be compared. Similar data is given in Table 6-2 for the pressure vessel inner radius. Again, the three pertinent exposure parameters are listed for both the design basis and the cycle 1 plant specific power distribution. It is important to note that the data for the vessel inner radius were taken at the clad/base metal interface; and, thus, represent the maximum exposure levels of the vessel wall itself.

Radial gradient information for neutron flux (E > 1.0 MeV), neutron flux (E > 0.1 MeV), and iron atom displacement rate is given in Tables 6-3, 6-4, and 6-5, respectively. The data, obtained from the forward neutron transport calculation, are presented on a relative basis for each exposure parameter at several azimuthal locations. Exposure parameter distributions within the wall may be obtained by normalizing the calculated or projected exposure at the vessel inner radius to the gradient data given in Tables 6-3 through 6-5.

For example, the neutron flux (E > 1.0 MeV) at the 1/4T position on the 45° azimuth is given by:

$$\phi_{1/4T}(45^\circ) = \phi(220.27,\ 45^\circ)\ F\ (225.75,\ 45^\circ)$$

where: $\phi_{1/4T}(45^\circ)$ = Projected neutron flux at the 1/4T position on the 45° azimuth

ϕ (220.27,45°) = Projected or calculated neutron flux at the vessel inner radius on the 45° azimuth.

F (225.75, 45°) = Relative radial distribution function from Table 6-3.

Similar expressions apply for exposure parameters in terms of ϕ (E > 0.1 MeV) and dpa/sec.

The DOT calculations were carried out for a typical octant of the reactor. However, for the neutron pad arrangement in Braidwood Unit 2, the pad extent for all octants is not the same. For the analysis of the flux to the pressure vessel, an octant was chosen with the neutron pad extending from 32.5 - 45.0 degrees which produces the maximum vessel flux. Other octants have neutron pads spanning larger azimuthal sectors which provide more shielding. For the octant with the 12.5 degree pad, the maximum flux to the vessel occurs near 25 degrees and the values in the tables for the 25 degree angle are vessel maximum values. Exposure values for 0, 15, and 45 can be used for all octants; values in the tables for 25 and 35 degrees are maximum values and only apply to octants with a 12.5 degree neutron pad.

6.3 Neutron Dosimetry

The passive neutron sensors included in the Braidwood Unit 2 surveillance program are listed in Table 6-6. Also given in Table 6-6 are the primary nuclear reactions and associated nuclear constants that were used in the evaluation of the neutron energy spectrum within the capsule and the subsequent determination of the various exposure parameters of interest [ϕ (E > 1.0 MeV), ϕ (E > 0.1 MeV), dpa].

The relative locations of the neutron sensors within the capsules are shown in Figure 4-2. The iron, nickel, copper, and cobalt-aluminum monitors, in wire form, were placed in holes drilled in spacers at several axial levels within the capsules. The cadmium-shielded neptunium and uranium fission monitors were accommodated within the dosimeter block located near the center of the capsule.

The use of passive monitors such as those listed in Table 6-6 does not yield a direct measure of the energy dependent flux level at the point of interest. Rather, the activation or fission process is a measure of the integrated effect that the time- and energy-dependent neutron flux has on the target material over the course of the irradiation period. An accurate assessment of the average neutron flux level incident on the various monitors may be derived from the activation measurements only if the irradiation parameters are well known. In particular, the following variables are of interest:

- The specific activity of each monitor.
- The operating history of the reactor.
- The energy response of the monitor.
- The neutron energy spectrum at the monitor location.
- The physical characteristics of the monitor.

The specific activity of each of the neutron monitors was determined using established ASTM procedures [15 through 28]. Following sample preparation and weighing, the activity of each monitor was determined by means of a lithium-drifted germanium, Ge(Li), gamma spectrometer. The irradiation history of the Braidwood Unit 2 reactor during cycle 1 was obtained from NUREG-0020, "Licensed Operating Reactors Status Summary Report" for the applicable period.

The irradiation history applicable to capsule U is given in Table 6-7. Measured and saturated reaction product specific activities as well as measured full power reaction rates are listed in Table 6-8. Reaction rate values were derived using the pertinent data from Tables 6-6 and 6-7.

Values of key fast neutron exposure parameters were derived from the measured reaction rates using the FERRET least squares adjustment code [29]. The FERRET approach used the measured reaction rate data and the calculated neutron energy spectrum at the the center of the surveillance capsule as input and proceeded to adjust a priori (calculated) group fluxes to produce a best fit (in a least squares sense) to the reaction rate data. The exposure parameters along with associated uncertainties where then obtained from the adjusted spectra.

In the FERRET evaluations, a log normal least-squares algorithm weights both the a priori values and the measured data in accordance with the assigned uncertainties and correlations. In general, the measured values f are linearly related to the flux ϕ by some response matrix A:

$$f^{(s,\alpha)} = \sum_g A_{ig}^{(s)} \phi_g^{(\alpha)}$$

where i indexes the measured values belonging to a single data set s, g designates the energy group and a delineates spectra that may be simultaneously adjusted. For example,

$$R_i = \sum_g \sigma_{ig} \phi_g$$

relates a set of measured reaction rates R_i to a single spectrum ϕ_g by the multigroup cross section σ_{ig}. In this case, FERRET also adjusts the cross-sections. The lognormal approach automatically accounts for the physical constraint of positive fluxes, even with the large assigned uncertainties.

In the FERRET analysis of the dosimetry data, the continuous quantities (i.e., fluxes and cross-sections) were approximated in 53 groups. The calculated fluxes from the discrete ordinates analysis were expanded into the FERRET group structure using the SAND-II code [30]. This procedure was carried out by first expanding the a priori spectrum into the SAND-II 620 group structure using a SPLINE interpolation procedure for interpolation in regions where group boundaries do not coincide. The 620-point spectrum was then easily collapsed to the group scheme used in FERRET.

The cross-sections were also collapsed into the 53 energy-group structure using SAND II with calculated spectra (as expanded to 620 groups) as weighting functions. The cross sections were taken from the ENDF/B-V dosimetry file. Uncertainty estimates and 53 x 53 covariance matrices were constructed for each cross section. Correlations between cross sections were neglected due to data and code limitations, but are expected to be unimportant.

For each set of data or a priori values, the inverse of the corresponding relative covariance matrix M is used as a statistical weight. In some cases, as for the cross sections, a multigroup covariance matrix is used. More often, a simple parameterized form is used:

$$M_{gg'} = R_N^2 + R_g R_{g'} P_{gg'}$$

where R_N specifies an overall fractional normalization uncertainty (i.e., complete correlation) for the corresponding set of values. The fractional uncertainties R_g specify additional random uncertainties for group g that are correlated with a correlation matrix:

$$P_{gg'} = (1 - \theta)\, \delta_{gg'} + \theta \exp \left[\frac{-(g-g')^2}{2\partial^2}\right]$$

The first term specifies purely random uncertainties while the second term describes short-range correlations over a range ϑ (θ specifies the strength of the latter term).

For the a priori calculated fluxes, a short-range correlation of $\vartheta = 6$ groups was used. This choice implies that neighboring groups are strongly correlated when r is close to 1. Strong long-range correlations (or anticorrelations) were justified based on information presented by R.E. Maerker[31]. Maerker's results are closely duplicated when $\vartheta = 6$. For the integral reaction rate covariances, simple normalization and random uncertainties were combined as deduced from experimental uncertainties.

Results of the FERRET evaluation of the capsule U dosimetry are given in Table 6-9. The data summarized in Table 6-9 indicated that the capsule received an integrated exposure of 3.91×10^{18} n/cm^2 (E > 1.0 MeV) with an associated uncertainty of $\pm$ 8%. Also reported are capsule exposures in terms of fluence (E > 0.1 MeV) and iron atom displacements (dpa). Summaries of the fit of the adjusted spectrum are provided in Table 6-10. In general, excellent results were achieved in the fits of the adjusted spectrum to the individual experimental reaction rates. The adjusted spectrum itself is tabulated in Table 6-11 for the FERRET 53 energy group structure.

A summary of the measured and calculated neutron exposure of capsule U is presented in Table 6-12. The agreement between calculation and measurement falls within $\pm$ 12% for all fast neutron exposure parameters listed. The thermal neutron exposure calculated for cycle 1 underpredicted the measured value by 59 percent.

Neutron exposure projections at key locations on the pressure vessel inner radius are given in Table 6-13. Along with the current (1.15 EFPY) exposure derived from the capsule U measurements, projections are also provided for an exposure period of 16 EFPY and to end of vessel design life (32 EFPY). The calculated design basis exposure rates given in Table 6-2 were used to perform projections beyond the end of cycle 1.

In the calculation of exposure gradients for the Braidwood Unit 2 reactor coolant system, exposure projections to 16 EFPY and 32 EFPY were employed. Data based on both a fluence (E > 1.0 MeV) slope and a plant specific dpa slope through the vessel wall are provided in Table 6-14. In order to access RT_{NDT} vs. fluence trend curves, dpa equivalent fast neutron fluence levels for the 1/4T and 3/4T positions were defined by the relations

$$\phi' \text{ (1/4T)} = \phi \text{ (Surface) } \left(\frac{\text{dpa (1/4T)}}{\text{dpa (Surface)}}\right)$$

$$\phi' \text{ (3/4T)} = \phi \text{ (Surface) } \left(\frac{\text{dpa (3/4T)}}{\text{dpa (Surface)}}\right)$$

Using this approach results in the dpa equivalent fluence values listed in Table 6-14.

In Table 6-15 updated lead factors are listed for each of the Braidwood Unit 2 surveillance capsules. These data may be used as a guide in establishing future withdrawal schedules for the remaining capsules.

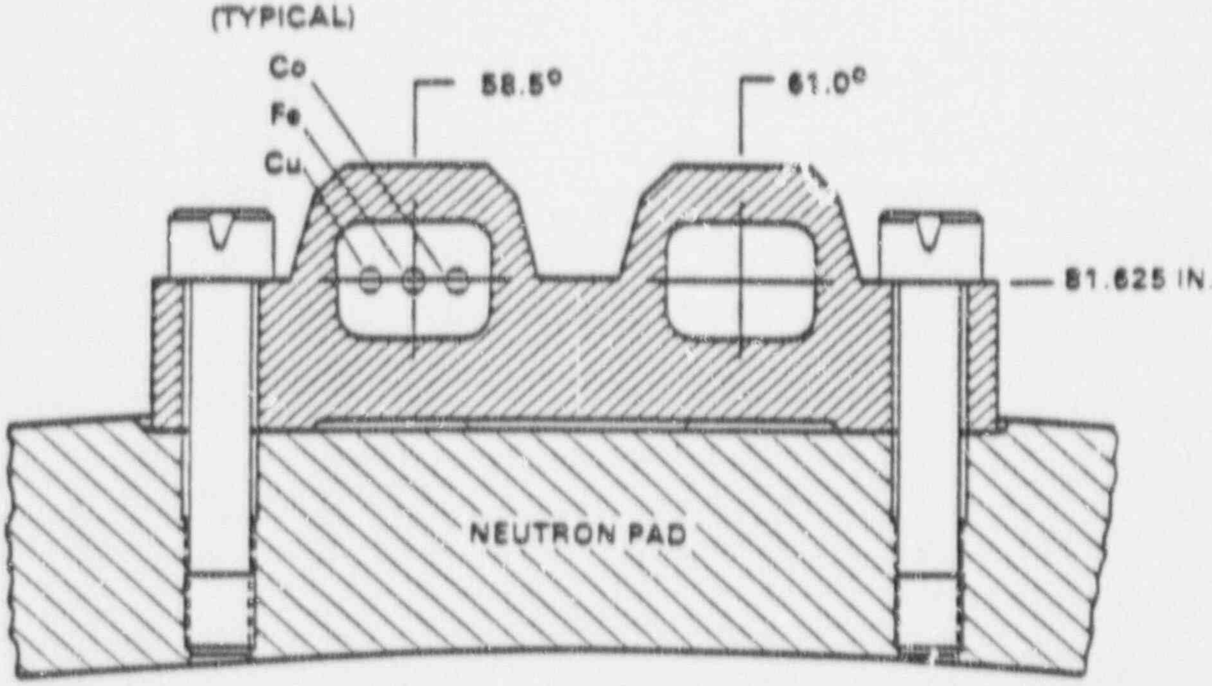

Figure 6-1. Plan View of a Dual Reactor Vessel Surveillance Capsule

0.74 1.01	0.70 1.04	0.76 0.96	0.59 0.77	Cycle 1 Design Basis	
0.99 1.02	1.02 1.10	0.97 1.00	0.95 1.05	0.84 1.10	0.57 0.71
1.13 1.05	1.09 0.87	1.07 0.87	1.05 1.07	0.98 1.00	1.01 1.05
1.14 1.09	1.13 1.06	1.13 0.88	1.14 1.10	1.08 1.04	
1.18 0.90	1.14 1.04	1.14 1.12	1.20 0.92		

Figure 6-2. Core Power Distributions Used in Transport Calculations for Braidwood Unit 2

TABLE 6-1

CALCULATED FAST NEUTRON EXPOSURE PARAMETERS
AT THE SURVEILLANCE CAPSULE CENTER

	DESIGN BASIS		CYCLE 1	
	29.0°	31.5°	29.0°	31.5°
ϕ (E > 1.0 MeV) (n/cm^2-sec)	1.13×10^{11}	1.21×10^{11}	8.84×10^{10}	9.51×10^{10}
ϕ (E > 0.1 MeV) (n/cm^2-sec)	5.07×10^{11}	5.44×10^{11}	3.97×10^{11}	4.28×10^{11}
dpa/sec	2.21×10^{-10}	2.37×10^{-10}	1.73×10^{-10}	1.86×10^{-10}

TABLE 6-2

CALCULATED FAST NEUTRON EXPOSURE PARAMETERS AT
THE PRESSURE VESSEL CLAD/BASE METAL INTERFACE

DESIGN BASIS

	0°	15°	25°	35°	45°
ϕ(E > 1.0MeV) (n/cm^2-sec)	1.78×10^{10}	2.66×10^{10}	3.01×10^{10}	2.45×10^{10}	2.81×10^{10}
ϕ(E > 0.1MeV) (n/cm^2-sec)	3.70×10^{10}	5.60×10^{10}	8.22×10^{10}	6.96×10^{10}	7.04×10^{10}
dpa/sec	2.77×10^{-11}	4.12×10^{-11}	5.04×10^{-11}	4.15×10^{-11}	4.48×10^{-11}

CYCLE 1 SPECIFIC

	0°	15°	25°	35°	45°
ϕ(E > 1.0MeV) (n/cm^2-sec)	1.32×10^{10}	2.06×10^{10}	2.38×10^{10}	1.98×10^{10}	2.31×10^{10}
ϕ(E > 0.1MeV) (n/cm^2-sec)	2.74×10^{10}	4.34×10^{10}	6.50×10^{10}	5.62×10^{10}	5.79×10^{10}
dpa/sec	2.05×10^{-11}	3.19×10^{-11}	3.99×10^{-11}	3.35×10^{-11}	3.68×10^{-11}

TABLE 6-3

RELATIVE RADIAL DISTRIBUTIONS OF NEUTRON FLUX (E > 1.0 MeV)
WITHIN THE PRESSURE VESSEL WALL

Radius (cm)	0°	15°	25°	35°	45°
220.27[1]	1.00	1.00	1.00	1.00	1.00
220.64	0.976	0.979	0.980	0.977	0.979
221.66	0.888	0.891	0.893	0.891	0.889
222.99	0.768	0.770	0.772	0.770	0.766
224.31	0.653	0.653	0.657	0.655	0.648
225.63	0.551	0.550	0.554	0.552	0.543
226.95	0.462	0.460	0.465	0.463	0.452
228.28	0.386	0.384	0.388	0.386	0.375
229.60	0.321	0.319	0.324	0.321	0.311
230.92	0.267	0.265	0.271	0.267	0.257
232.25	0.221	0.219	0.223	0.221	0.211
233.57	0.183	0.181	0.185	0.183	0.174
234.89	0.151	0.149	0.153	0.151	0.142
236.22	0.124	0.122	0.126	0.124	0.116
237.54	0.102	0.100	0.104	0.102	0.0945
238.86	0.0823	0.0817	0.0846	0.0835	0.0762
240.19	0.0671	0.0660	0.0689	0.0679	0.0608
241.51	0.0538	0.0522	0.0550	0.0545	0.0471
242.17[2]	0.0506	0.0488	0.0518	0.0521	0.0438

NOTES: 1) Base Metal Inner Radius
2) Base Metal Outer Radius

TABLE 6-4

RELATIVE RADIAL DISTRIBUTIONS OF NEUTRON FLUX (E > 0.1 MeV)
WITHIN THE PRESSURE VESSEL WALL

Radius (cm)	0°	15°	25°	35°	45°
220.27 (1)	1.00	1.00	1.00	1.00	1.00
220.64	1.00	1.00	1.00	1.00	1.00
221.66	1.00	1.00	1.00	0.999	0.995
222.99	0.974	0.969	0.974	0.959	0.956
224.31	0.927	0.920	0.927	0.907	0.901
225.63	0.874	0.865	0.874	0.850	0.842
226.95	0.818	0.808	0.818	0.792	0.782
228.28	0.761	0.750	0.716	0.734	0.721
229.60	0.705	0.693	0.704	0.677	0.662
230.92	0.649	0.637	0.649	0.621	0.605
232.25	0.594	0.582	0.594	0.567	0.549
233.57	0.540	0.529	0.542	0.515	0.495
234.89	0.487	0.478	0.490	0.465	0.443
236.22	0.436	0.428	0.440	0.416	0.392
237.54	0.386	0.380	0.392	0.369	0.343
238.86	0.337	0.333	0.344	0.324	0.295
240.19	0.289	0.287	0.298	0.279	0.248
241.51	0.244	0.238	0.249	0.233	0.201
242.17 (2)	0.233	0.226	0.237	0.223	0.188

NOTES: 1) Base Metal Inner Radius
2) Base Metal Outer Radius

TABLE 6-5

RELATIVE RADIAL DISTRIBUTIONS OF IRON DISPLACEMENT RATE (dpa) WITHIN THE PRESSURE VESSEL WALL

Radius (cm)	0°	15°	25°	35°	45°
220.27[1]	1.00	1.00	1.00	1.00	1.00
220.64	0.984	0.981	0.984	0.983	0.984
221.66	0.912	0.909	0.917	0.921	0.915
222.99	0.815	0.812	0.826	0.833	0.821
224.31	0.722	0.719	0.737	0.747	0.730
225.63	0.638	0.634	0.656	0.668	0.647
226.95	0.563	0.559	0.584	0.597	0.572
228.28	0.497	0.493	0.519	0.533	0.506
229.60	0.439	0.435	0.462	0.475	0.447
230.92	0.387	0.383	0.410	0.423	0.394
232.25	0.341	0.338	0.364	0.376	0.347
233.57	0.300	0.297	0.322	0.334	0.305
234.89	0.263	0.261	0.285	0.295	0.266
236.22	0.230	0.228	0.250	0.260	0.231
237.54	0.199	0.198	0.218	0.227	0.199
238.86	0.171	0.170	0.189	0.196	0.169
240.19	0.145	0.144	0.161	0.167	0.140
241.51	0.121	0.119	0.135	0.139	0.113
242.17[2]	0.116	0.113	0.128	0.134	0.106

NOTES: 1) Base Metal Inner Radius
2) Base Metal Outer Radius

TABLE 6-6

NUCLEAR PARAMETERS FOR NEUTRON FLUX MONITORS

Monitor Material	Reaction of Interest	Target Weight Fraction	Response Range	Product Half-Life	Fission Yield (%)
Copper	$Cu^{63}(n,\alpha)Co^{60}$	0.6917	E > 4.7 MeV	5.272 yrs	
Iron	$Fe^{54}(n,p)Mn^{54}$	0.0582	E > 1.0 MeV	312.2 days	
Nickel	$Ni^{58}(n,p)Co^{58}$	0.6830	E > 1.0 MeV	70.90 days	
Uranium-238*	$U^{238}(n,f)Cs^{137}$	1.0	E > 0.4 MeV	30.12 yrs	5.99
Neptunium-237*	$Np^{237}(n,f)Cs^{137}$	1.0	E > 0.08 MeV	30.12 yrs	6.50
Cobalt-Aluminum*	$Co^{59}(n,\partial)Co^{60}$	0.0015	0.4ev>E>0.015 MeV	5.272 yrs	
Cobalt-Aluminum	$Co^{59}(n,\partial)Co^{60}$	0.0015	E > 0.015 MeV	5.272 yrs	

*Denotes that monitor is cadmium shielded.

TABLE 6-7

IRRADIATION HISTORY OF NEUTRON SENSORS
CONTAINED IN CAPSULE U

Irradiation Period	P_j (MW_t)	$\frac{P_j}{P_{Ref.}}$	Irradiation Time (days)	Decay Time (days)
5/88	691	.203	7	869
6/88	741	.217	30	839
7/88	1572	.461	31	808
8/88	2576	.755	31	777
9/88	1368	.401	30	747
10/88	670	.196	31	716
11/88	2248	.659	30	686
12/88	2636	.773	31	655
1/89	3016	.884	31	624
2/89	1078	.316	28	596
3/89	408	.120	31	565
4/89	3164	.928	30	535
5/89	2252	.660	31	504
6/89	2381	.698	30	474
7/89	2496	.732	31	443
8/89	2821	.827	31	412
9/89	2651	.777	30	382
10/89	2960	.868	31	351
11/89	3172	.930	30	321
12/89	3323	.974	31	290
1/90	2636	.773	31	259
2/90	1862	.546	28	231
3/90	1505	.441	15	216

NOTE: Reference Power = 3411 MW_t

TABLE 6-8

MEASURED SENSOR ACTIVITIES AND REACTION RATES

Monitor and Axial Location	Measured Activity (dis/sec-gm)	Saturated Activity (dis/sec-gm)	Reaction Rate (RPS/NUCLEUS)
Cu-63 (n,α) Co-60			
Top	5.41×10^{4}	4.30×10^{5}	
Middle	4.78×10^{4}	3.80×10^{5}	
Bottom	4.81×10^{4}	3.82×10^{5}	
Average	5.00×10^{4}	3.97×10^{5}	6.06×10^{-17}
Fe-54(n,p) Mn-54			
Top	1.31×10^{6}	4.03×10^{6}	
Middle	1.16×10^{6}	3.57×10^{6}	
Bottom	1.14×10^{6}	3.51×10^{6}	
Average	1.20×10^{6}	3.70×10^{6}	5.90×10^{-15}
Ni-58 (n,p) Co-58			
Top	4.99×10^{6}	5.77×10^{7}	
Middle	4.46×10^{6}	5.15×10^{7}	
Bottom	4.44×10^{6}	5.13×10^{7}	
Average	4.63×10^{6}	5.35×10^{7}	7.63×10^{-15}
U-238 (n,f) Cs-137 (Cd)			
Middle	1.34×10^{5}	5.25×10^{5}	3.46×10^{-14}

TABLE 6-8

MEASURED SENSOR ACTIVITIES AND REACTION RATES - cont'd

Monitor and Axial Location	Measured Activity (dis/sec-gm)	Saturated Activity (dis/sec-gm)	Reaction Rate (RPS/NUCLEUS)
Np-237(n,f) Cs-137 (Cd)			
Middle	1.39×10^{6}	5.44×10^{7}	3.30×10^{-13}
Co-59 (n,γ) Co-60			
Top	1.08×10^{7}	8.58×10^{7}	
Middle	1.07×10^{7}	8.50×10^{7}	
Bottom	1.06×10^{7}	8.42×10^{7}	
Average	1.07×10^{7}	8.50×10^{7}	5.54×10^{-12}
Co-59 (n,γ) Co-60 (Cd)			
Top	5.42×10^{6}	4.30×10^{7}	
Middle	5.57×10^{6}	4.42×10^{7}	
Bottom	5.56×10^{6}	4.42×10^{7}	
Average	5.52×10^{6}	5.81×10^{7}	2.86×10^{-12}

TABLE 6-6

SUMMARY OF NEUTRON DOSIMETRY RESULTS

	TIME AVERAGED EXPOSURE RATES	
ϕ (E > 1.0 MeV) {n/cm^2-sec}	1.08×10^{11}	± 8%
ϕ (E > 0.1 MeV) {n/cm^2-sec}	4.76×10^{11}	± 15%
dpa/sec	2.08×10^{-10}	± 11%
ϕ (E < 0.414 eV) {n/cm^2-sec}	1.11×10^{11}	± 21%
	INTEGRATED CAPSULE EXPOSURE	
Φ (E > 1.0 MeV) {n/cm^2}	3.91×10^{18}	± 8%
Φ (E > 0.1 MeV) {n/cm^2}	1.72×10^{19}	± 15%
dpa	7.53×10^{-3}	± 11%
Φ (E < 0.414 eV) {n/cm^2}	4.02×10^{18}	± 21%

NOTE: Total Irradiation Time = 1.15 EFPY

TABLE 6-10

COMPARISON OF MEASURED AND FERRET CALCULATED
REACTION RATES AT THE SURVEILLANCE CAPSULE CENTER

Reaction	Measured	Adjusted Calculation	C/M
Cu-63 (n,α) Co-60	6.06×10^{-17}	5.93×10^{-17}	0.98
Fe-54 (n,p) Mn-54	5.90×10^{-15}	5.79×10^{-15}	0.98
Ni-58 (n,p) Co-58	7.63×10^{-15}	7.72×10^{-15}	1.01
U-238 (n,f) Cs-137 (Cd)	3.46×10^{-14}	3.31×10^{-14}	0.96
Np-237 (n,f) Cs-137 (Cd)	3.30×10^{-13}	3.38×10^{-13}	1.02
Co-59 (n,γ) Co-60 (Cd)	2.86×10^{-12}	2.87×10^{-12}	0.99
Co-59 (n,γ) Co-60	5.54×10^{-12}	5.50×10^{-12}	1.00

TABLE 6-11

ADJUSTED NEUTRON ENERGY SPECTRUM AT THE SURVEILLANCE CAPSULE CENTER

Group	Energy (MeV)	Adjusted Flux (n/cm^2-sec)	Group	Energy (MeV)	Adjusted Flux (n/cm^2-sec)
1	1.73×10^{1}	8.15×10^{6}	28	9.12×10^{-3}	2.18×10^{10}
2	1.49×10^{1}	1.90×10^{7}	29	5.53×10^{-3}	2.83×10^{10}
3	1.35×10^{1}	7.34×10^{7}	30	3.36×10^{-3}	8.83×10^{9}
4	1.16×10^{1}	1.64×10^{8}	31	2.84×10^{-3}	8.44×10^{9}
5	1.00×10^{1}	3.60×10^{8}	32	2.40×10^{-3}	8.13×10^{9}
6	8.61×10^{0}	6.14×10^{8}	33	2.04×10^{-3}	2.29×10^{10}
7	7.41×10^{0}	1.41×10^{9}	34	1.23×10^{-3}	2.11×10^{10}
8	6.07×10^{0}	2.02×10^{9}	35	7.49×10^{-4}	1.95×10^{10}
9	4.97×10^{0}	4.26×10^{9}	36	4.54×10^{-4}	1.86×10^{10}
10	3.68×10^{0}	5.60×10^{9}	37	2.75×10^{-4}	2.00×10^{10}
11	2.87×10^{0}	1.19×10^{10}	38	1.67×10^{-4}	2.14×10^{10}
12	2.23×10^{0}	1.65×10^{10}	39	1.01×10^{-4}	2.16×10^{10}
13	1.74×10^{0}	2.32×10^{10}	40	6.14×10^{-5}	2.15×10^{10}
14	1.35×10^{0}	2.59×10^{10}	41	3.73×10^{-5}	2.10×10^{10}
15	1.11×10^{0}	4.75×10^{10}	42	2.26×10^{-5}	2.04×10^{10}
16	8.21×10^{-1}	5.43×10^{10}	43	1.37×10^{-5}	1.98×10^{10}
17	6.39×10^{-1}	5.64×10^{10}	44	8.32×10^{-6}	1.89×10^{10}
18	4.98×10^{-1}	4.09×10^{10}	45	5.04×10^{-6}	1.74×10^{10}
19	3.88×10^{-1}	5.75×10^{10}	46	3.06×10^{-6}	1.63×10^{10}
20	3.02×10^{-1}	5.91×10^{10}	47	1.86×10^{-6}	1.50×10^{10}
21	1.83×10^{-1}	5.86×10^{10}	48	1.13×10^{-6}	1.11×10^{10}
22	1.11×10^{-1}	4.69×10^{10}	49	6.83×10^{-7}	1.43×10^{10}
23	6.74×10^{-2}	3.26×10^{10}	50	4.14×10^{-7}	1.90×10^{10}
24	4.09×10^{-2}	1.85×10^{10}	51	2.51×10^{-7}	1.90×10^{9}
25	2.55×10^{-2}	2.42×10^{10}	52	1.52×10^{-7}	1.81×10^{9}
26	1.99×10^{-2}	1.19×10^{10}	53	9.24×10^{-8}	5.46×10^{10}
27	1.50×10^{-2}	1.51×10^{10}			

NOTE: Tabulated energy levels represent the upper energy of each group.

TABLE 6-12

COMPARISON OF CALCULATED AND MEASURED EXPOSURE LEVELS FOR CAPSULE U

	Calculated	Measured	C/M
$\Phi(E > 1.0\ MeV)\ (n/cm^2)$	3.44×10^{18}	3.91×10^{18}	0.88
$\Phi(E > 0.1\ MeV)\ (n/cm^2)$	1.55×10^{19}	1.72×10^{19}	0.90
dpa	6.74×10^{-3}	7.53×10^{-3}	0.90
$\Phi(E < 0.414\ eV)\ (n/cm^2)$	1.65×10^{18}	4.02×10^{18}	0.41

TABLE 6-13

NEUTRON EXPOSURE PROJECTIONS AT KEY LOCATIONS

ON THE PRESSURE VESSEL CLAD/BASE METAL INTERFACE FOR BRAIDWOOD UNIT 2

AZIMUTHAL ANGLE

	0°	15°	25°(a)	35°	45°
1.15 EFPY					
Φ(E>1.0 MeV) (n/cm^2)	5.43×10^{17}	8.48×10^{17}	9.80×10^{17}	8.15×10^{17}	9.51×10^{17}
Φ(E>0.1 MeV) (n/cm^2)	1.10×10^{18}	1.74×10^{18}	2.61×10^{18}	2.26×10^{18}	2.33×10^{18}
dpa	8.30×10^{-4}	1.30×10^{-3}	1.62×10^{-3}	1.35×10^{-3}	1.49×10^{-3}
16.0 EFPY					
Φ(E>1.0 MeV) (n/cm^2)	8.88×10^{18}	1.33×10^{19}	1.51×10^{19}	1.23×10^{19}	1.41×10^{19}
Φ(E>0.1 MeV) (n/cm^2)	1.84×10^{19}	2.80×10^{19}	4.11×10^{19}	3.49×10^{19}	3.53×10^{19}
dpa	1.38×10^{-2}	2.06×10^{-2}	2.52×10^{-2}	2.08×10^{-2}	2.25×10^{-2}
32.0 EFPY					
Φ(E>1.0 MeV) (n/cm^2)	1.79×10^{19}	2.68×10^{19}	3.03×10^{19}	2.47×10^{19}	2.83×10^{19}
Φ(E>0.1 MeV) (n/cm^2)	3.71×10^{19}	5.62×10^{19}	8.26×10^{19}	7.00×10^{19}	7.08×10^{19}
dpa	2.78×10^{-2}	4.14×10^{-2}	5.07×10^{-2}	4.17×10^{-2}	4.51×10^{-2}

(a) Maximum point on the pressure vessel

TABLE 6-14

NEUTRON EXPOSURE VALUES FOR USE IN THE GENERATION OF HEATUP/COOLDOWN CURVES

16 EFPY

	NEUTRON FLUENCE (E > 1.0 MeV) SLOPE (n/cm^2)			dpa SLOPE (equivalent n/cm^2)		
	Surface	1/4 T	3/4 T	Surface	1/4 T	3/4 T
0°	8.88×10^{18}	4.82×10^{18}	1.03×10^{18}	8.88×10^{18}	5.60×10^{18}	1.95×10^{18}
15°	1.33×10^{19}	7.20×10^{18}	1.51×10^{18}	1.33×10^{19}	8.34×10^{18}	2.88×10^{18}
25°(a)	1.51×10^{19}	8.24×10^{18}	1.78×10^{18}	1.51×10^{19}	9.80×10^{18}	3.59×10^{18}
35°	1.23×10^{19}	6.69×10^{18}	1.43×10^{18}	1.23×10^{19}	8.15×10^{18}	3.05×10^{18}
45°	1.41×10^{19}	7.54×10^{18}	1.52×10^{18}	1.41×10^{19}	9.02×10^{18}	3.09×10^{18}

32 EFPY

	NEUTRON FLUENCE (E > 1.0 MeV) SLOPE (n/cm^2)			dpa SLOPE (equivalent n/cm^2)		
	Surface	1/4 T	3/4 T	Surface	1/4 T	3/4 T
0°	1.79×10^{19}	9.72×10^{18}	2.07×10^{18}	1.79×10^{19}	1.13×10^{19}	3.92×10^{18}
15°	2.68×10^{19}	1.45×10^{19}	3.05×10^{18}	2.68×10^{19}	1.69×10^{19}	5.81×10^{18}
25°(a)	3.03×10^{19}	1.66×10^{19}	3.57×10^{18}	3.03×10^{19}	1.97×10^{19}	7.21×10^{18}
35°	2.47×10^{19}	1.35×10^{19}	2.86×10^{18}	2.47×10^{19}	1.64×10^{19}	6.12×10^{18}
45°	2.83×10^{19}	1.52×10^{19}	3.06×10^{18}	2.83×10^{19}	1.81×10^{19}	6.20×10^{18}

(a) Maximum point on the pressure vessel

TABLE 6-15

UPDATED LEAD FACTORS FOR BRAIDWOOD UNIT 2
SURVEILLANCE CAPSULES

Capsule	Lead Factor
U	4.00[a]
X	4.02
W	4.02
Z	4.02
V	3.75
Y	3.75

(a) Plant specific evaluation

SECTION 7.0
SURVEILLANCE CAPSULE REMOVAL SCHEDULE

The following removal schedule meets ASTM E185-82 and is recommended for future capsules to be removed from the Braidwood Unit 1 reactor vessel:

Capsule	Location (deg.)	Capsule Lead Factor	Removal Time [(b)]	Estimated Fluence (n/cm^2)
U	58.5	4.00	1.15 (Removed)[(a)]	3.91×10^{18} (Actual)
X	238.5	4.02	4.5	1.7×10^{19} (c)
V	61.0	3.75	9.0	3.2×10^{19} (d)
Y	241.0	3.75	15.0	5.3×10^{19}
W	121.5	4.02	Standby	---
Z	301.5	4.02	Standby	---

(a) Plant Specific Evaluation

(b) Effective Full Power Years (EFPY) from plant startup.

(c) Approximate fluence at 1/4 thickness of reactor vessel wall at end of life (32 EFPY).

(d) Approximate fluence at reactor vessel inner wall at end of life (32 EFPY).

SECTION 8.0
REFERENCES

1. Singer, L.R., "Commonwealth Edison Company Braidwood Station Unit No. 2 Reactor Vessel Radiation Surveillance Program," WCAP-11188, December 1986.

2. Code of Federal Regulations, 10CFR50, Appendix G, "Fracture Toughness Requirements", and Appendix H, "Reactor Vessel Material Surveillance Program Requirements," U.S. Nuclear Regulatory Commission, Washington, D.C.

3. Regulatory Guide 1.99, Revision 2, "Radiation Embrittlement of Reactor Vessel Materials", U.S. Nuclear Regulatory Commission, May, 1988.

4. Section III of the ASME Boiler and Pressure Vessel Code, Appendix G, "Protection Against Nonductile Failure."

5. ASTM E208, "Standard Test Method for Conducting Drop-Weight Test to Determine Nil-Ductility Transition Temperature of Ferritic Steels."

6. ASTM E185-82, "Standard Practice for Conducting Surveillance Tests for Light-Water Cooled Nuclear Power Reactor Vessels, E706 (IF)."

7. ASTM E23-88, "Standard Test Methods for Notched Bar Impact Testing of Metallic Materials."

8. ASTM A370-89, "Standard Test Methods and Definitions for Mechanical Testing of Steel Products."

9. ASTM E8-89b, "Standard Test Methods of Tension Testing of Metallic Materials."

10. ASTM E21-79 (1988), "Standard Practice for Elevated Temperature Tension Tests of Metallic Materials."

11. ASTM E83-85, "Standard Practice for Verification and Classification of Extensometers."

12. R. G. Soltesz, R. K. Disney, J. Jedruch, and S. L. Ziegler, "Nuclear Rocket Shielding Methods, Modification, Updating and Input Data Preparation. Vol. 5--Two-Dimensional Discrete Ordinates Transport Technique", WANL-PR(LL)-034, Vol. 5, August 1970.

13. "ORNL RSCI Data Library Collection DLC-76 SAILOR Coupled Self-Shielded, 47 Neutron, 20 Gamma-Ray, P3, Cross Section Library for Light Water Reactors".

14. J. V. Alexander, et. al., "Core Physics Parameters and Plant Operations Data for the Braidwood Generating Station Unit 2 Cycle 1", WCAP-11475, June 1987. (Proprietary)

15. ASTM Designation E482-82, "Standard Guide for Application of Neutron Transport Methods for Reactor Vessel Surveillance", in ASTM Standards, Section 12, American Society for Testing and Materials, Philadelphia, PA, 1984.

16. ASTM Designation E560-77, "Standard Recommended Practice for Extrapolating Reactor Vessel Surveillance Dosimetry Results", in ASTM Standards, Section 12, American Society for Testing and Materials, Philadelphia, PA, 1984.

17. ASTM Designation E693-79, "Standard Practice for Characterizing Neutron Exposures in Ferritic Steels in Terms of Displacements per Atom (dpa)", in ASTM Standards, Section 12, American Society for Testing and Materials, Philadelphia, PA, 1984.

18. ASTM Designation E706-81a, "Standard Master Matrix for Light-Water Reactor Pressure Vessel Surveillance Standard", in ASTM Standards, Section 12, American Society for Testing and Materials, Philadelphia, PA, 1984.

19. ASTM Designation E853-84, "Standard Practice for Analysis and Interpretation of Light-Water Reactor Surveillance Results", in ASTM Standards, Section 12, American Society for Testing and Materials, Philadelphia, PA, 1984.

20. ASTM Designation E261-77, "Standard Method for Determining Neutron Flux, Fluence, and Spectra by Radioactivation Techniques", in ASTM Standards, Section 12, American Society for Testing and Materials, Philadelphia, PA, 1984.

21. ASTM Designation E262-77, "Standard Method for Measuring Thermal Neutron Flux by Radioactivation Techniques", in ASTM Standards, Section 12, American Society for Testing and Materials, Philadelphia, PA, 1984.

22. ASTM Designation E263-82, "Standard Method for Determining Fast-Neutron Flux Density by Radioactivation of Iron", in ASTM Standards, Section 12, American Society for Testing and Materials, Philadelphia, PA, 1984.

23. ASTM Designation E264-82, "Standard Method for Determining Fast-Neutron Flux Density by Radioactivation of Nickel", in ASTM Standards, Section 12, American Society for Testing and Materials, Philadelphia, PA, 1984.

24. ASTM Designation E481-78, "Standard Method for Measuring Neutron-Flux Density by Radioactivation of Cobalt and Silver", in ASTM Standards, Section 12, American Society for Testing and Materials, Philadelphia, PA, 1984.

25. ASTM Designation E523-82, "Standard Method for Determining Fast-Neutron Flux Density by Radioactivation of Copper", in ASTM Standards, Section 12, American Society for Testing and Materials, Philadelphia, PA, 1984.

26. ASTM Designation E704-84, "Standard Method for Measuring Reaction Rates by Radioactivation of Uranium-238", in ASTM Standards, Section 12, American Society for Testing and Materials, Philadelphia, PA, 1984.

27. ASTM Designation E705-79, "Standard Method for Measuring Fast-Neutron Flux Density by Radioactivation of Neptunium-237", in ASTM Standards, Section 12, American Society for Testing and Materials, Philadelphia, PA, 1984.

28. ASTM Designation E1005-84, "Standard Method for Application and Analysis of Radiometric Monitors for Reactor Vessel Surveillance", in ASTM Standards, Section 12, American Society for Testing and Materials, Philadelphia, PA, 1984.

29. F. A. Schmittroth, FERRET Data Analysis Core, HEDL-TME 79-40, Hanford Engineering Development Laboratory, Richland, WA, September 1979.

30. W. N. McElroy, S. Berg and T. Crocket, A Computer-Automated Iterative Method of Neutron Flux Spectra Determined by Foil Activation, AFWL-TR-7-41, Vol. I-IV, Air Force Weapons Laboratory, Kirkland AFB, NM, July 1967.

31. EPRI-NP-2188, "Development and Demonstration of an Advanced Methodology for LWR Dosimetry Applications", R. E. Maerker, et al., 1981.

APPENDIX A

Load-Time Records for Charpy Specimen Tests

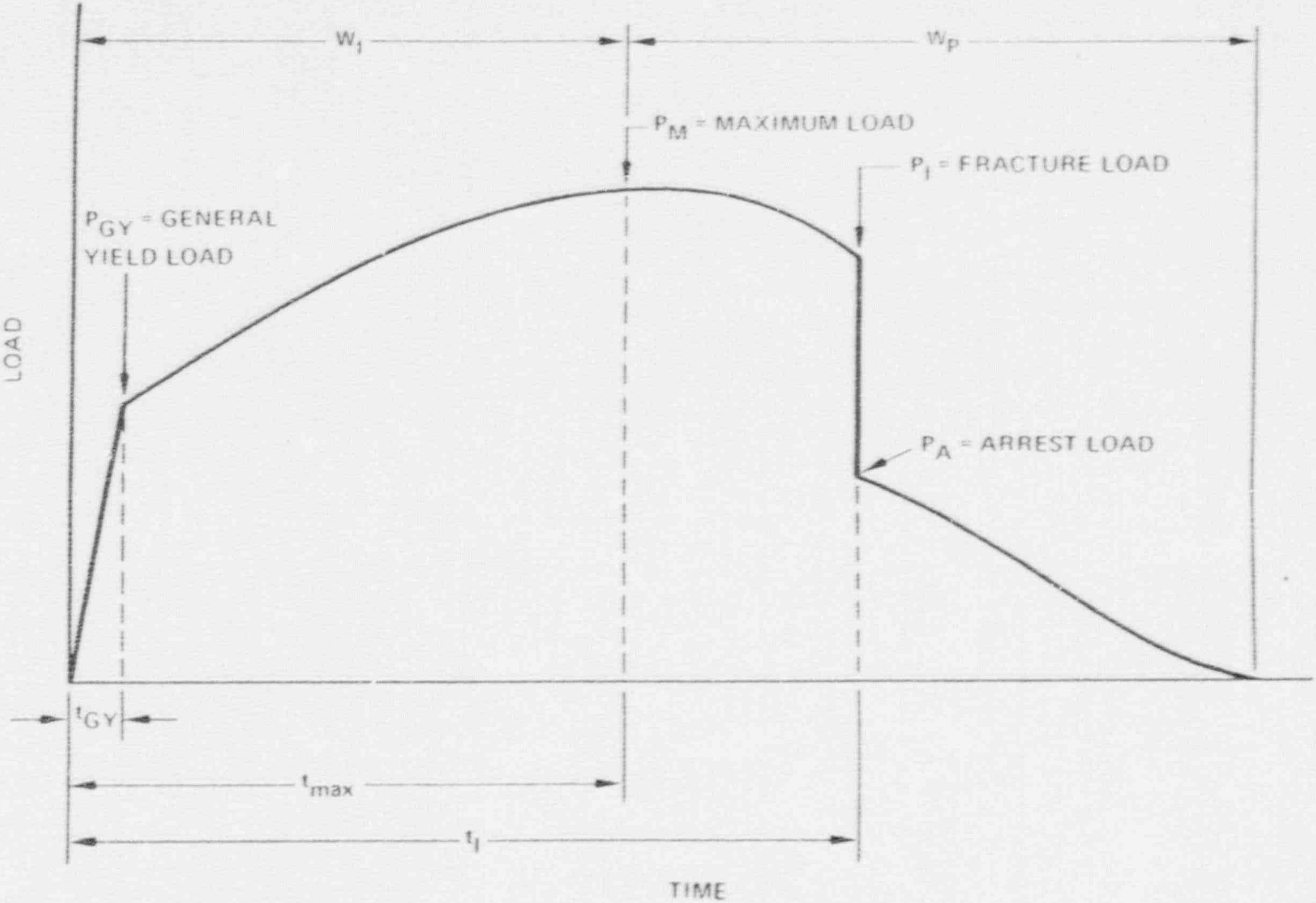

Figure A-1. Idealized load-time record.

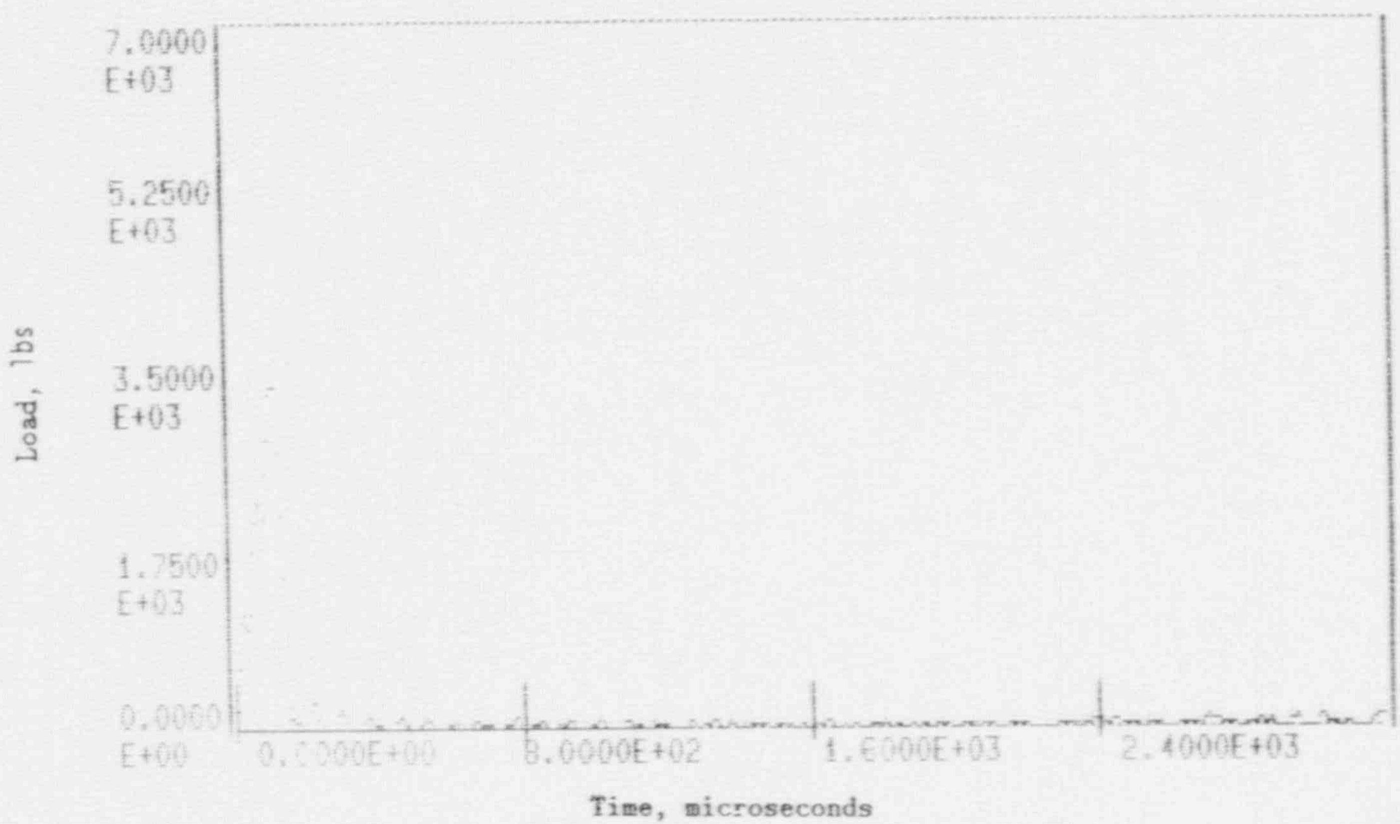

Figure A-2. Load-time record for Specimen FL12.

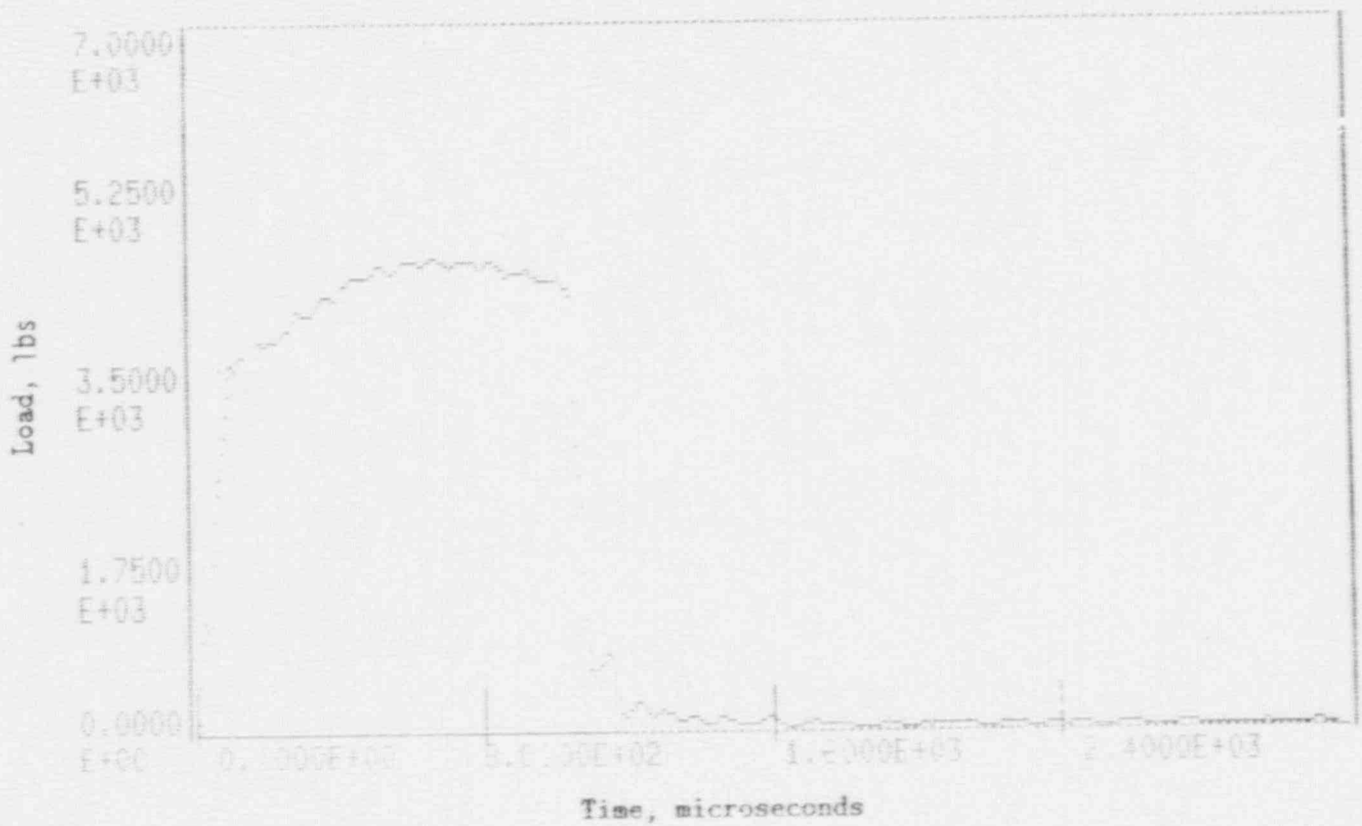

Figure A-3. Load-time record for Specimen FL13.

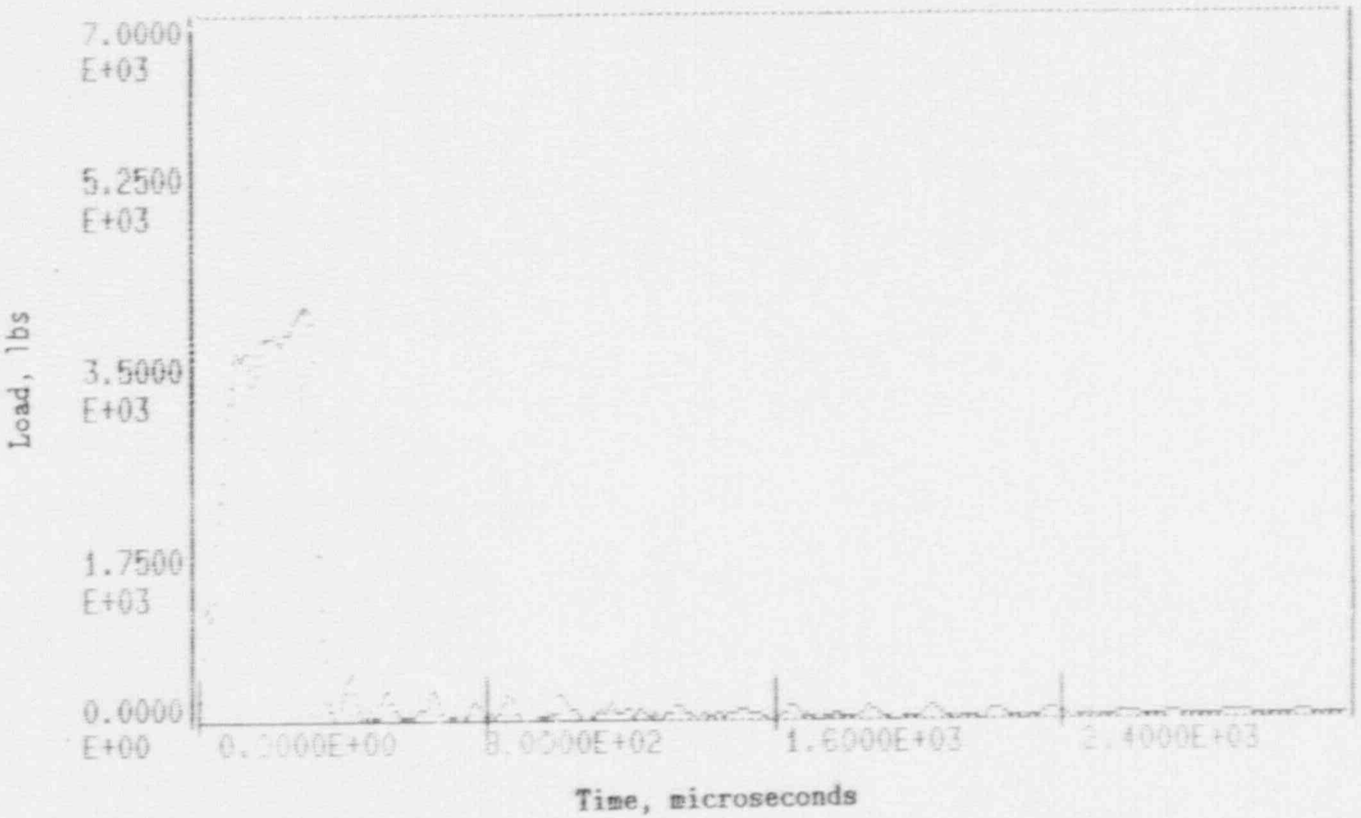

Figure A-4. Load-time record for Specimen FL4.

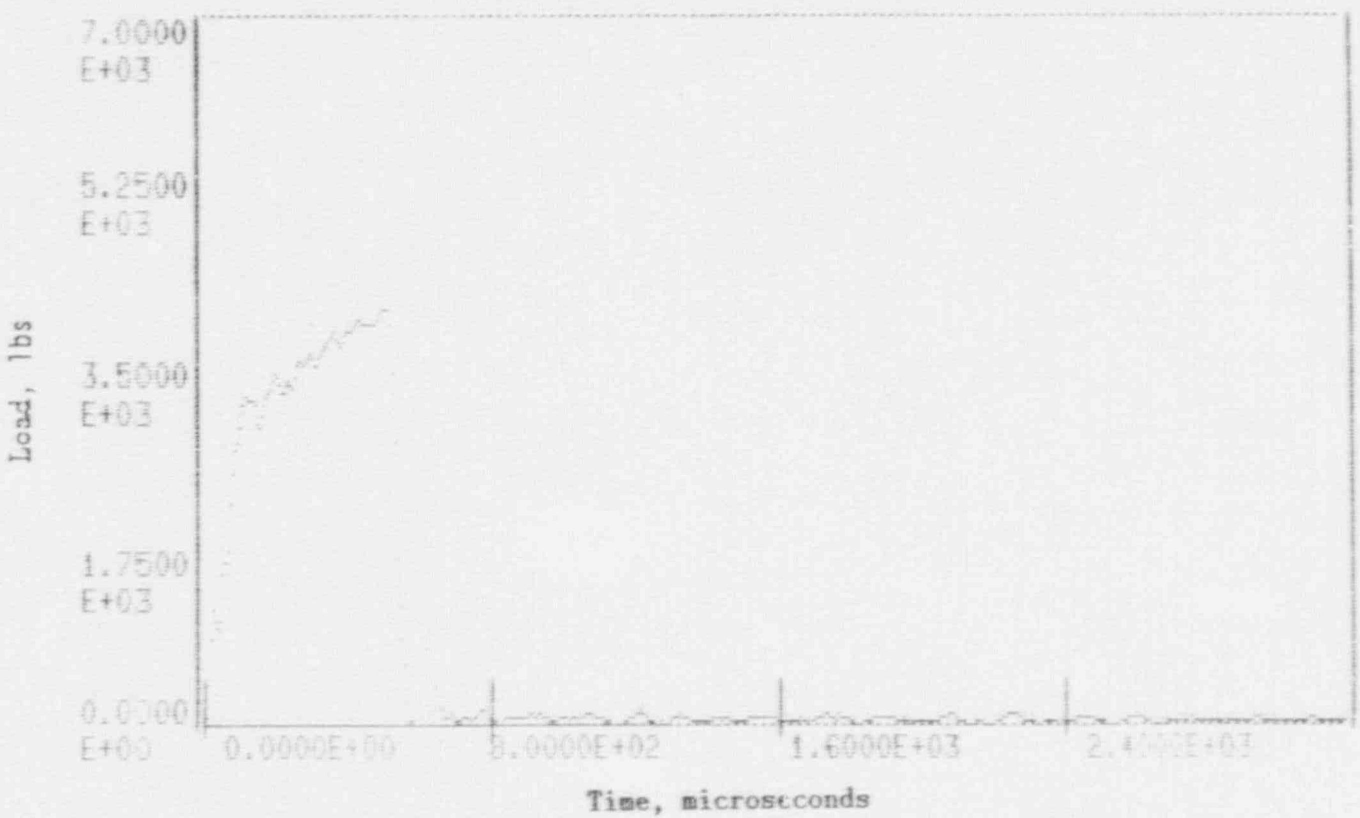

Figure A-5. Load-time record for Specimen FL9.

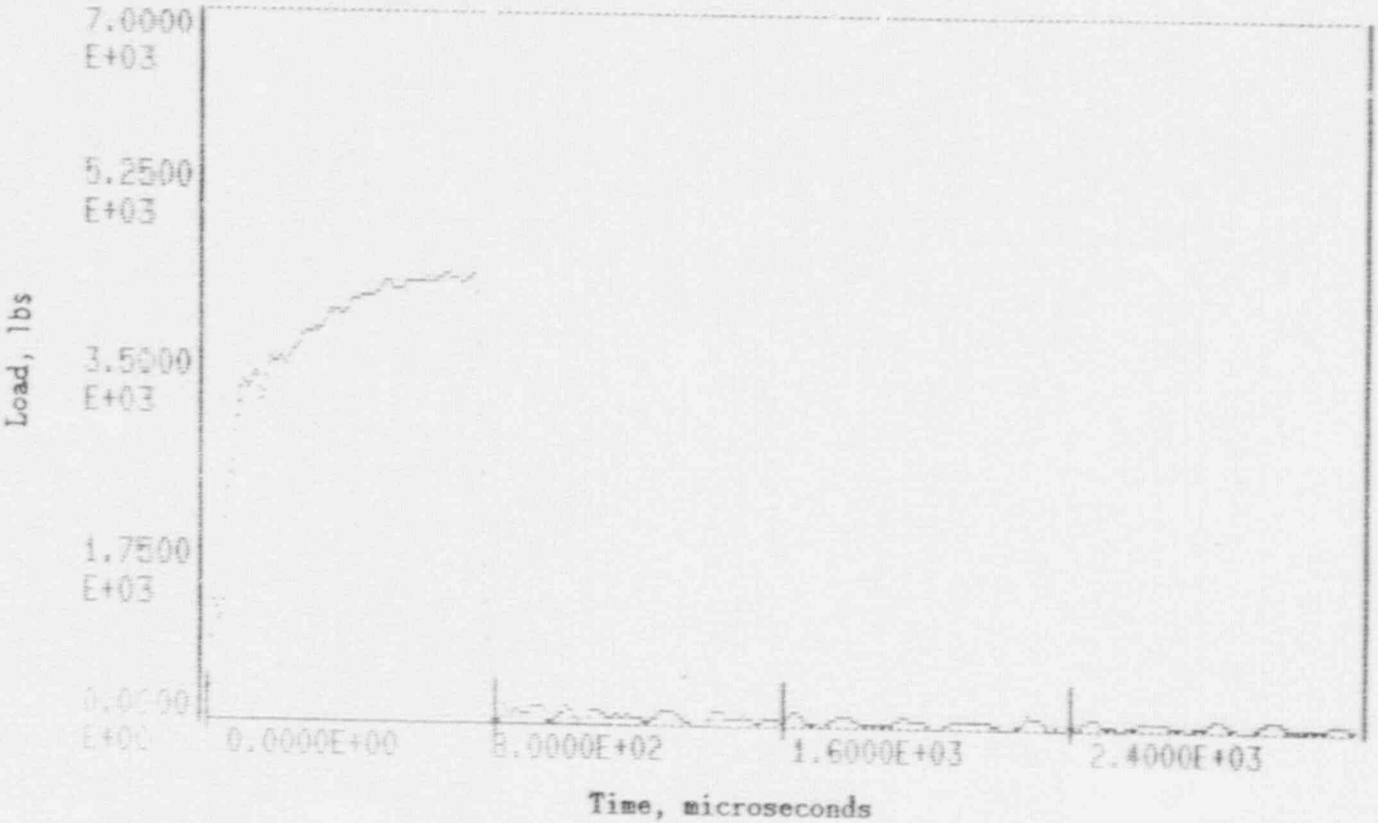

Figure A-6. Load-time record for Specimen FL5.

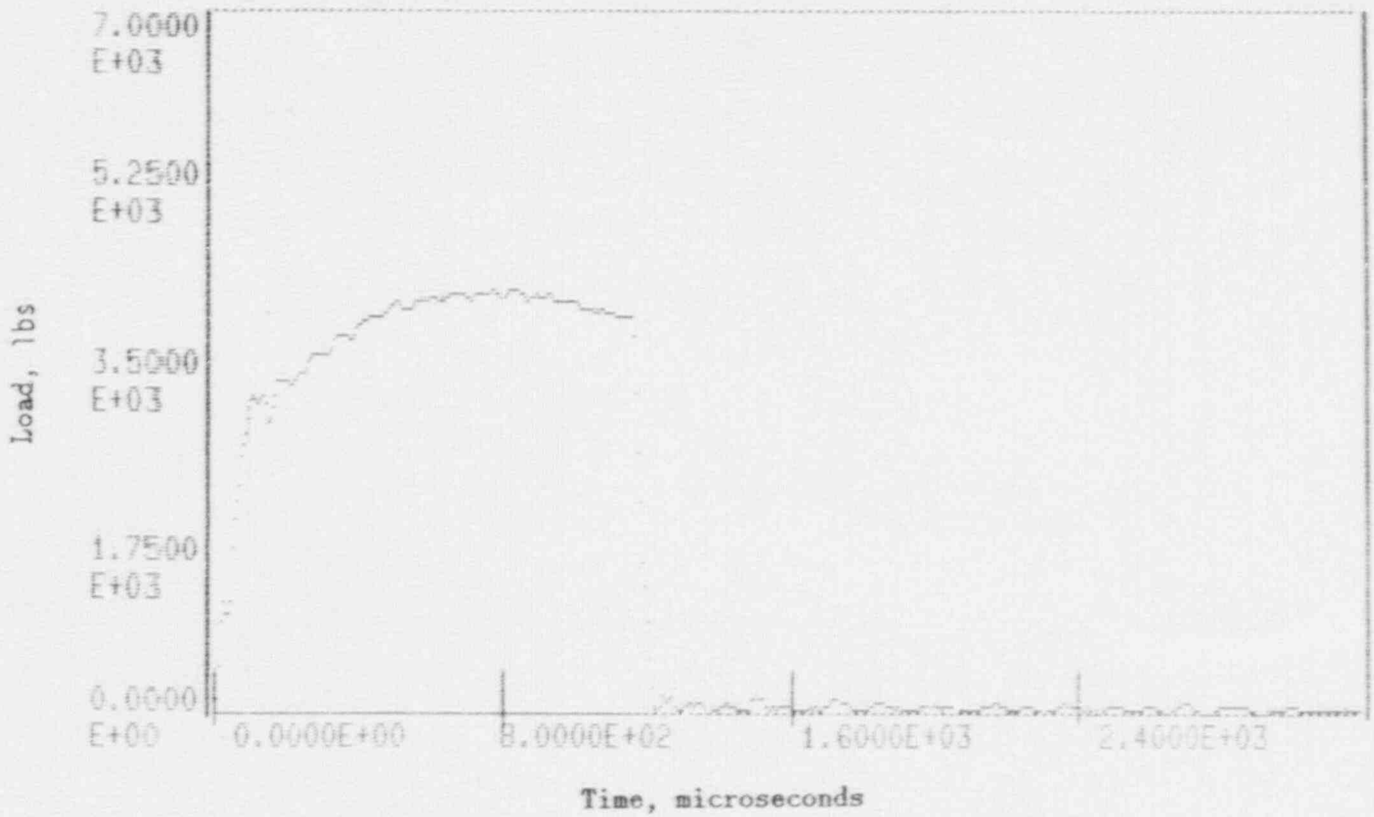

Figure A-7. Load-time record for Specimen FL11.

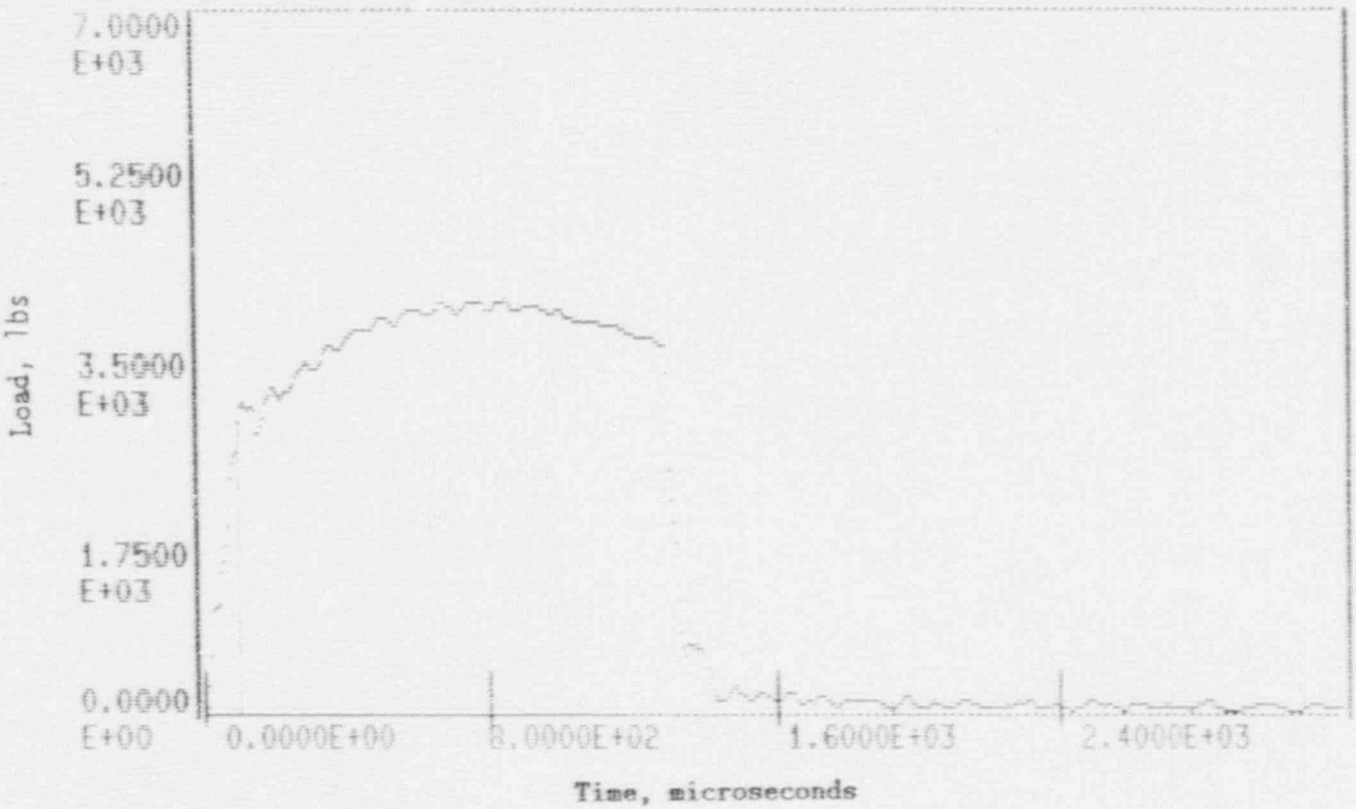

Figure A-8 Load-time record for Specimen FL10.

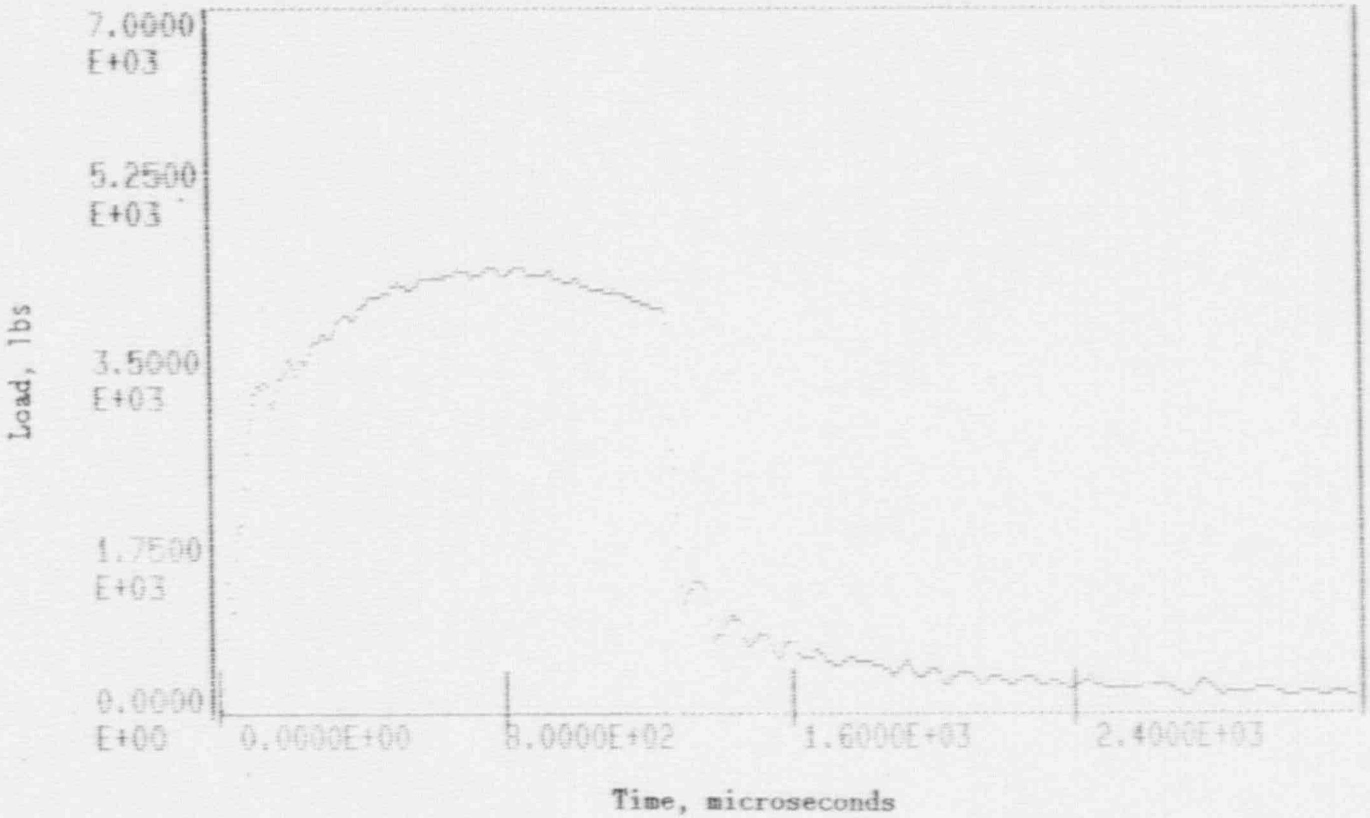

Figure A-9. Load-time record for Specimen FL6.

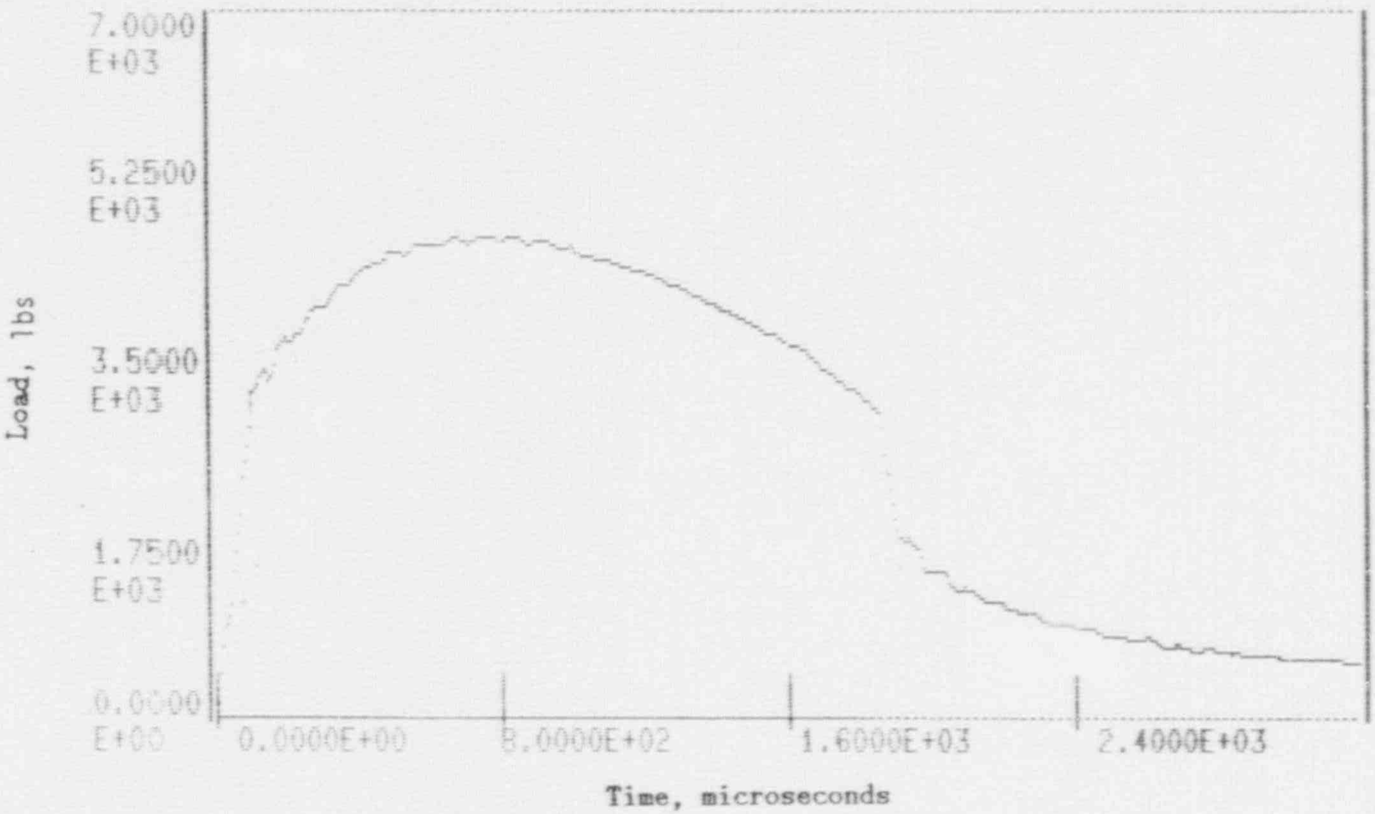

Figure A-10. Load-time record for Specimen FL14.

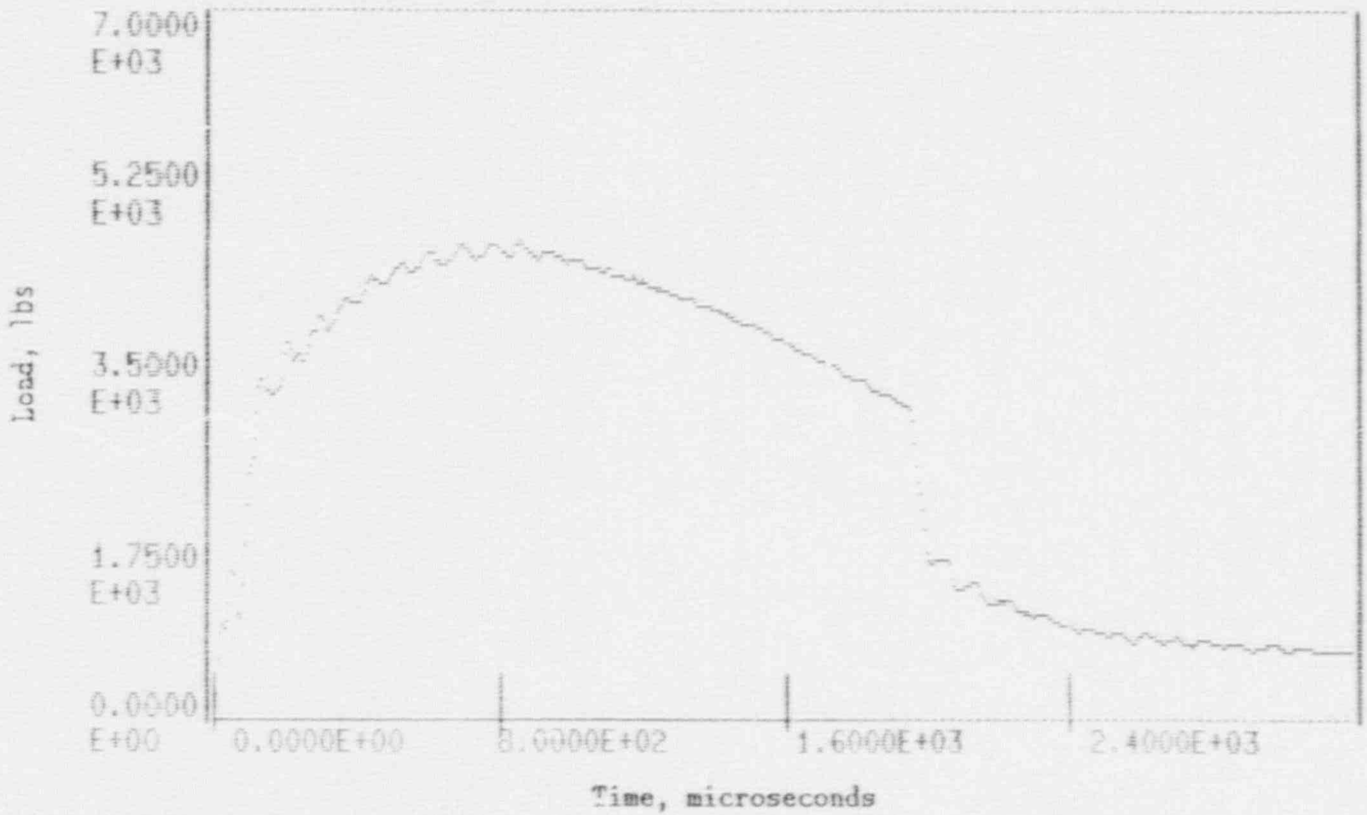

Figure A-11. Load-time record for Specimen FL7.

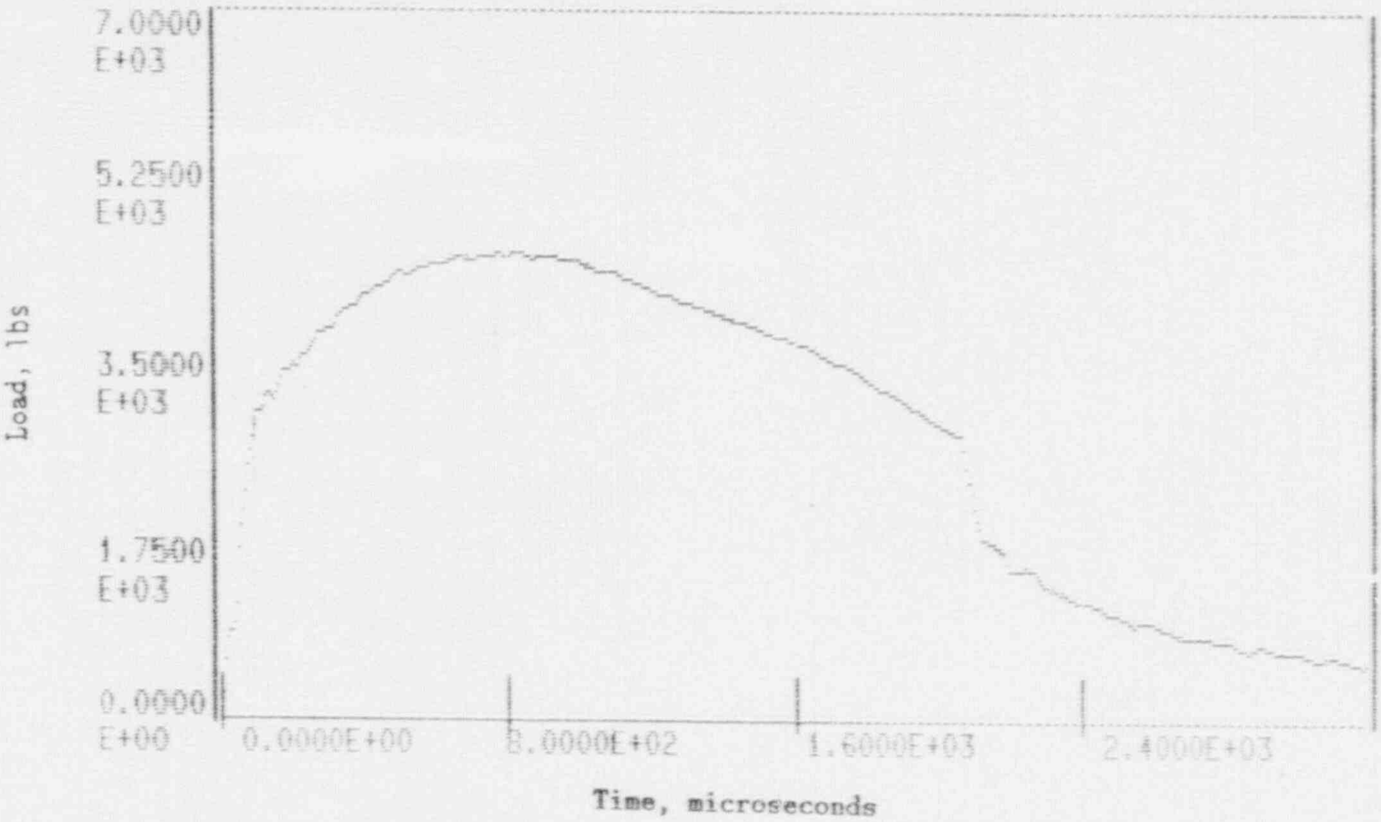

Figure A-12. Load-time record for Specimen FL3.

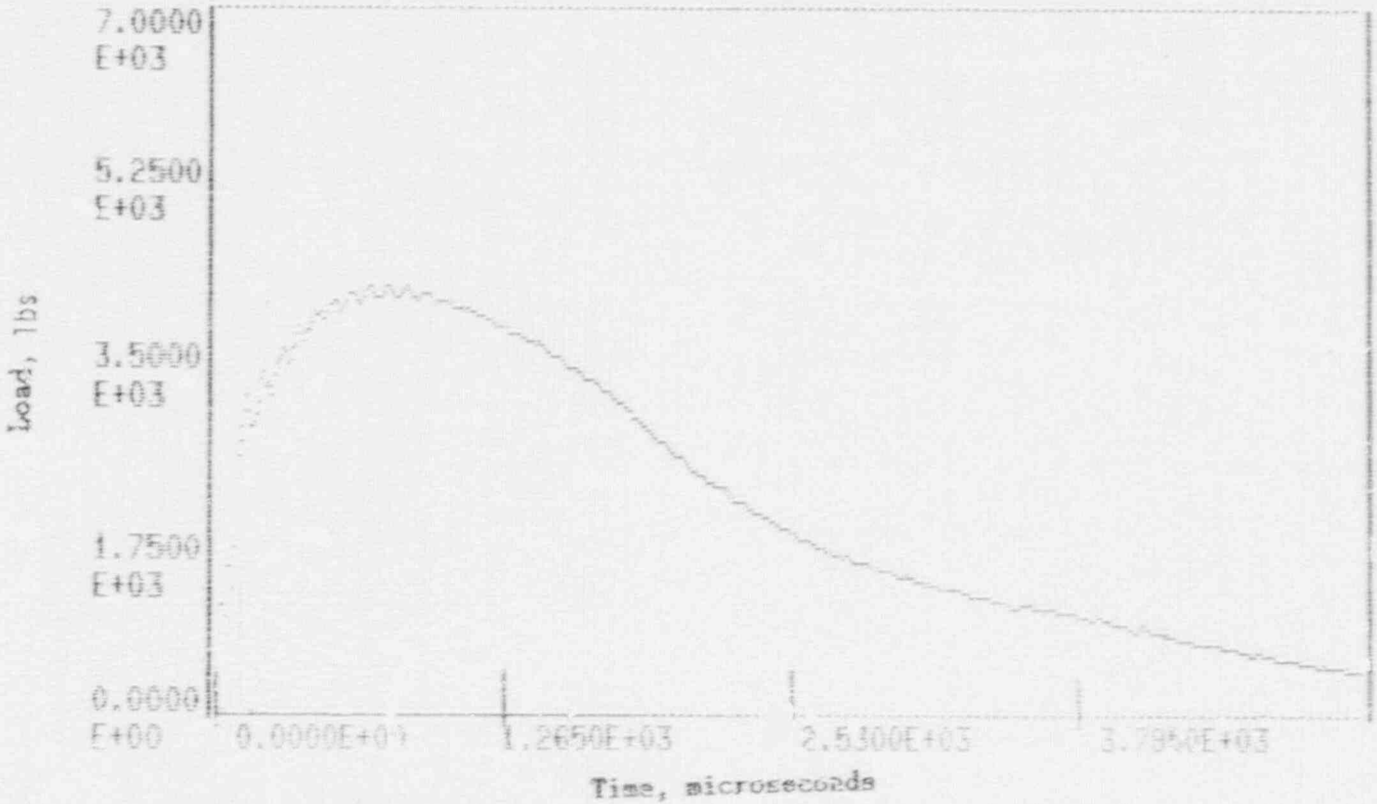

Figure A-13. Load-time record for Specimen KL2.

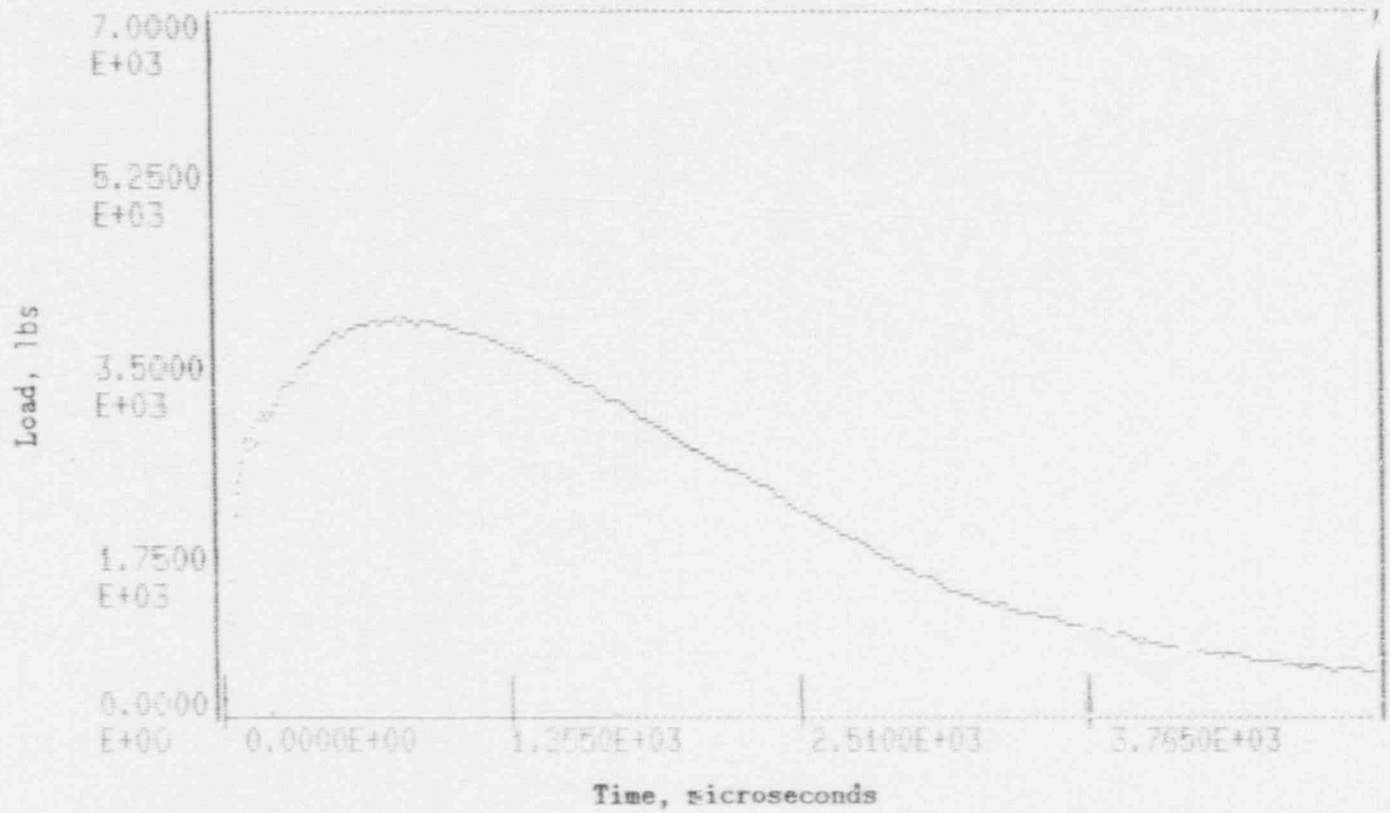

Figure A-14. Load-time record for Specimen FL15.

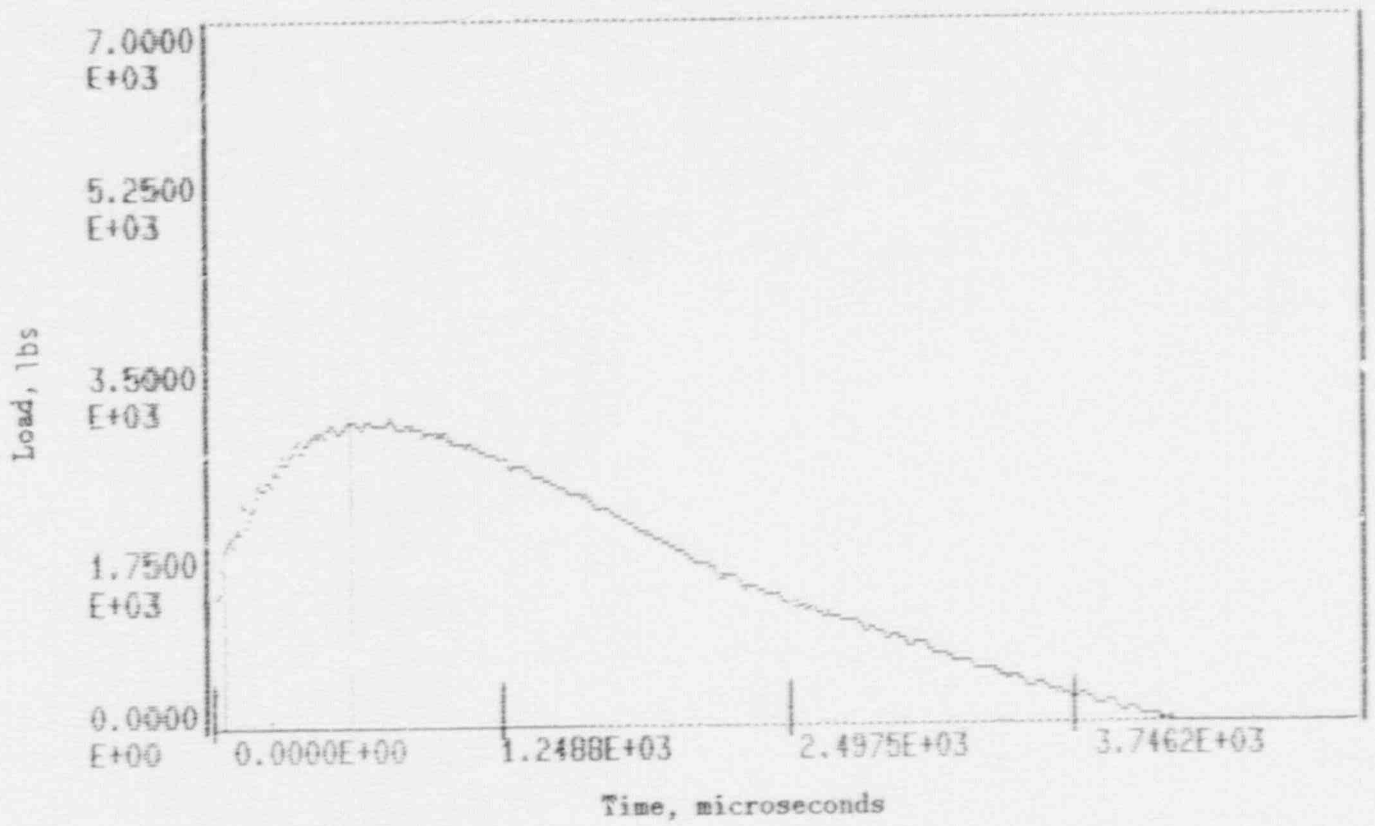

Figure A-15. Load-time record for Specimen FL1.

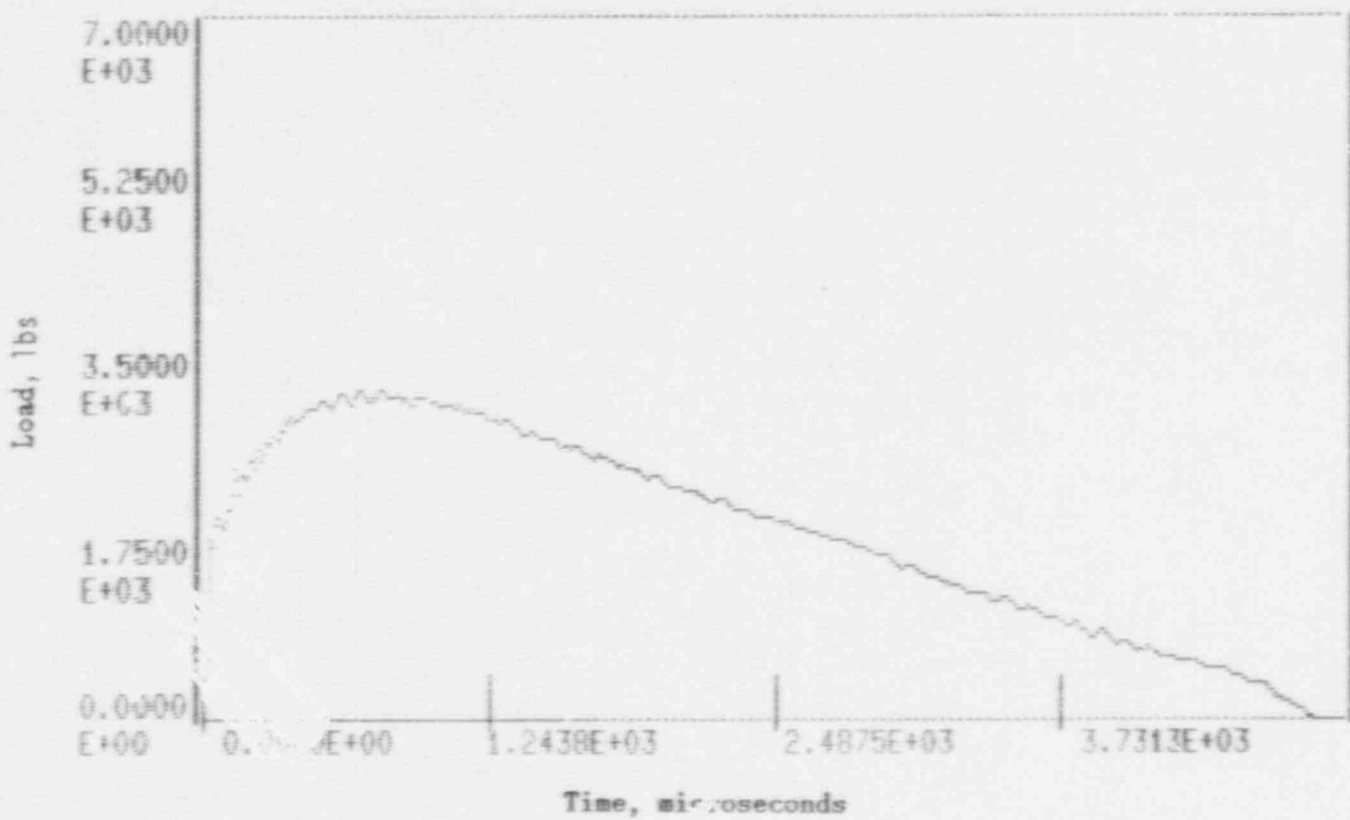

Figure A-16. Load-time record for Specimen FL8.

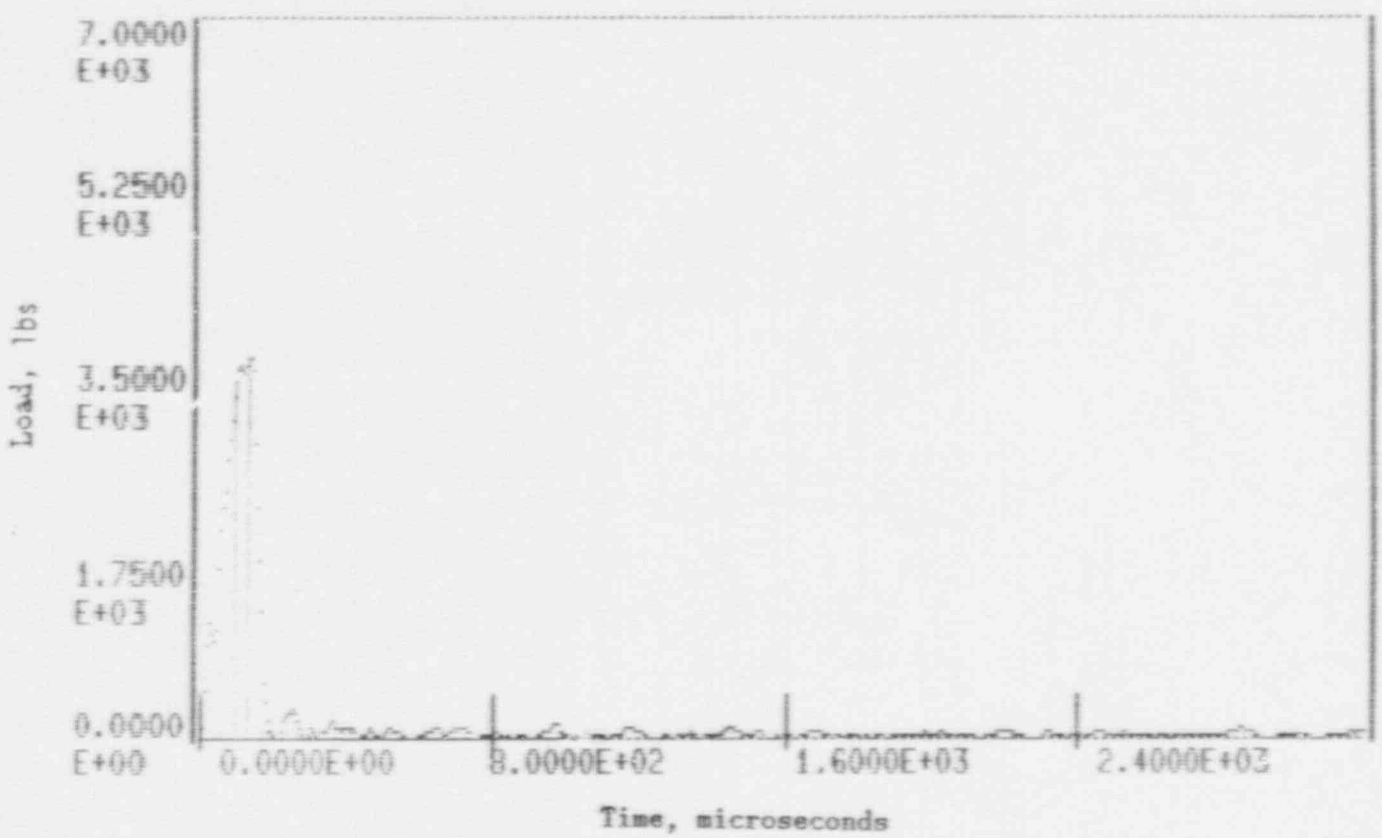

Figure A-17. Load-time record for Specimen FT3.

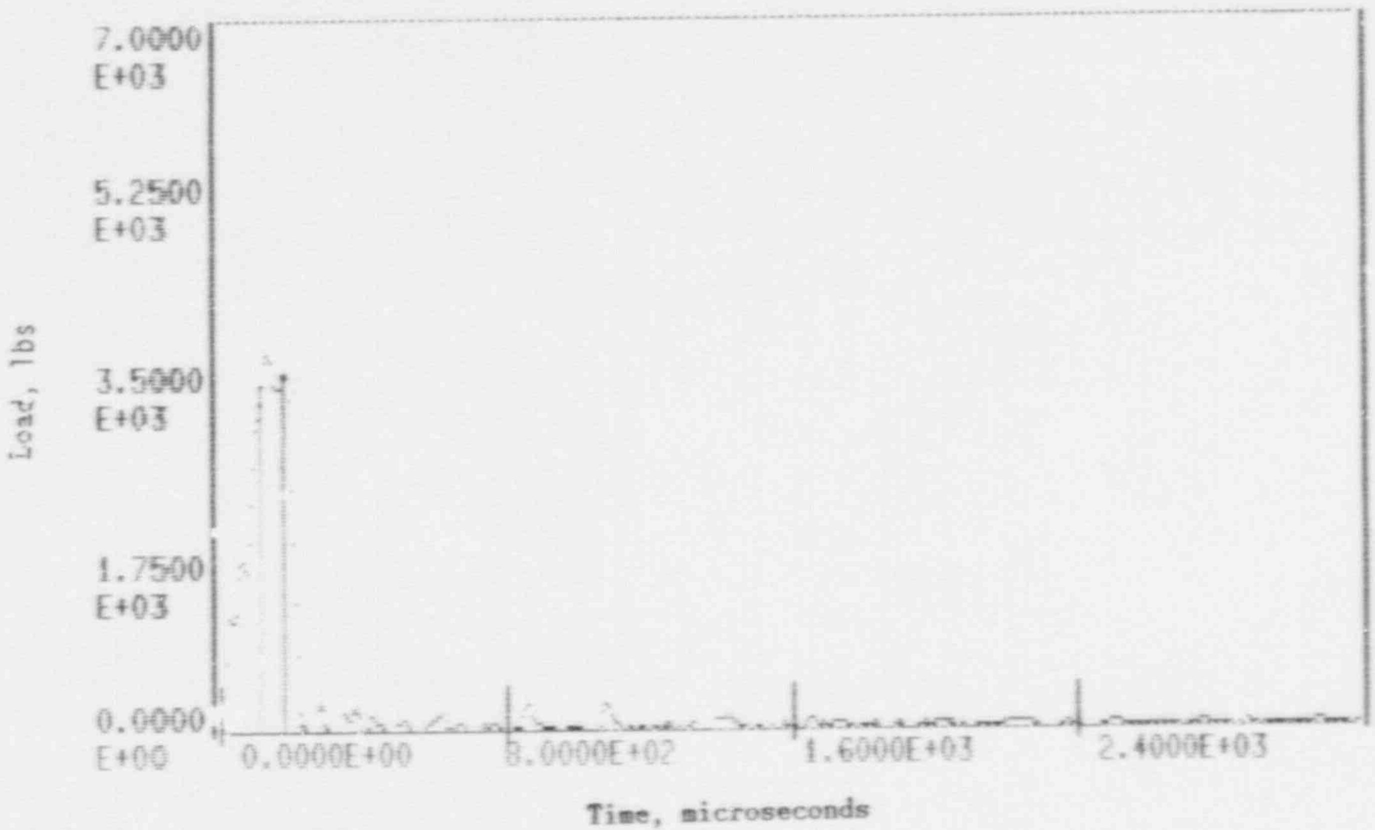

Figure 4-18. Load-time record for Specimen FT14.

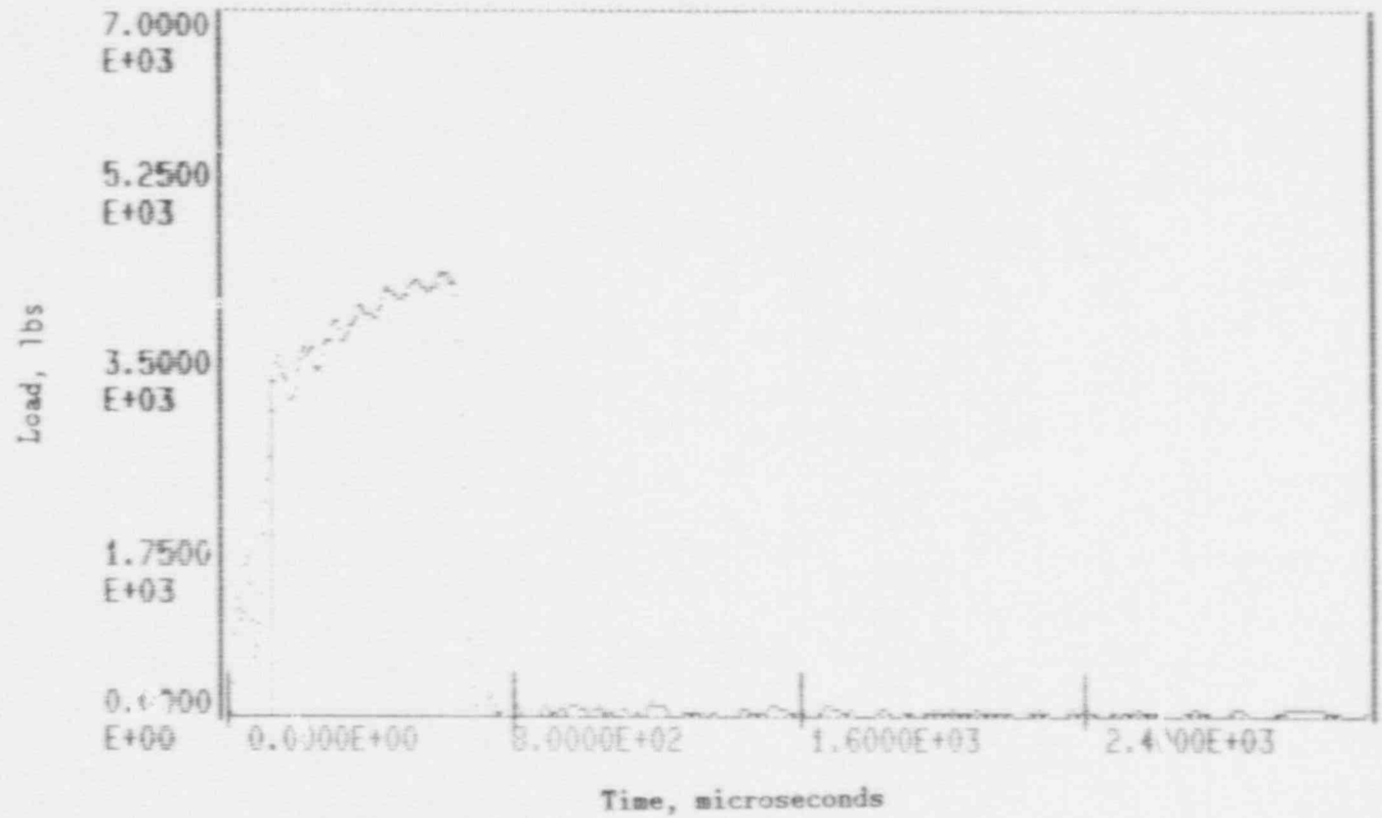

Figure A-19. Load-time record for Specimen FT6.

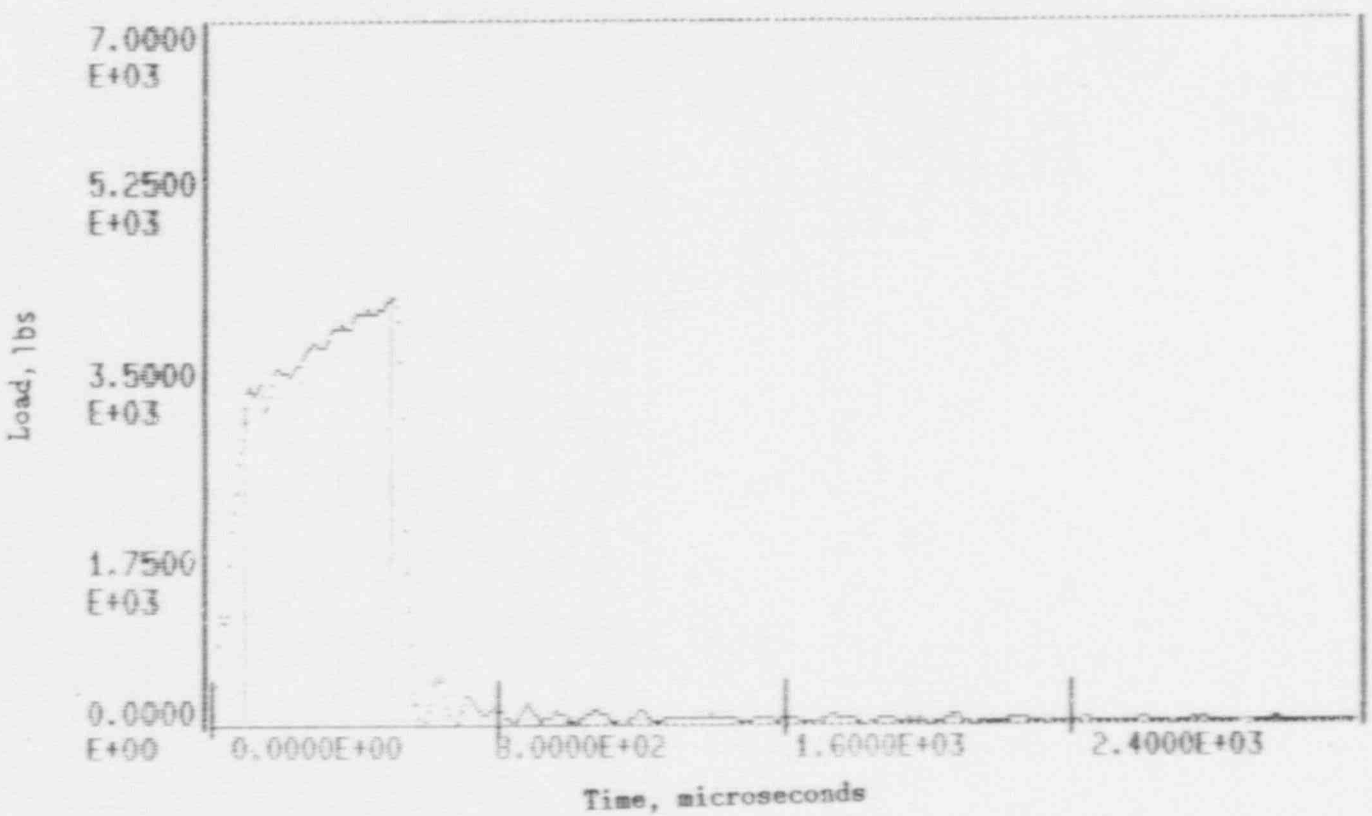

Figure A-20. Load-time record for Specimen FT4.

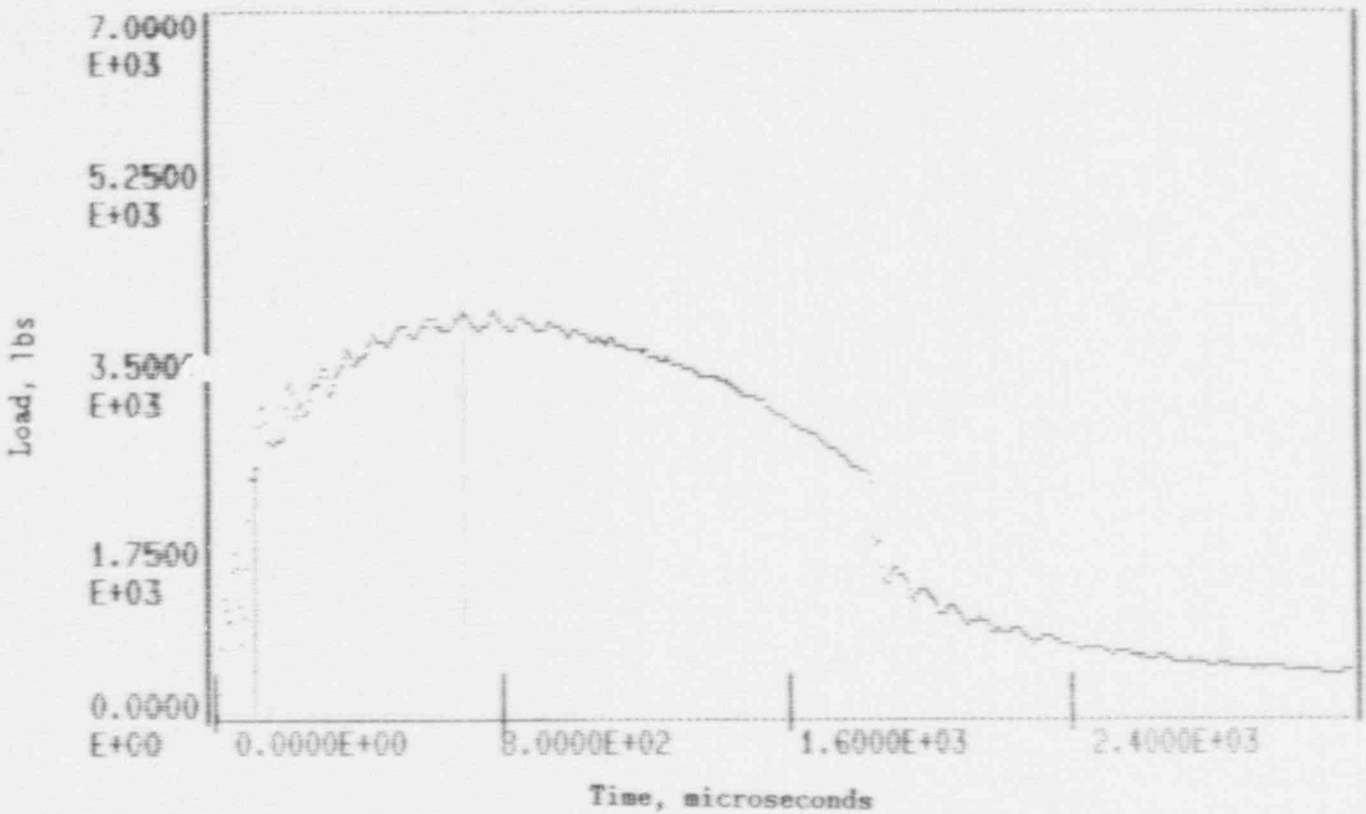

Figure A-21. Load-time record for Specimen FT8.

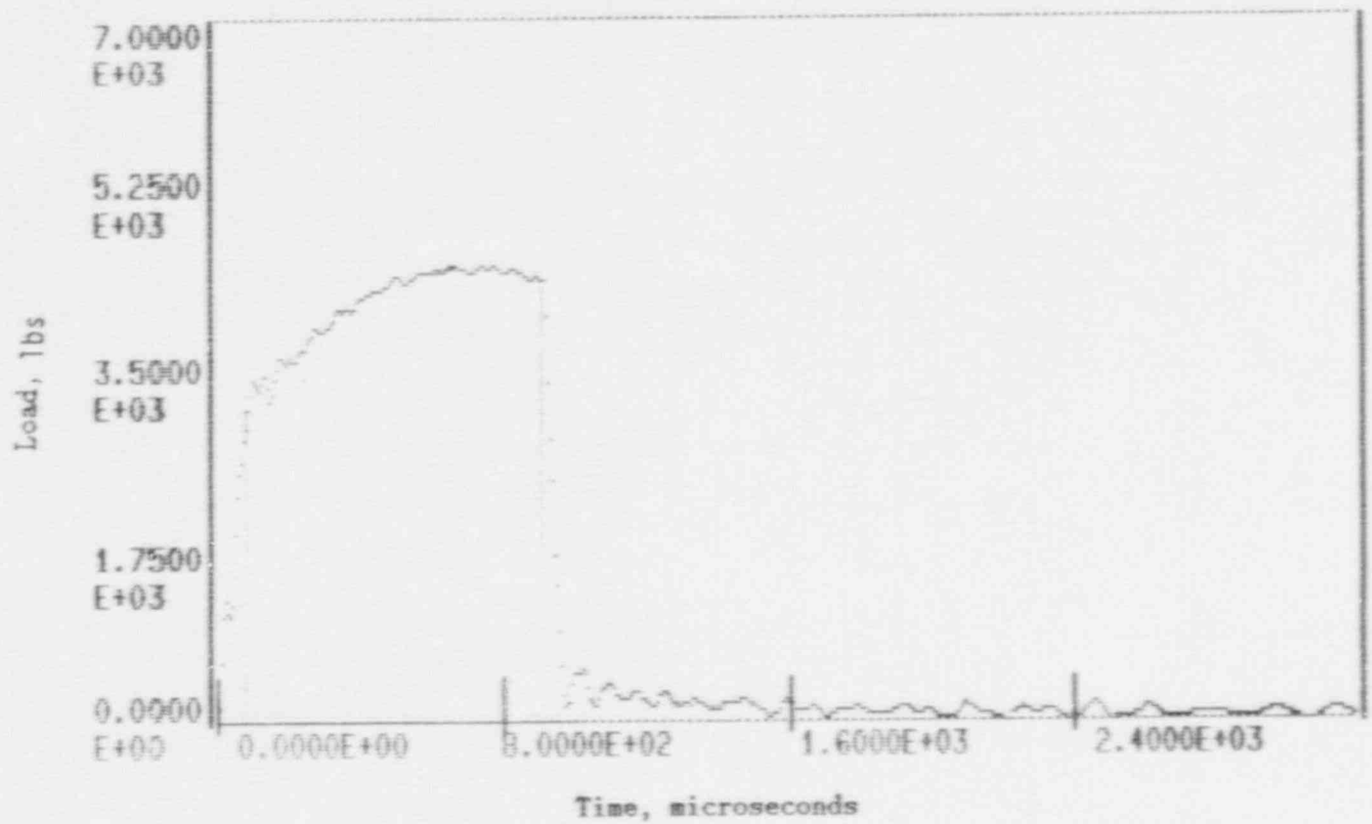

Figure A-22. Load-time record for Specimen FT1.

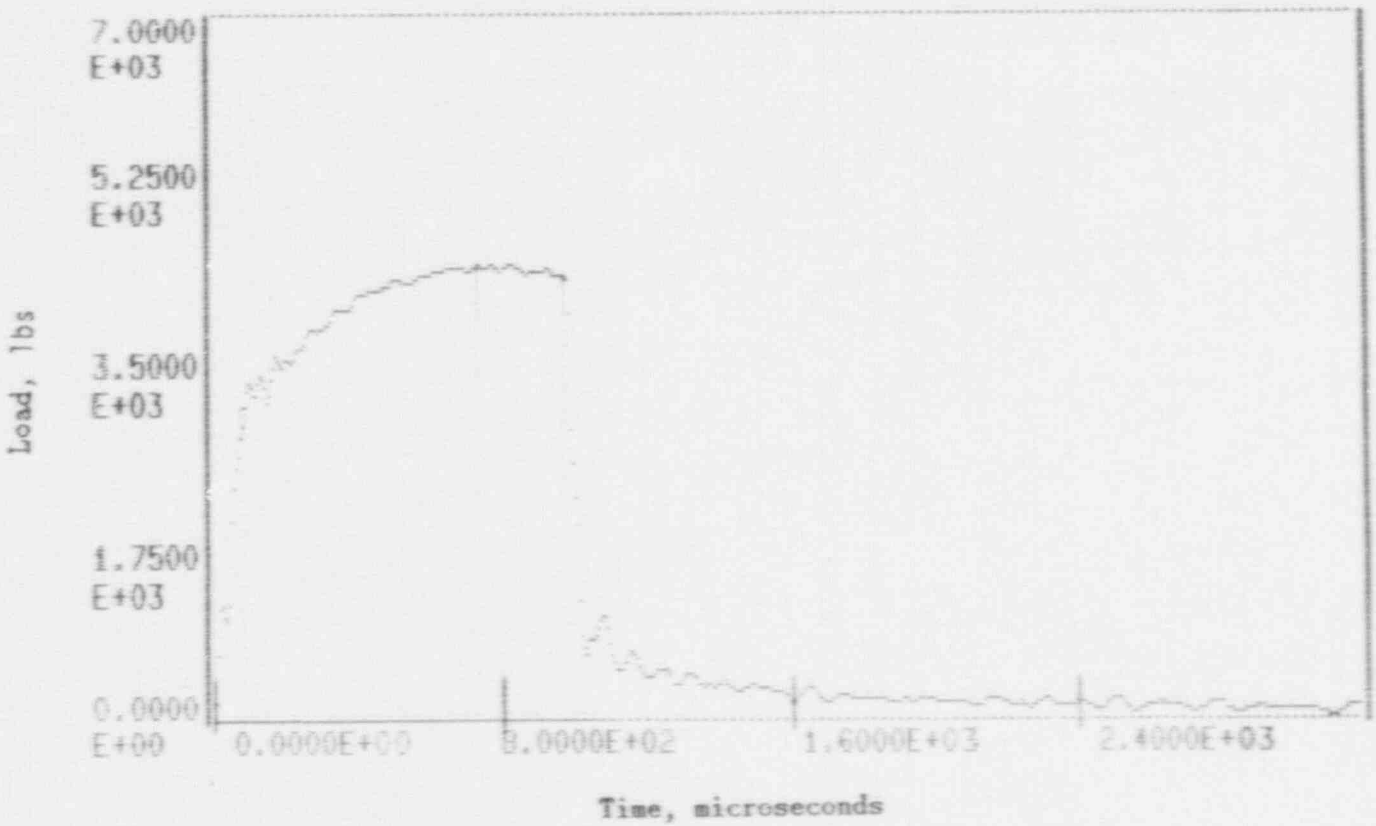

Figure A-23. Load-time record for Specimen FT2.

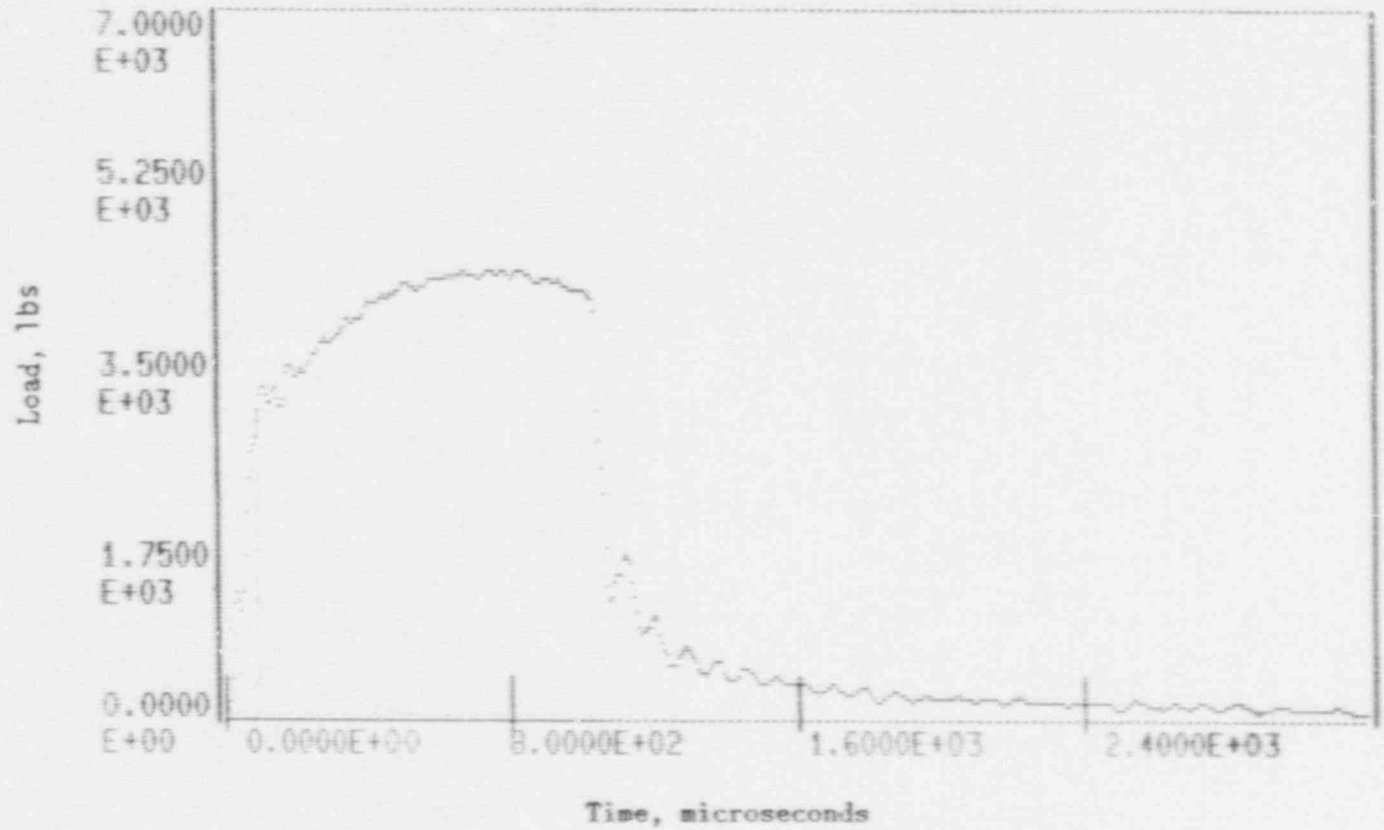

Figure A-24. Load-time record for Specimen FT11.

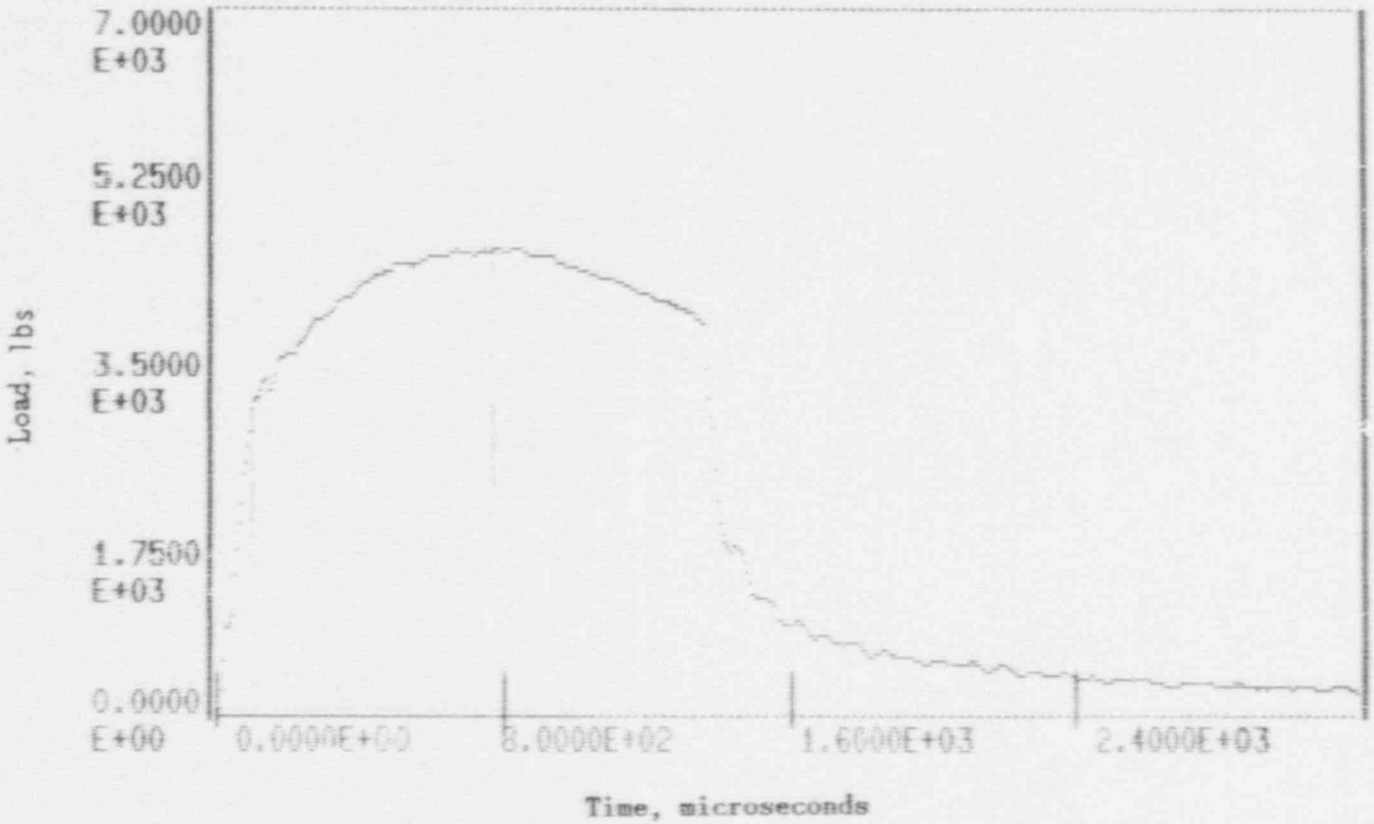

Figure A-25. Load-time record for Specimen FT15.

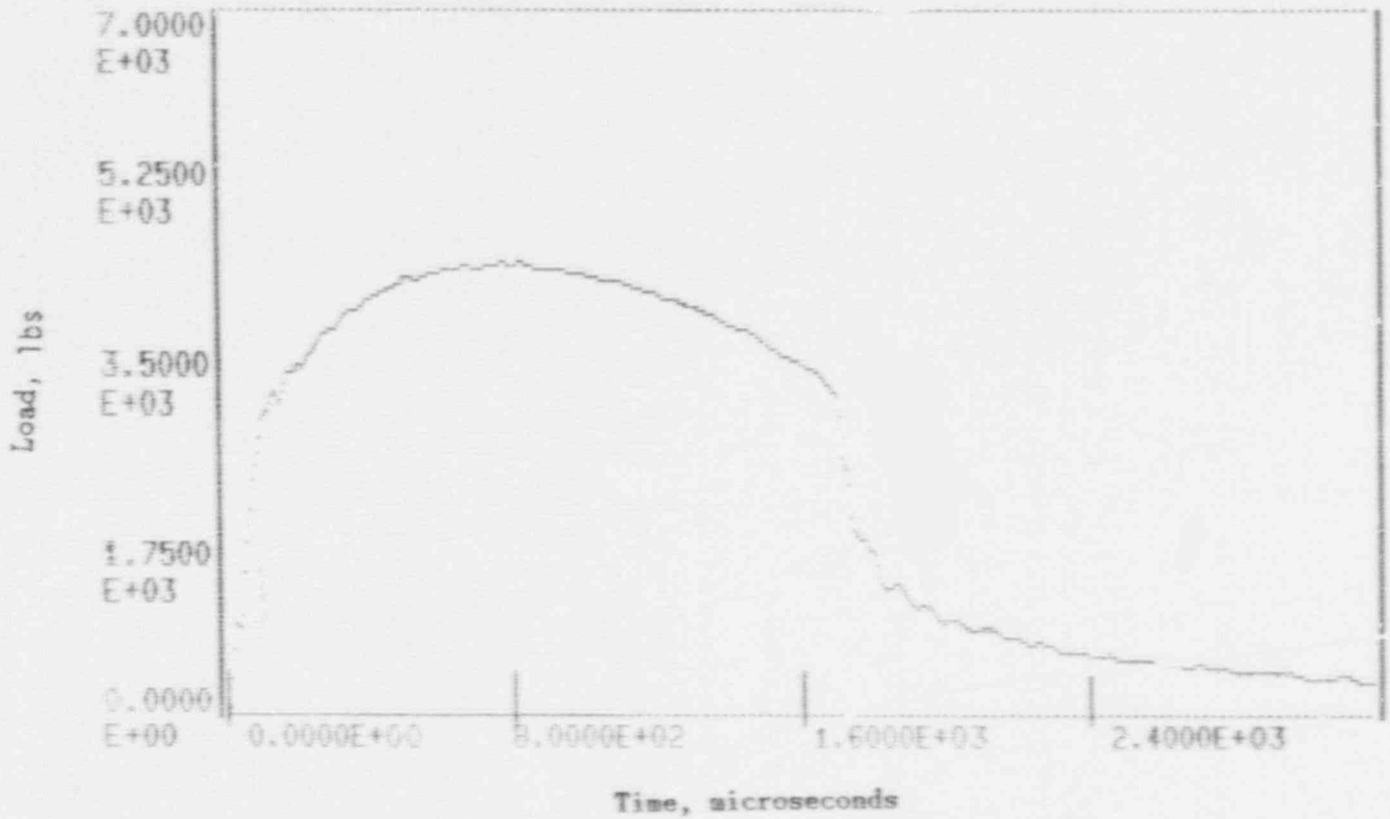

Figure A-26. Load-time record for Specimen FT13.

No record - computer malfunction

Figure A-27. Load-time record for Specimen FT10.

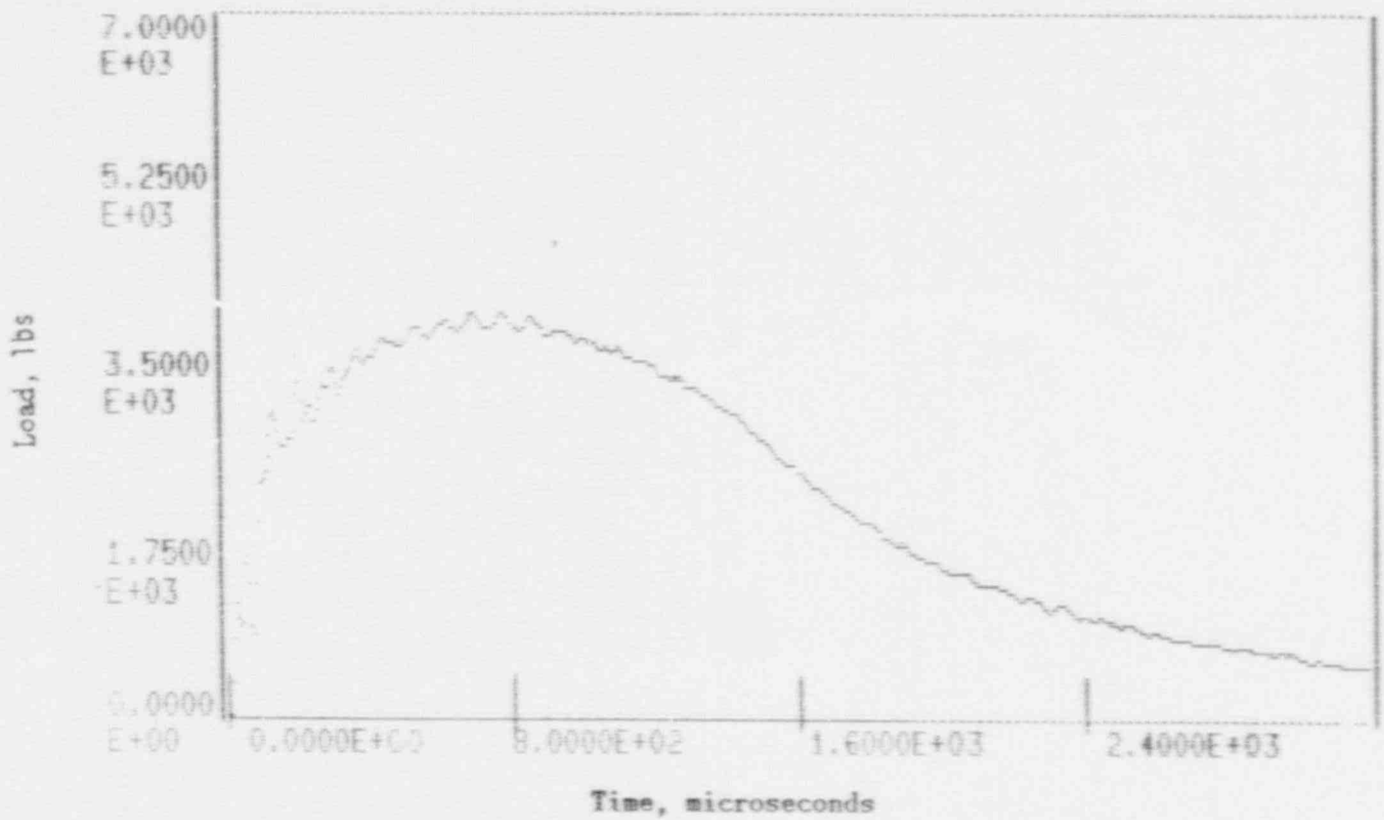

Figure A-28. Load-time record for Specimen FT5.

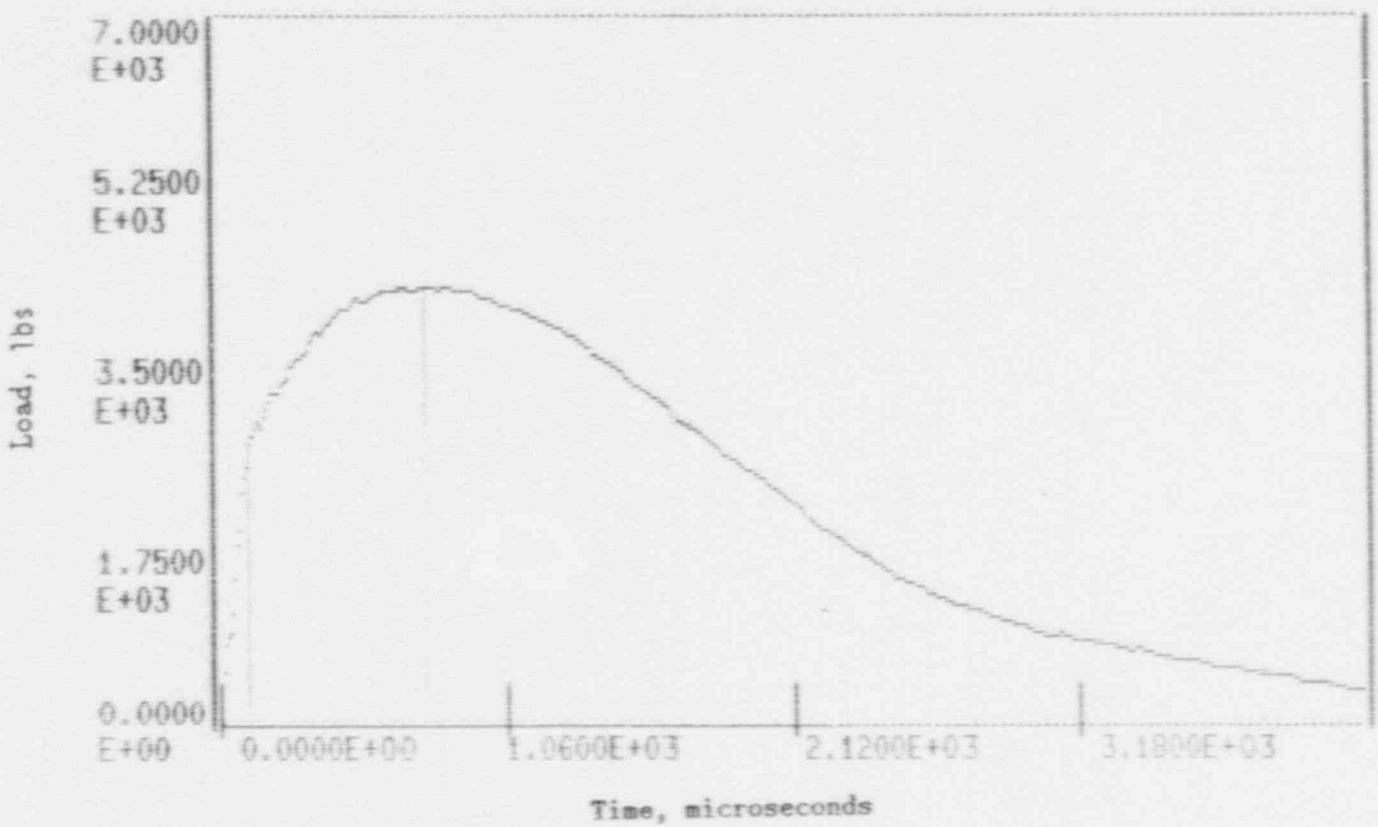

Figure A-29. Load-time record for Specimen FT9.

No record - computer malfunction

Figure A-30. Load-time record for Specimen FT12.

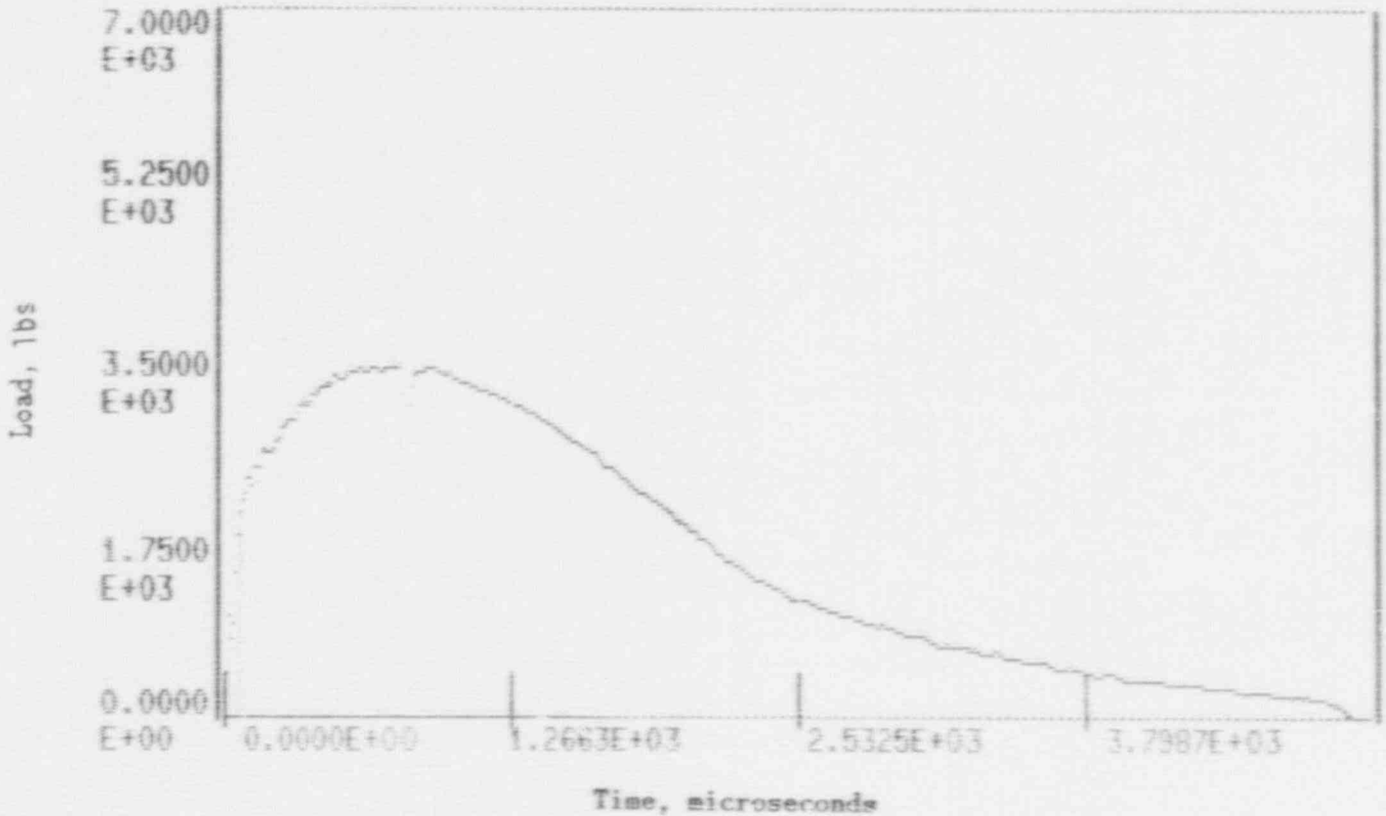

Figure A-31. Load-time record for Specimen FT7.

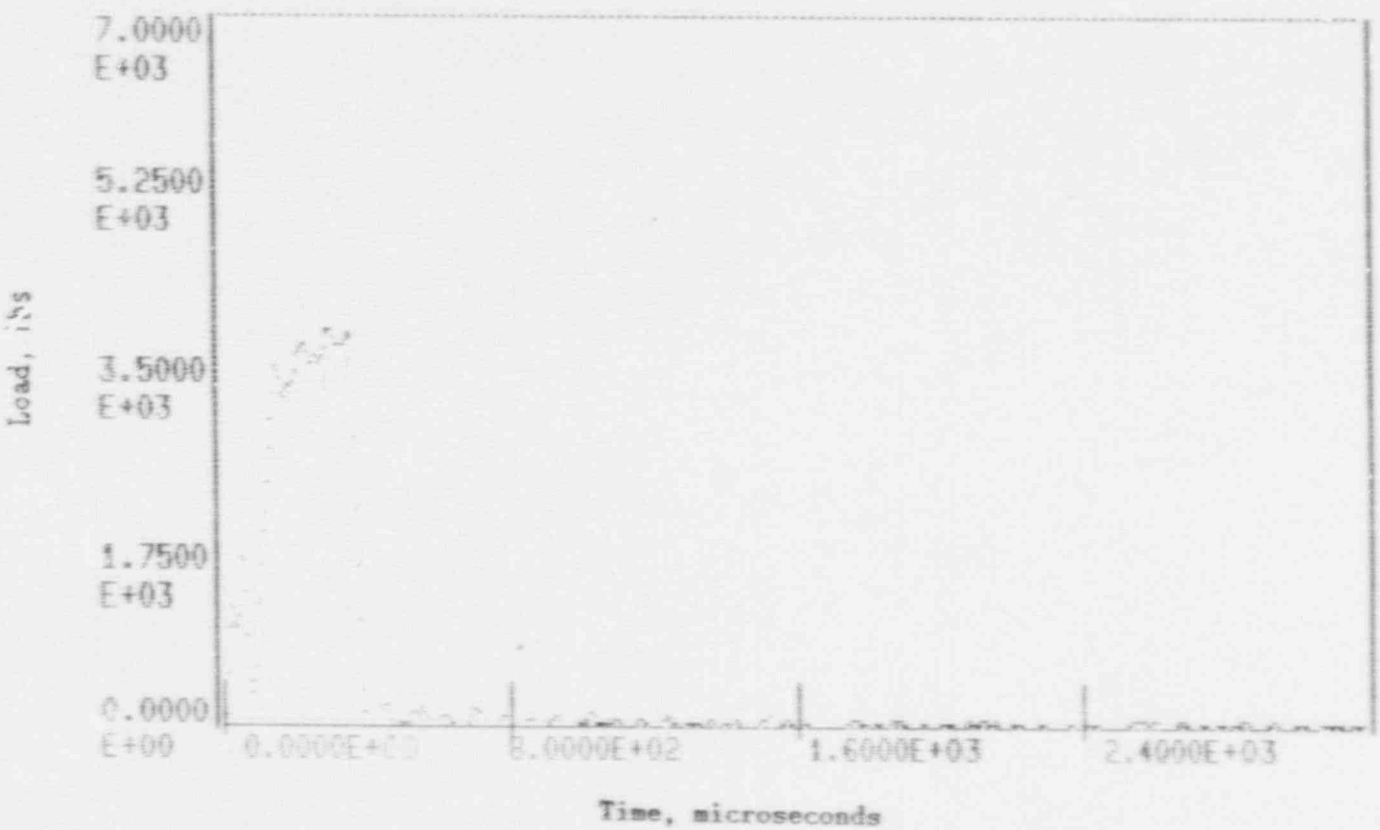

Figure A-32. Load-time record for Specimen FW11.

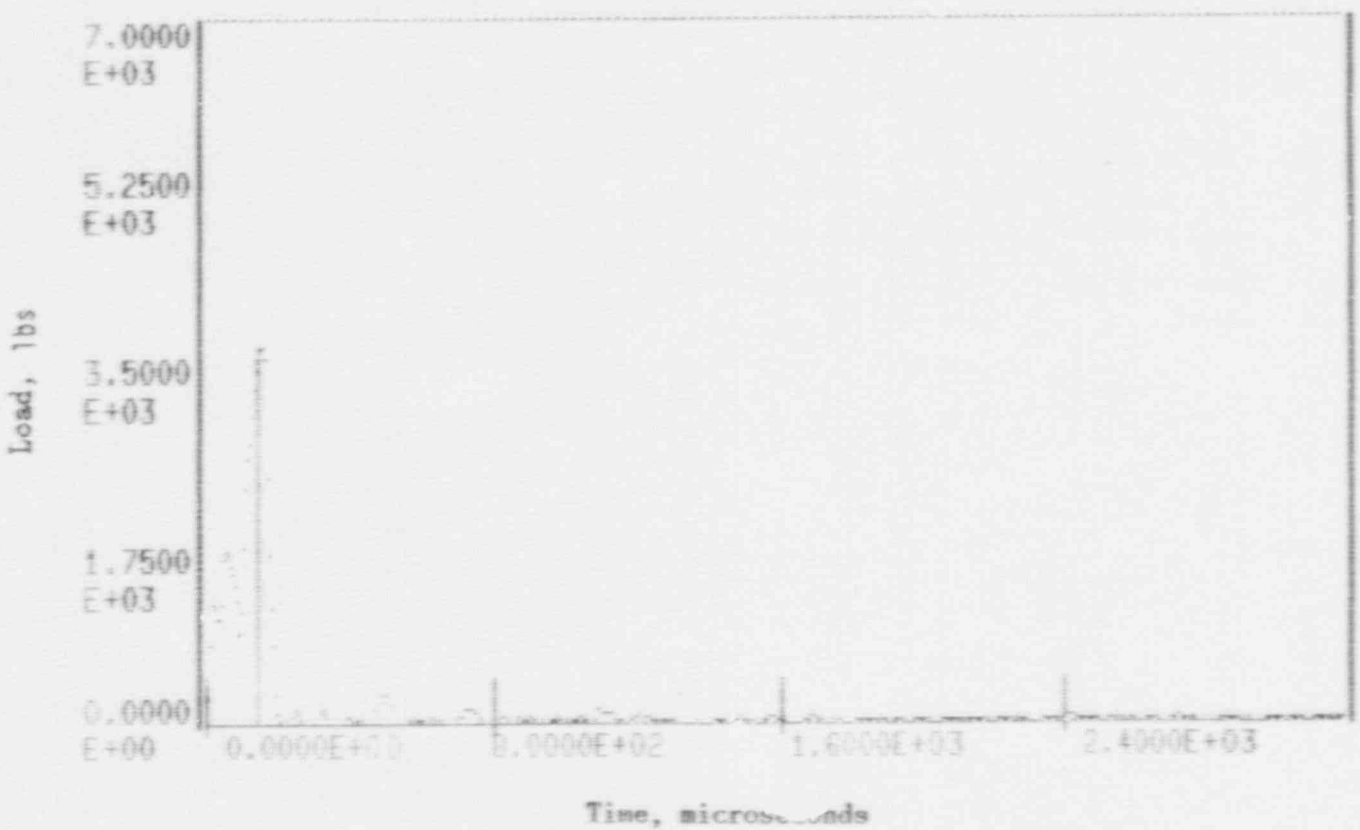

Figure A-33. Load-time record for Specimen FW8.

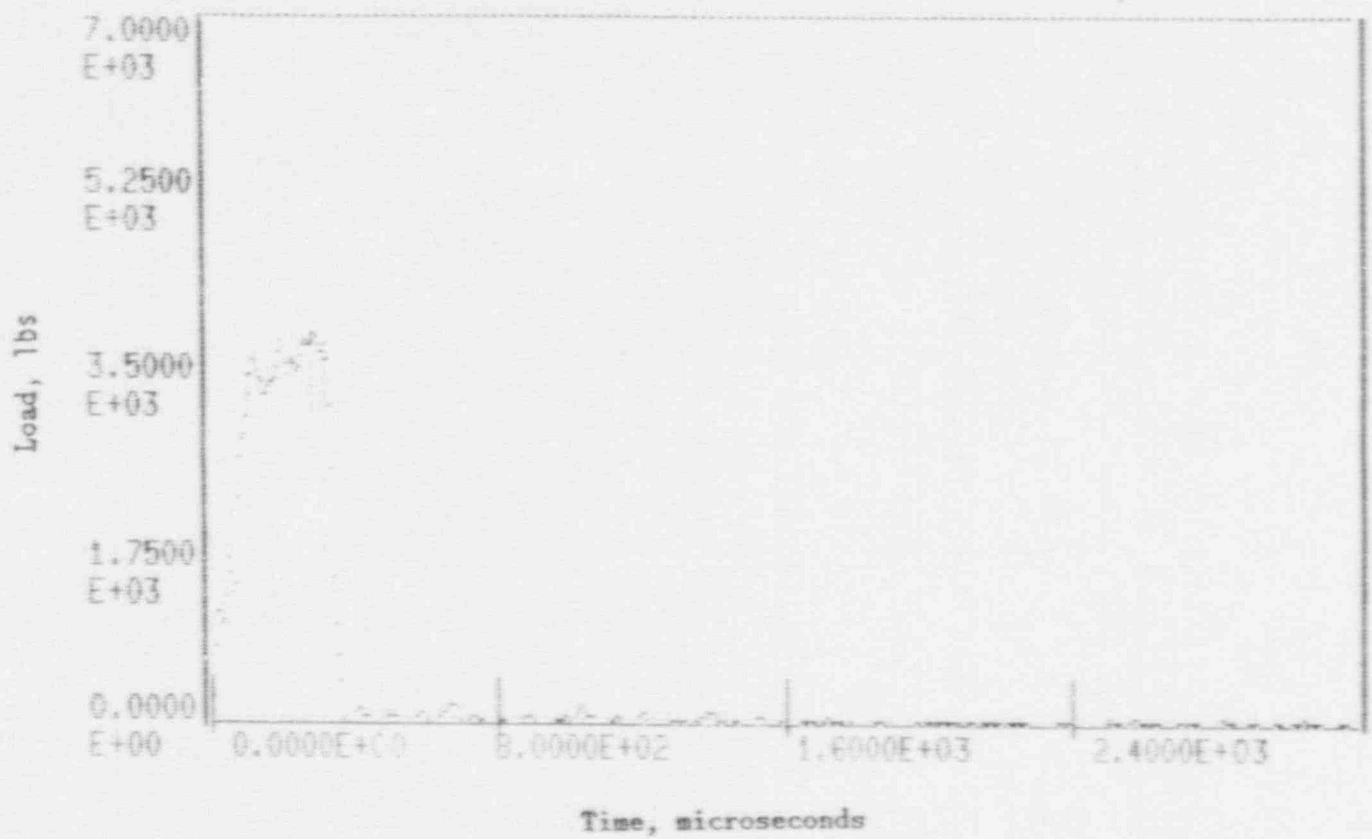

Figure A-34. Load-time record for Specimen FW7.

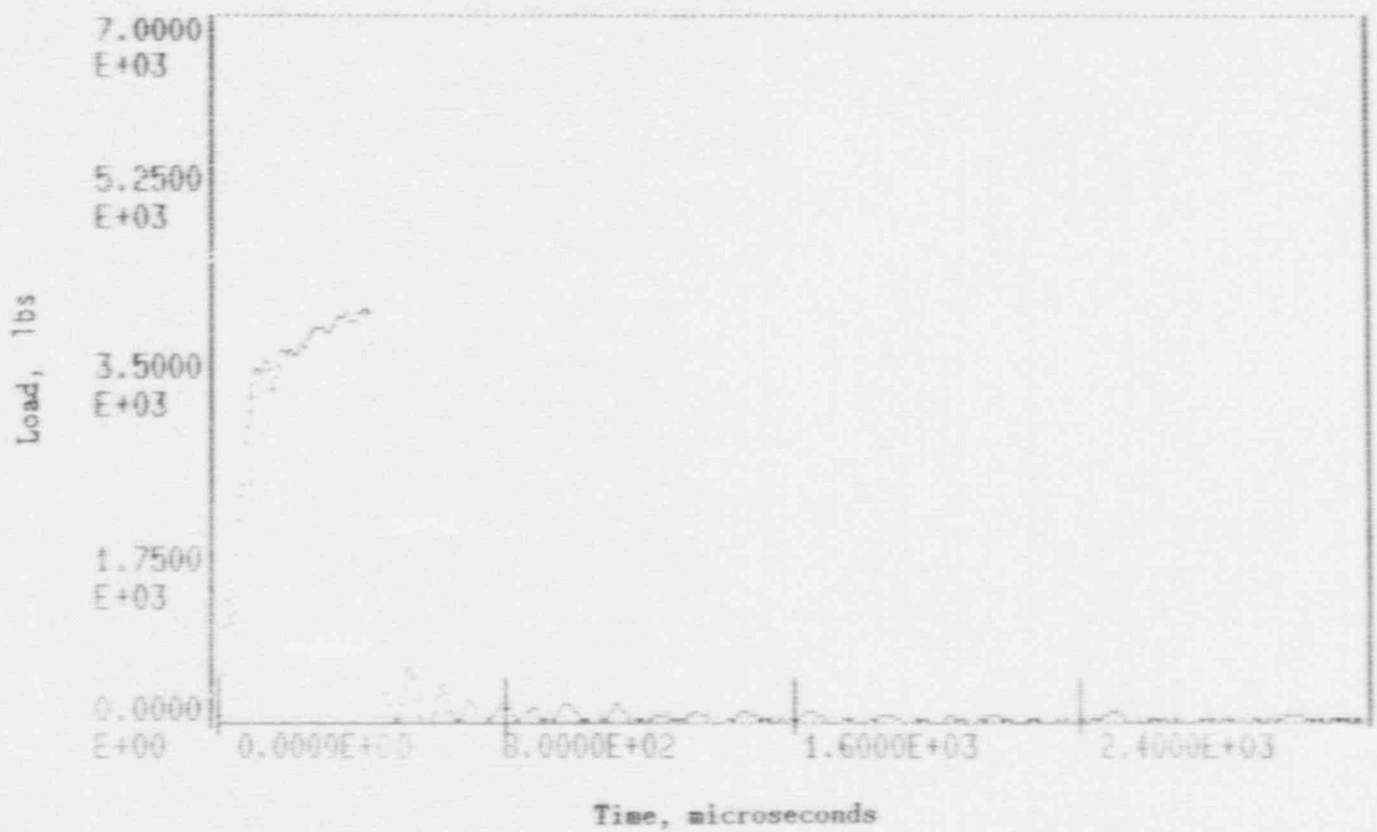

Figure A-35. Load-time record for Specimen FW5.

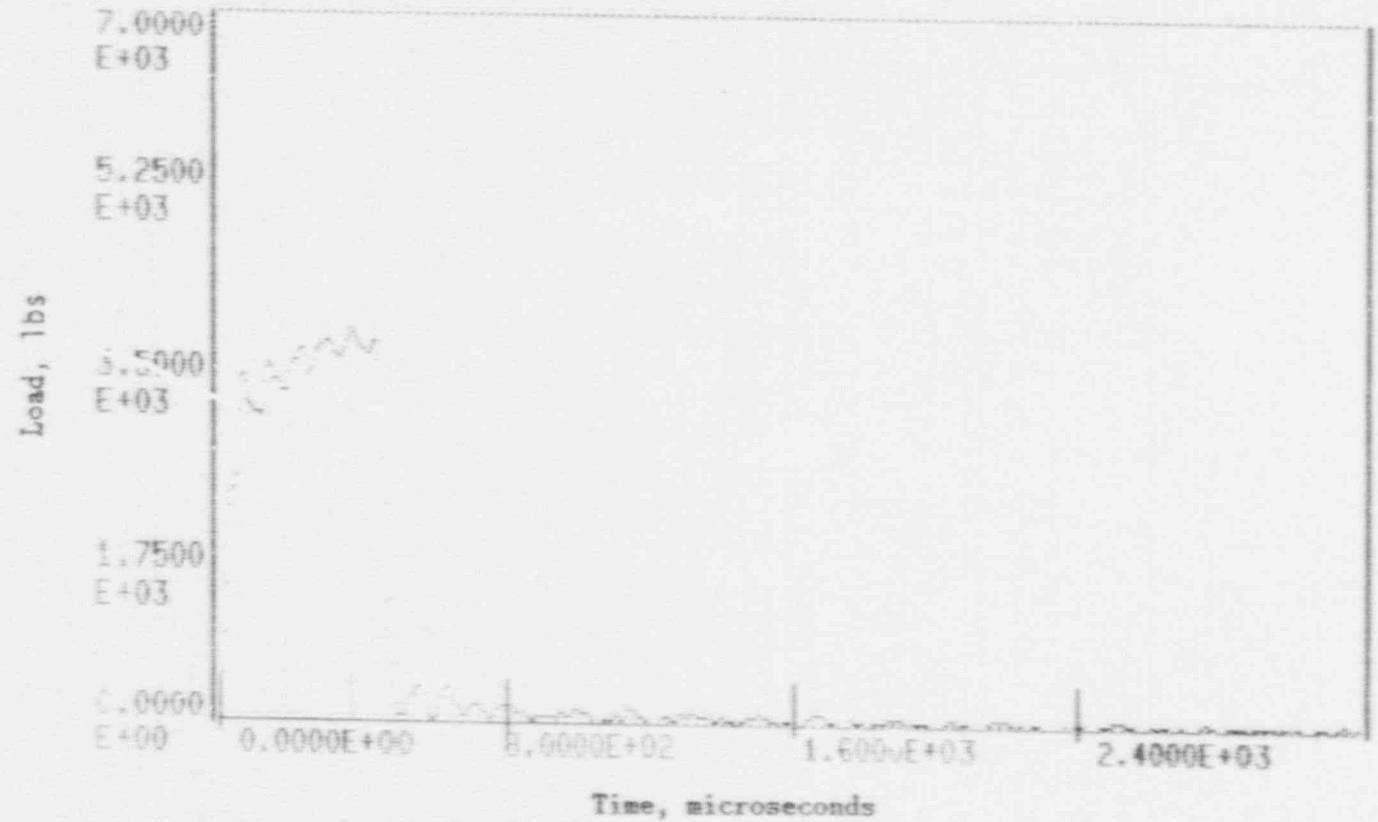

Figure A-36. Load-time record for Specimen FW1.

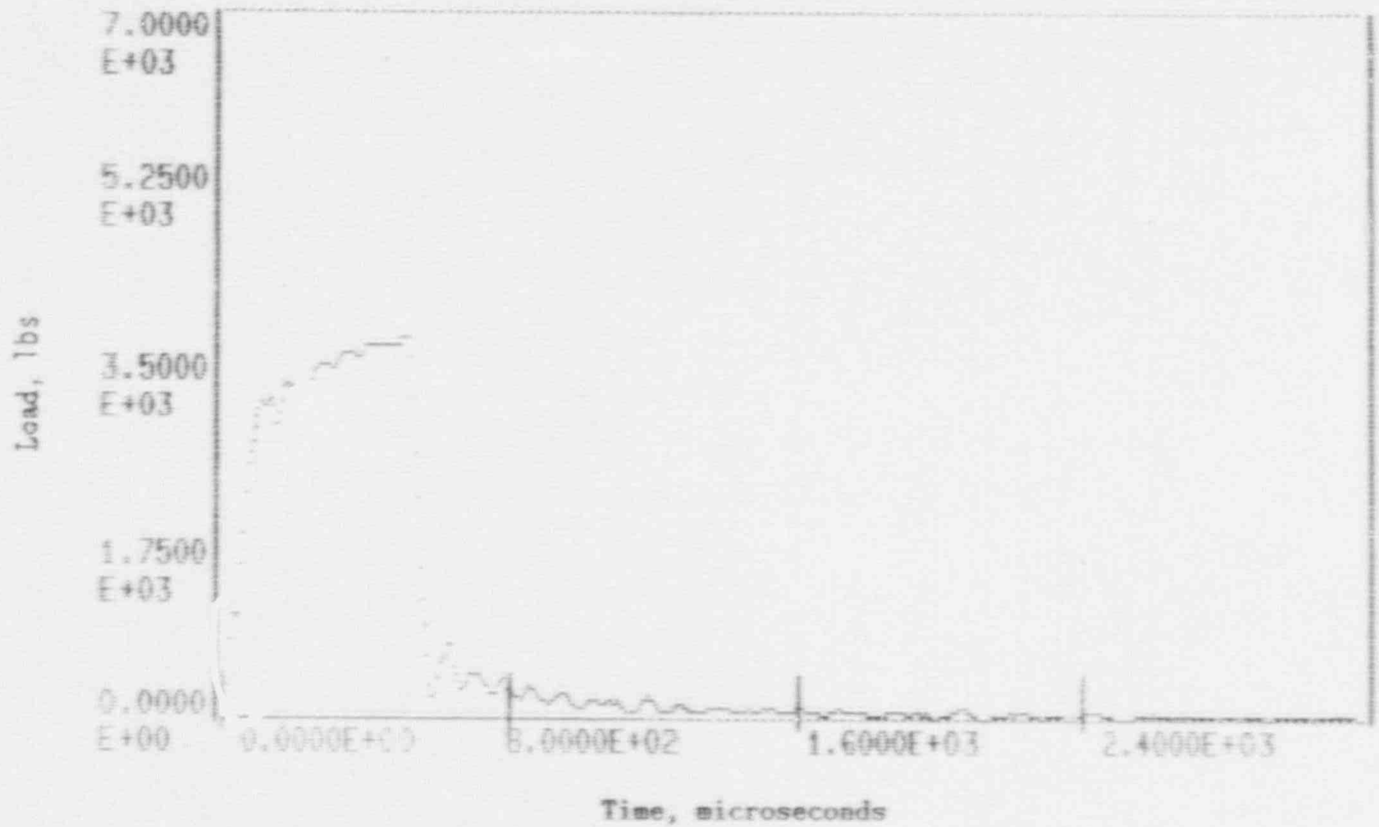

Figure A-37. Load-time record for Specimen FW3.

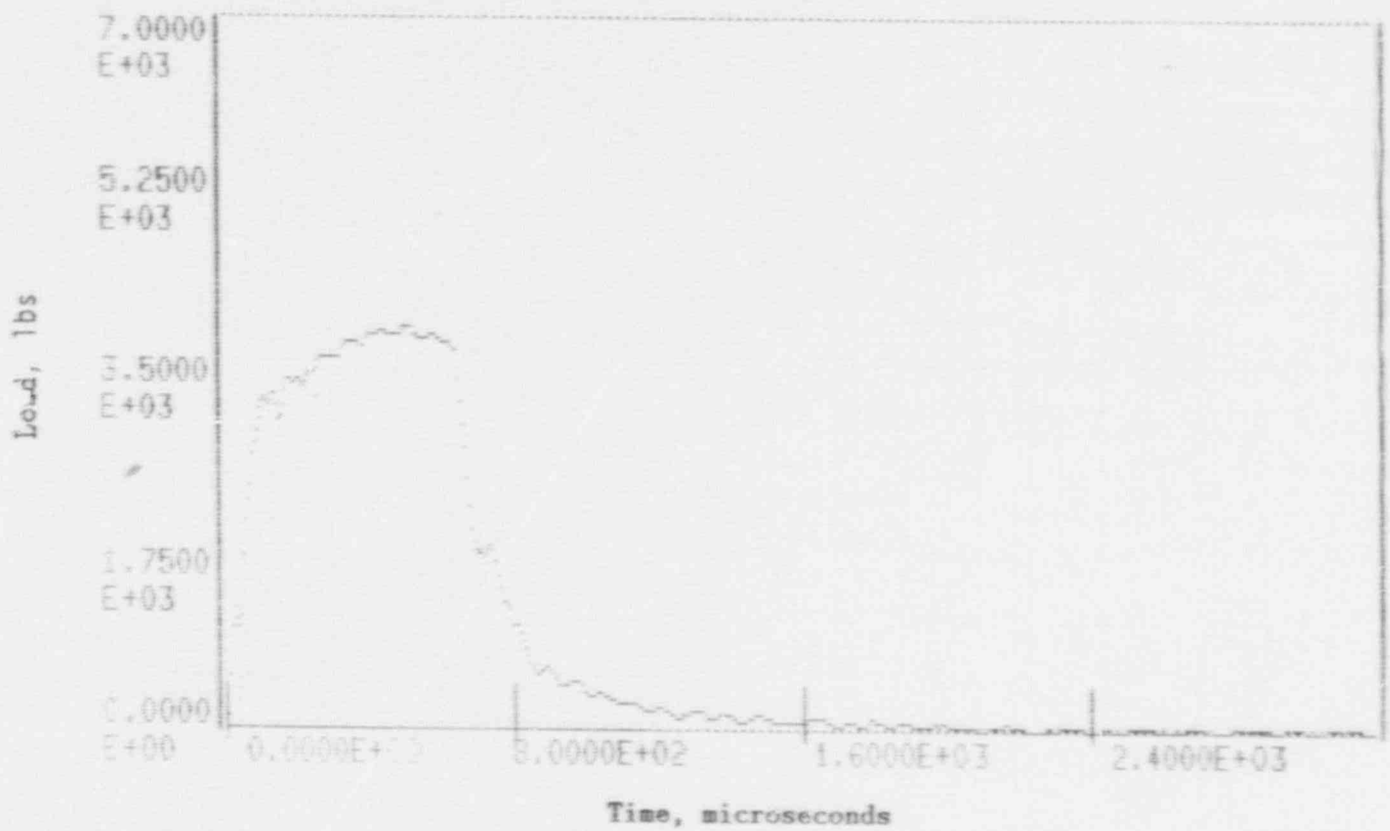

Figure A-38. Load-time record for Specimen FW12.

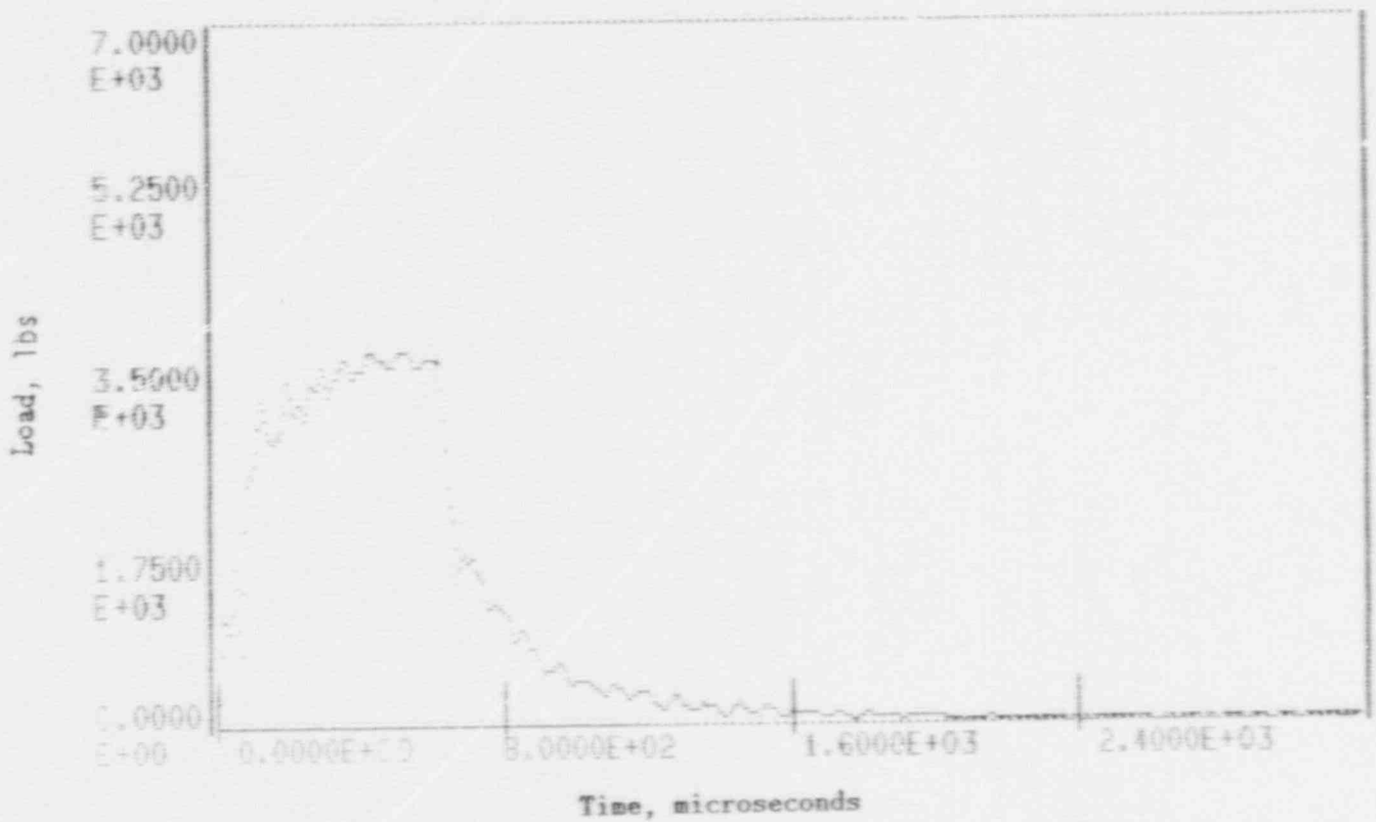

Figure A-39. Load-time record for Specimen FW14.

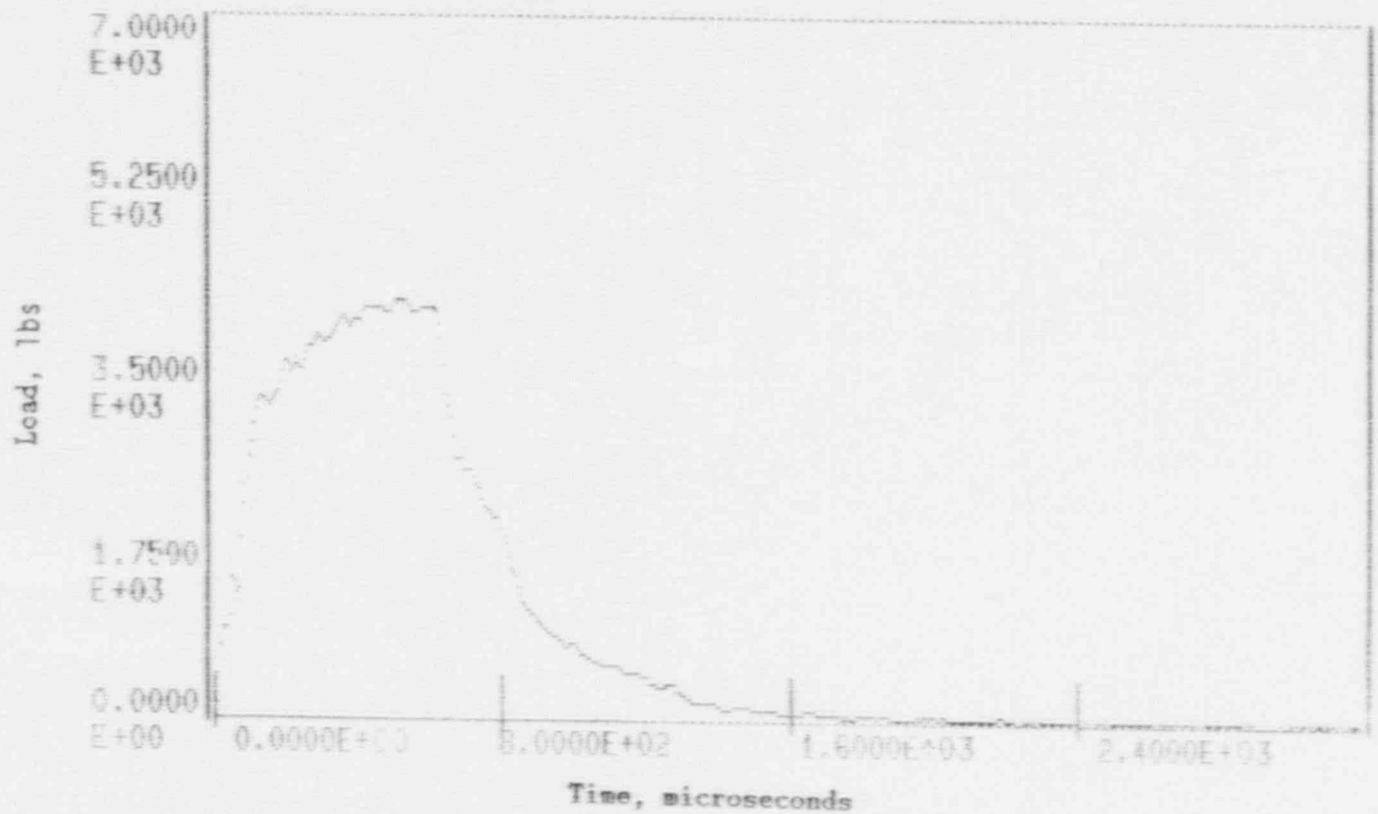

Figure A-40. Load-time record for Specimen FW9.

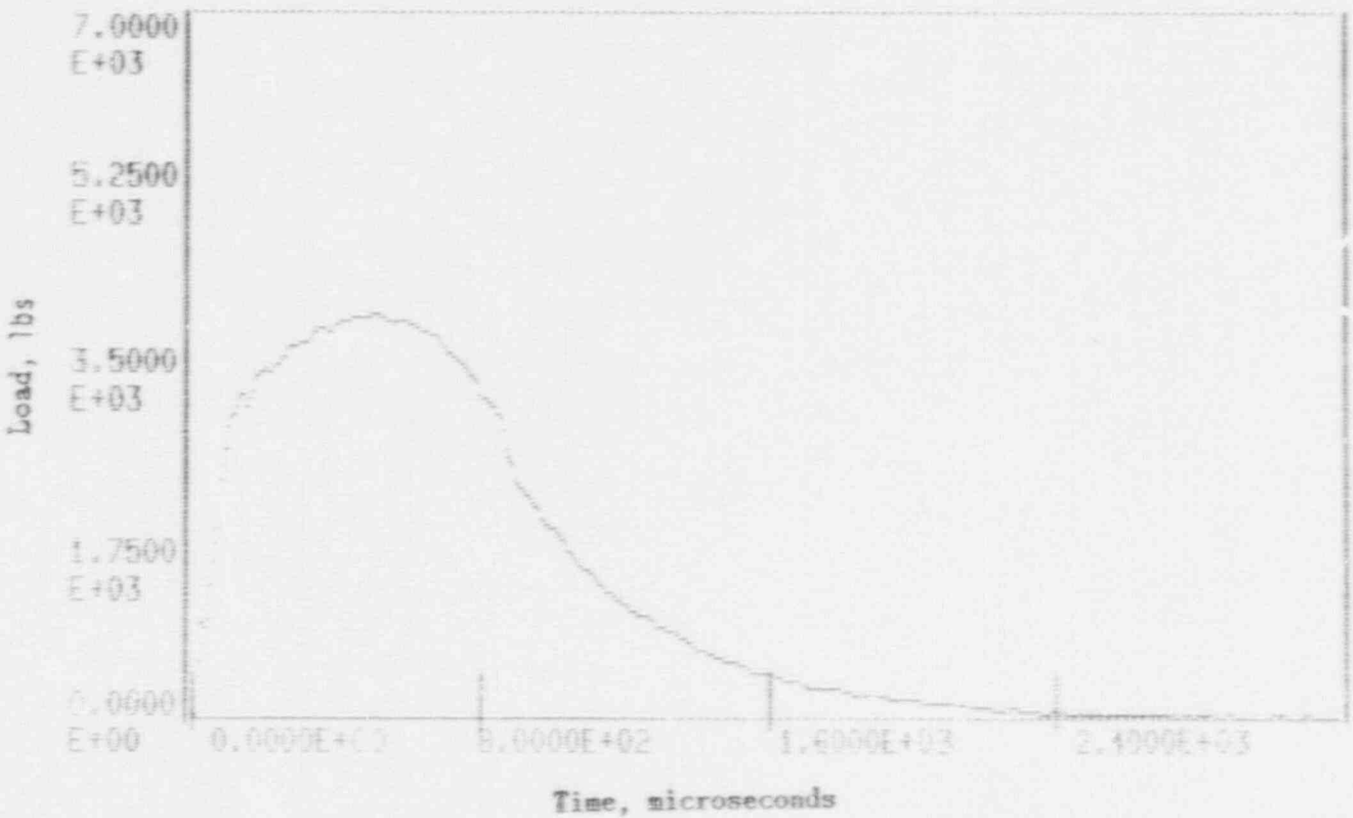

Figure A-41. Load-time record for Specimen FW6.

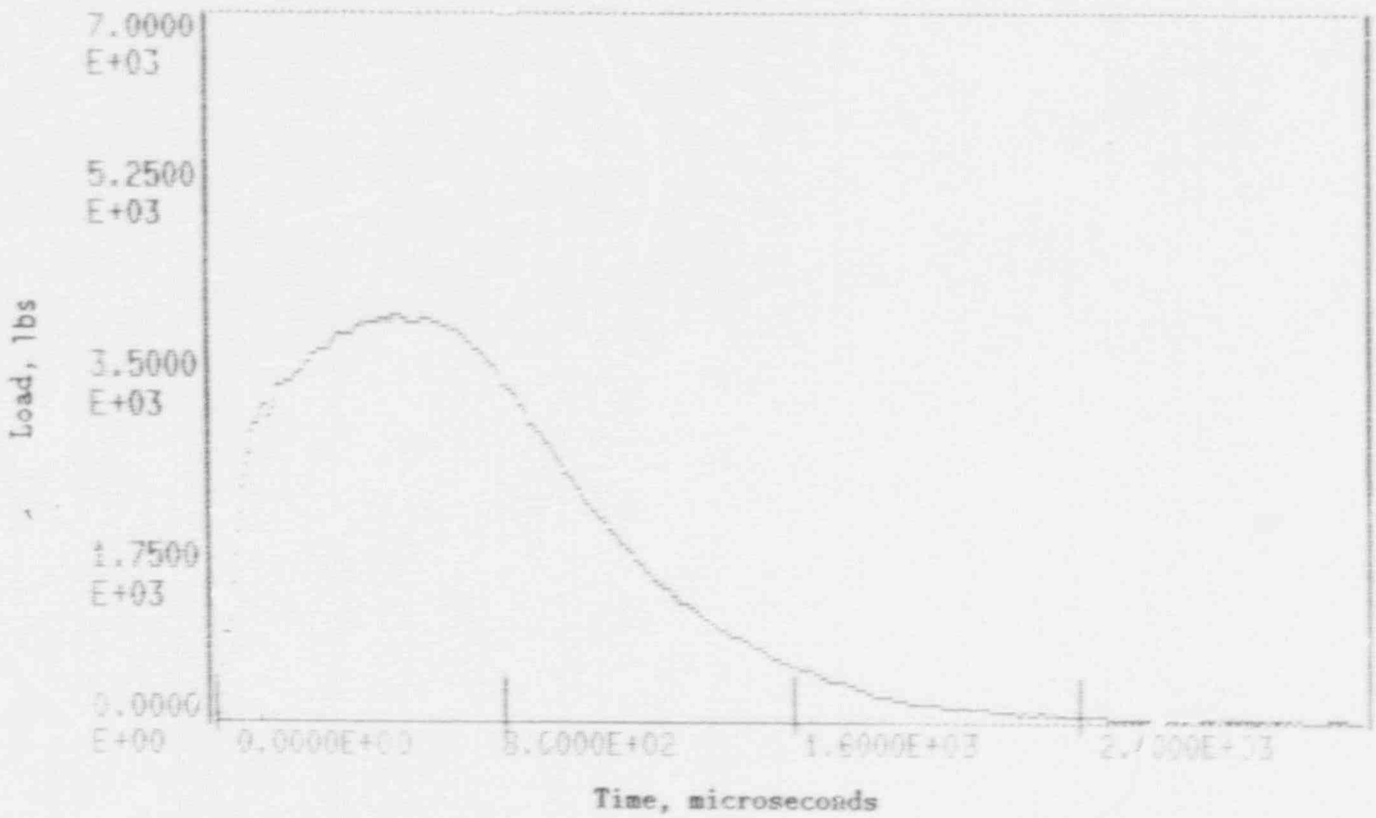

Figure A-42. Load-time record for Specimen FW4.

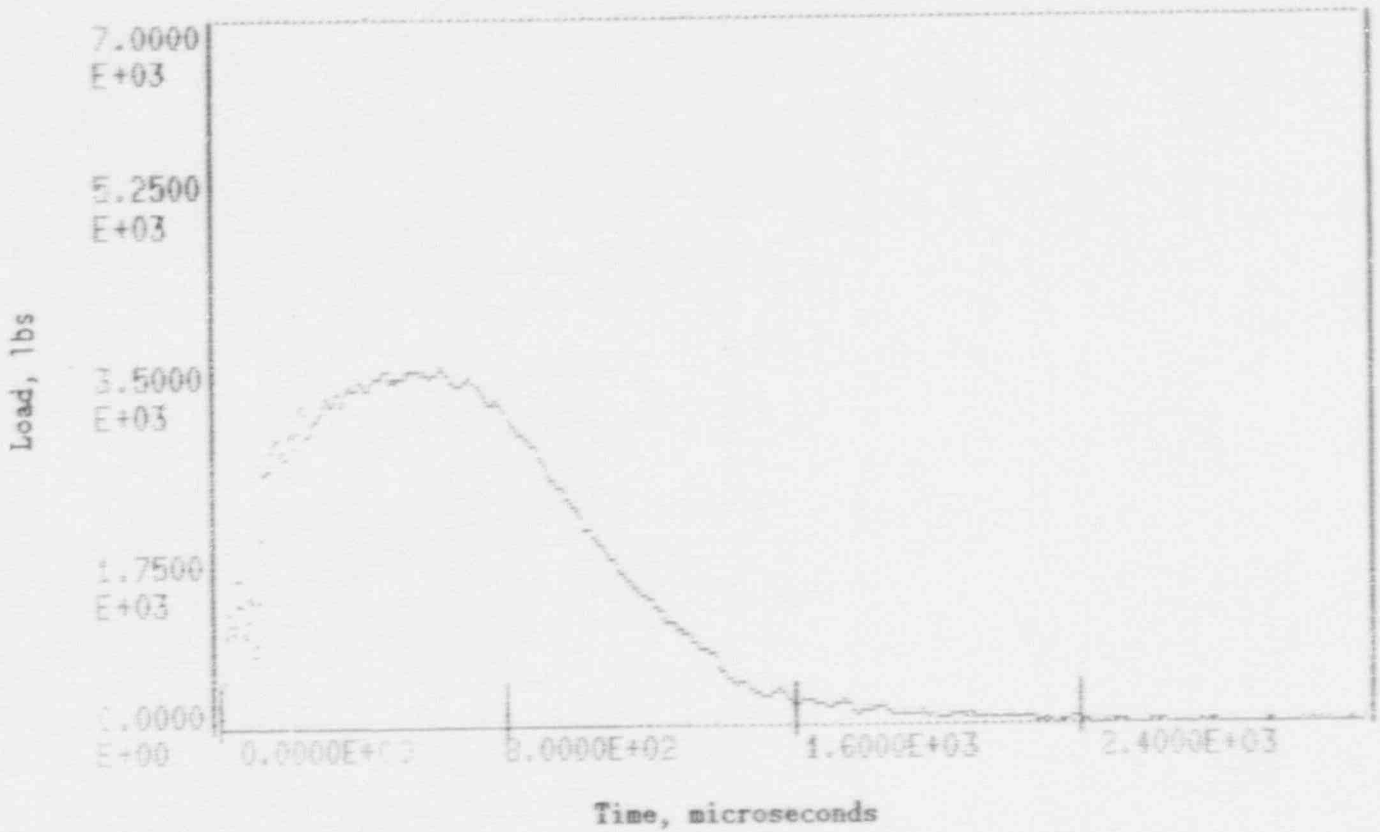

Figure A-43. Load-time record for Specimen FW10.

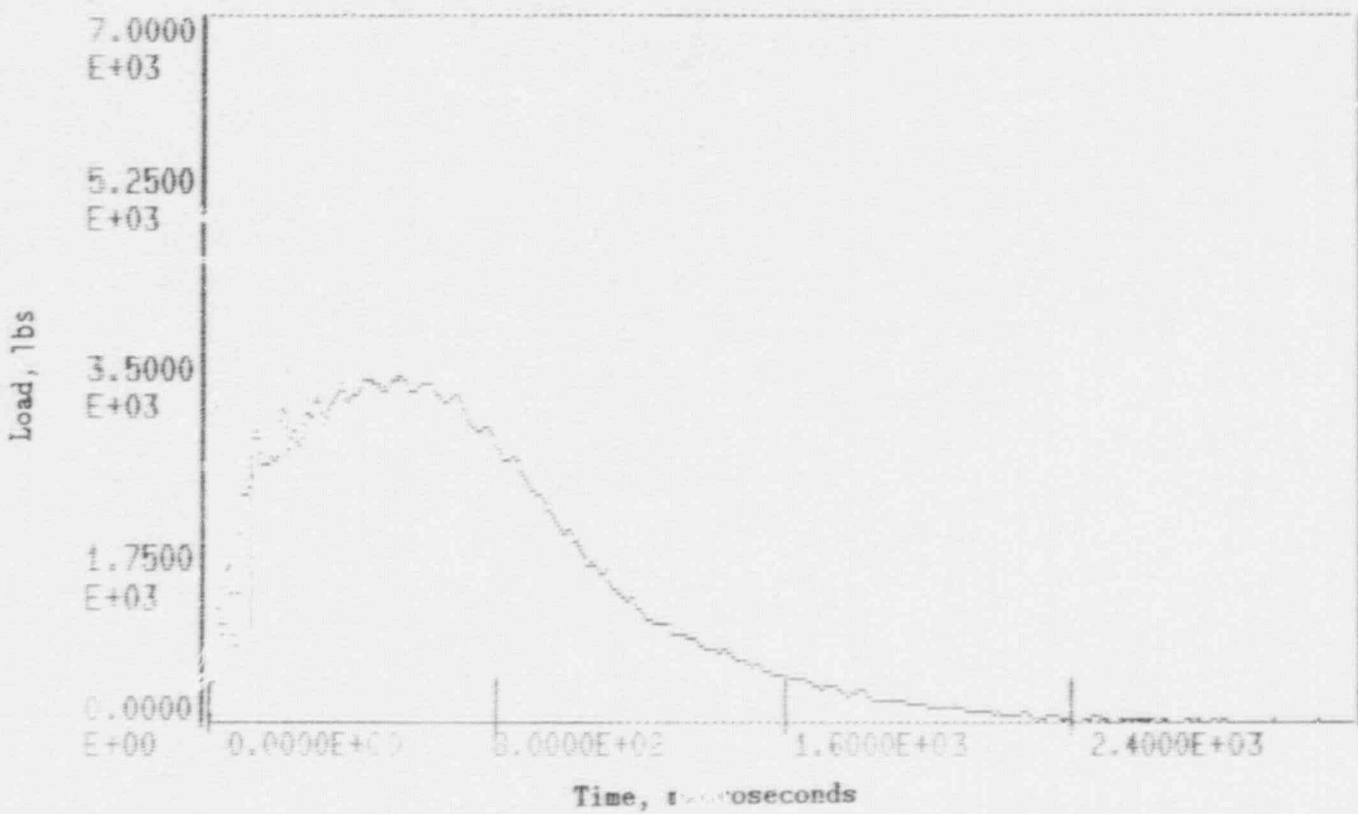

Figure A-44. Load-time record for Specimen FW2.

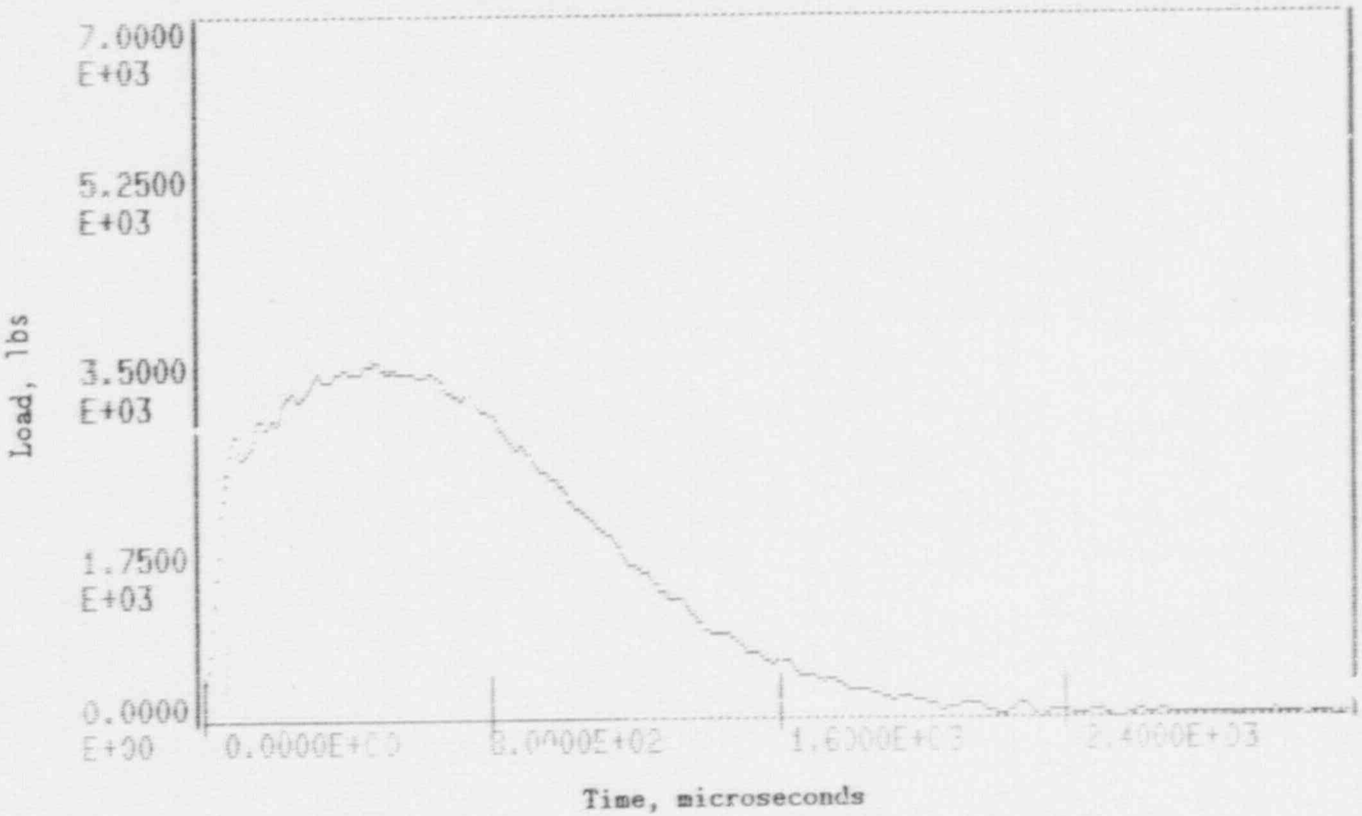

Figure A-45. Load-time record for Specimen FW15.

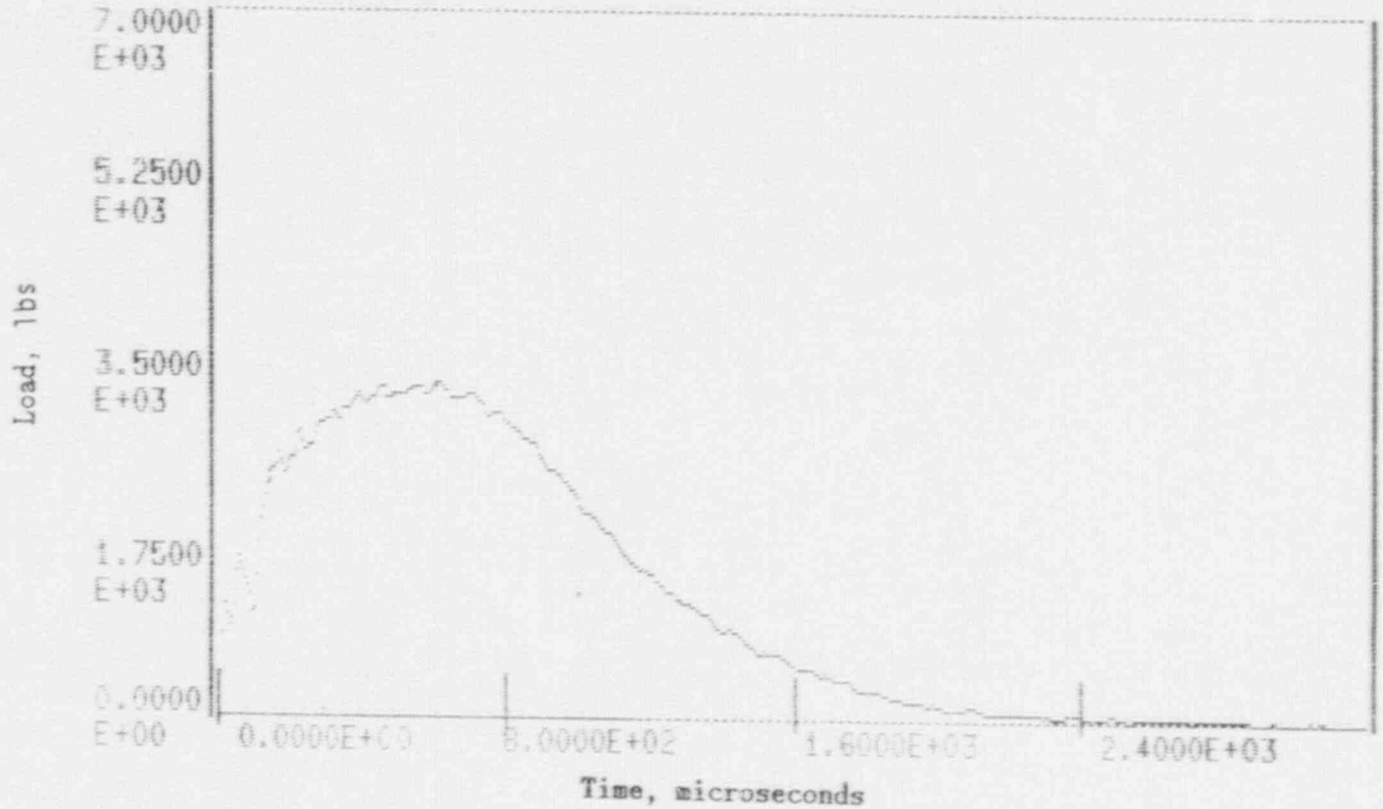

Figure A-46. Load-time record for Specimen FW13.

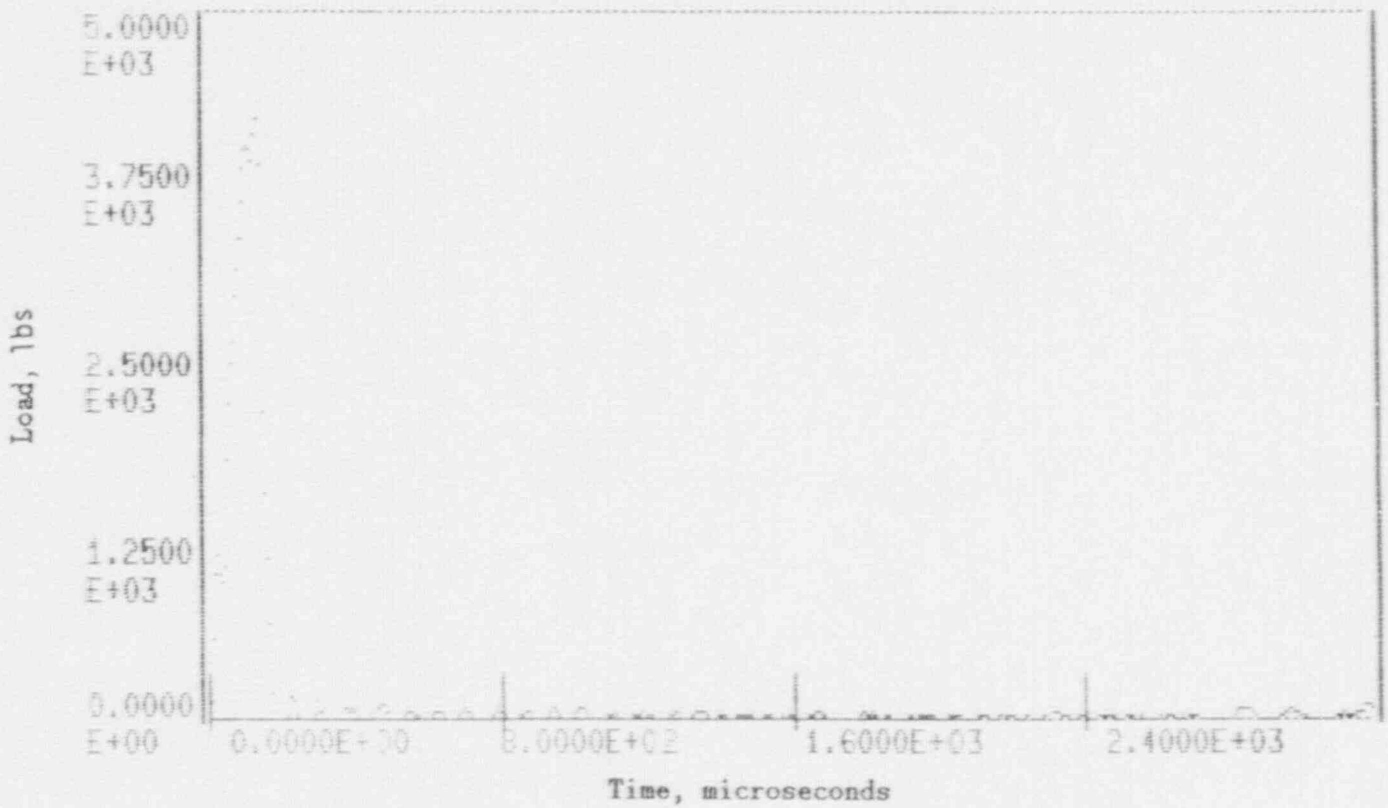

Figure A-47. Load-time record for specimen FH3.

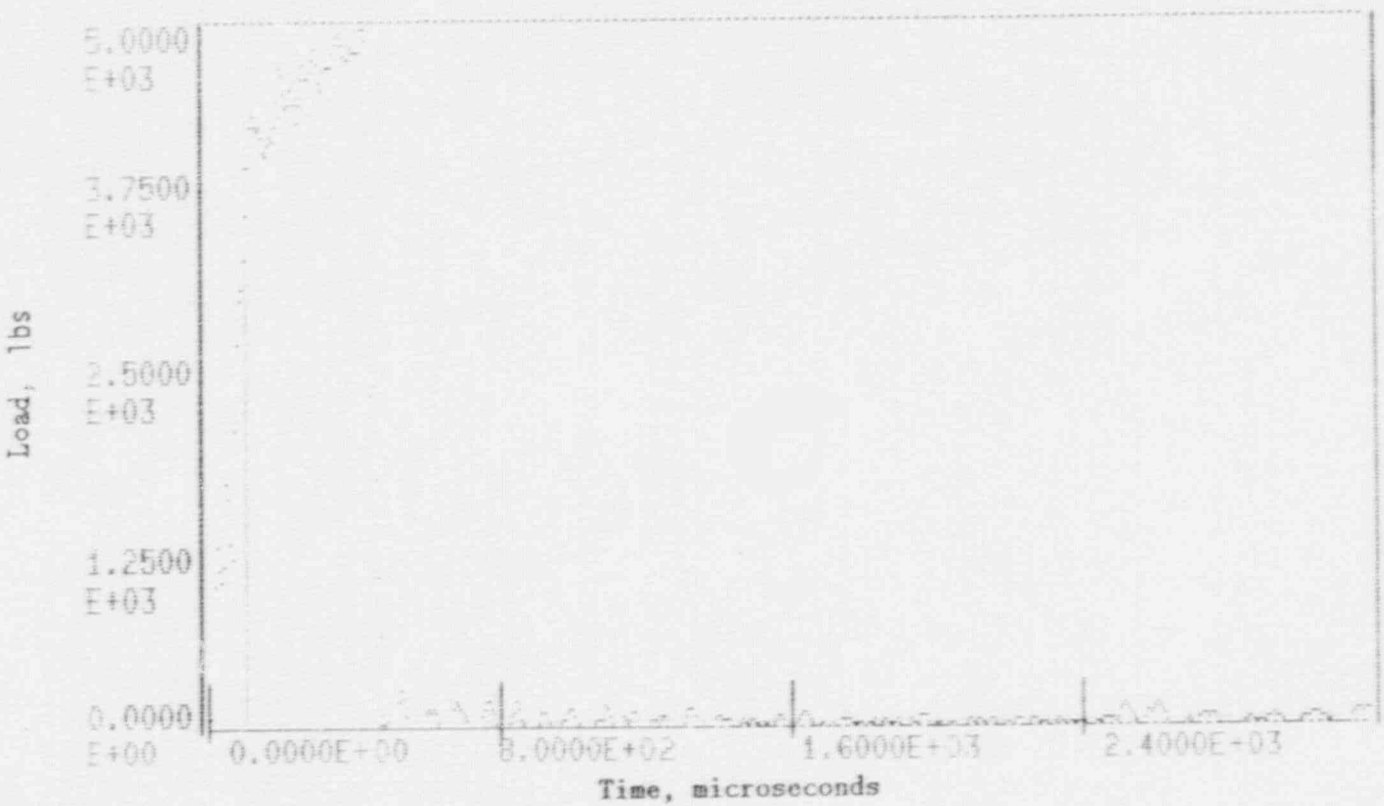

Figure A-48. Load-time record for Specimen FH8.

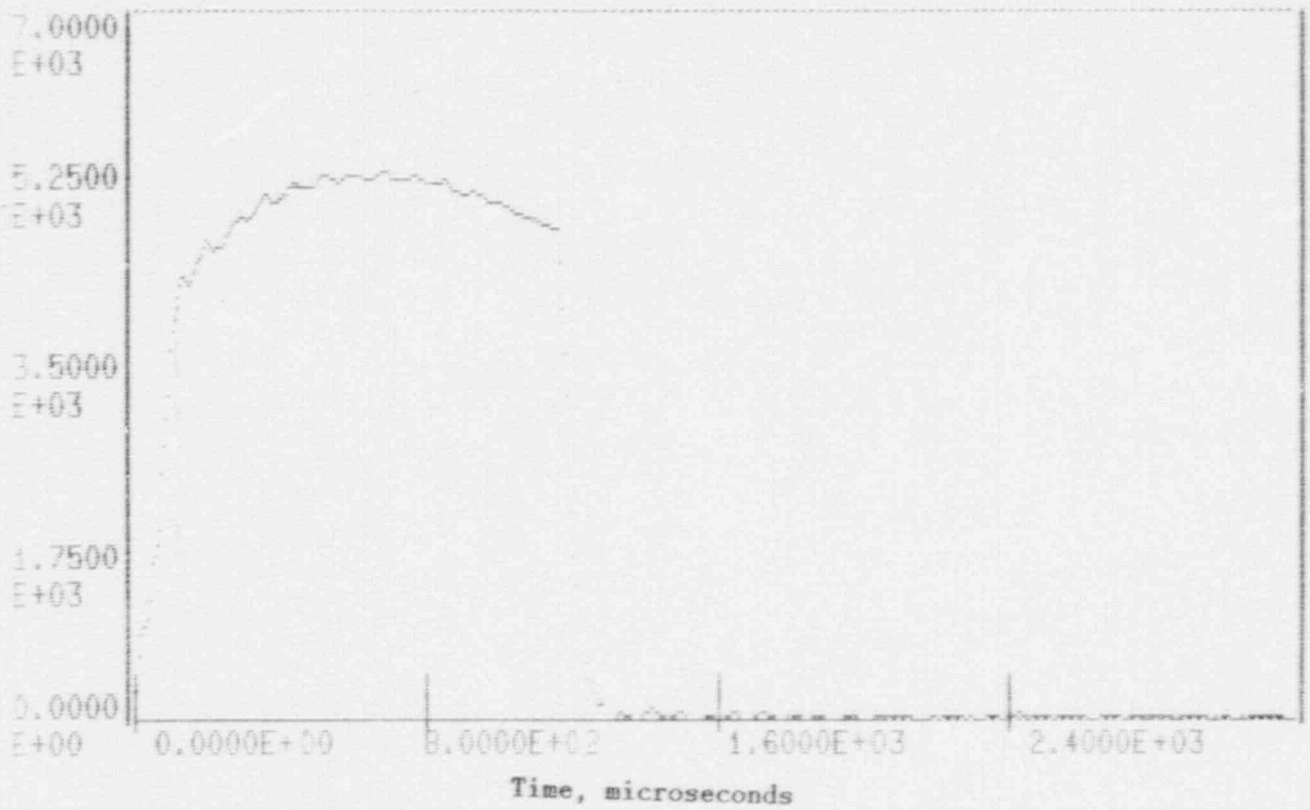

Figure A-49. Load-time record for Specimen FH4.

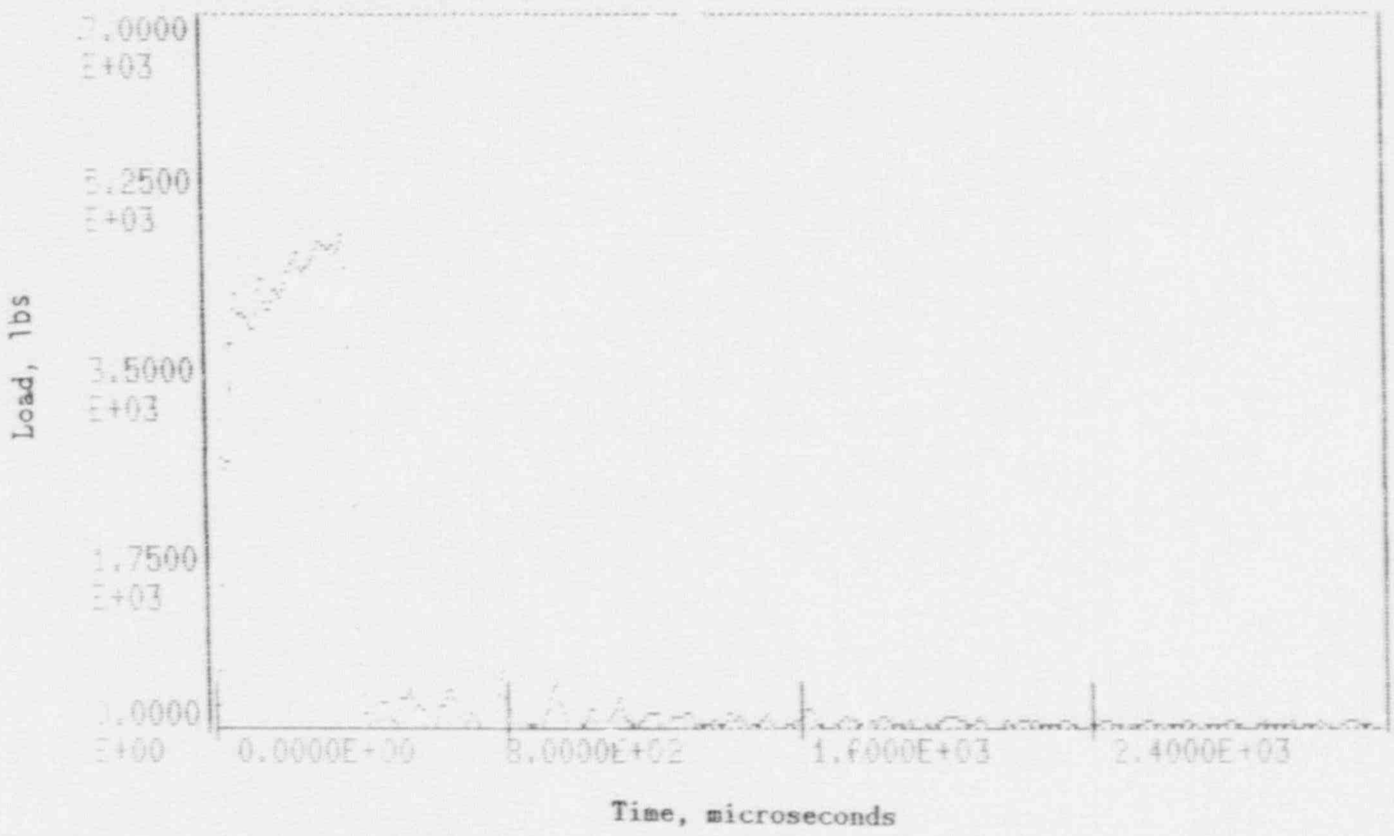

Figure A-50. Load-time record for Specimen FH6.

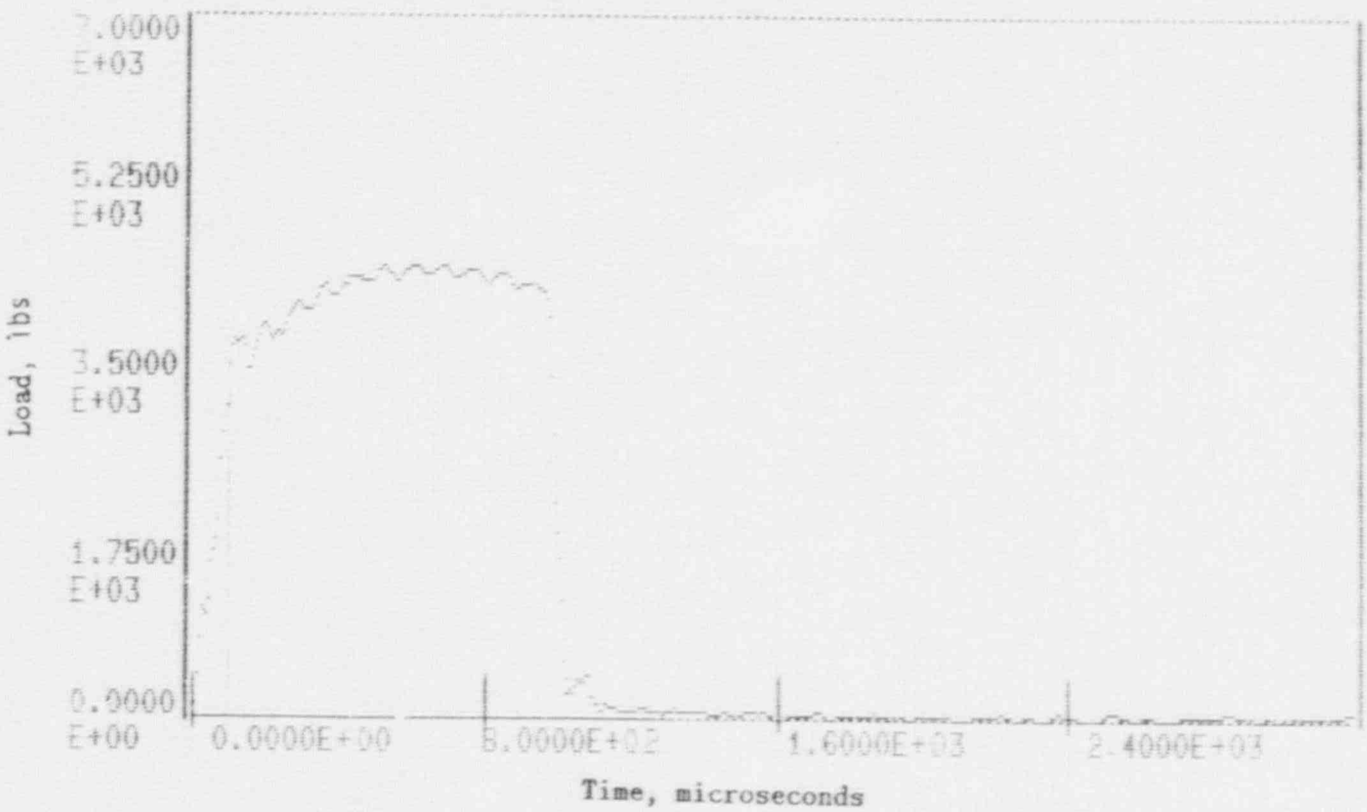

Figure A-51. Load-time record for Specimen FH15.

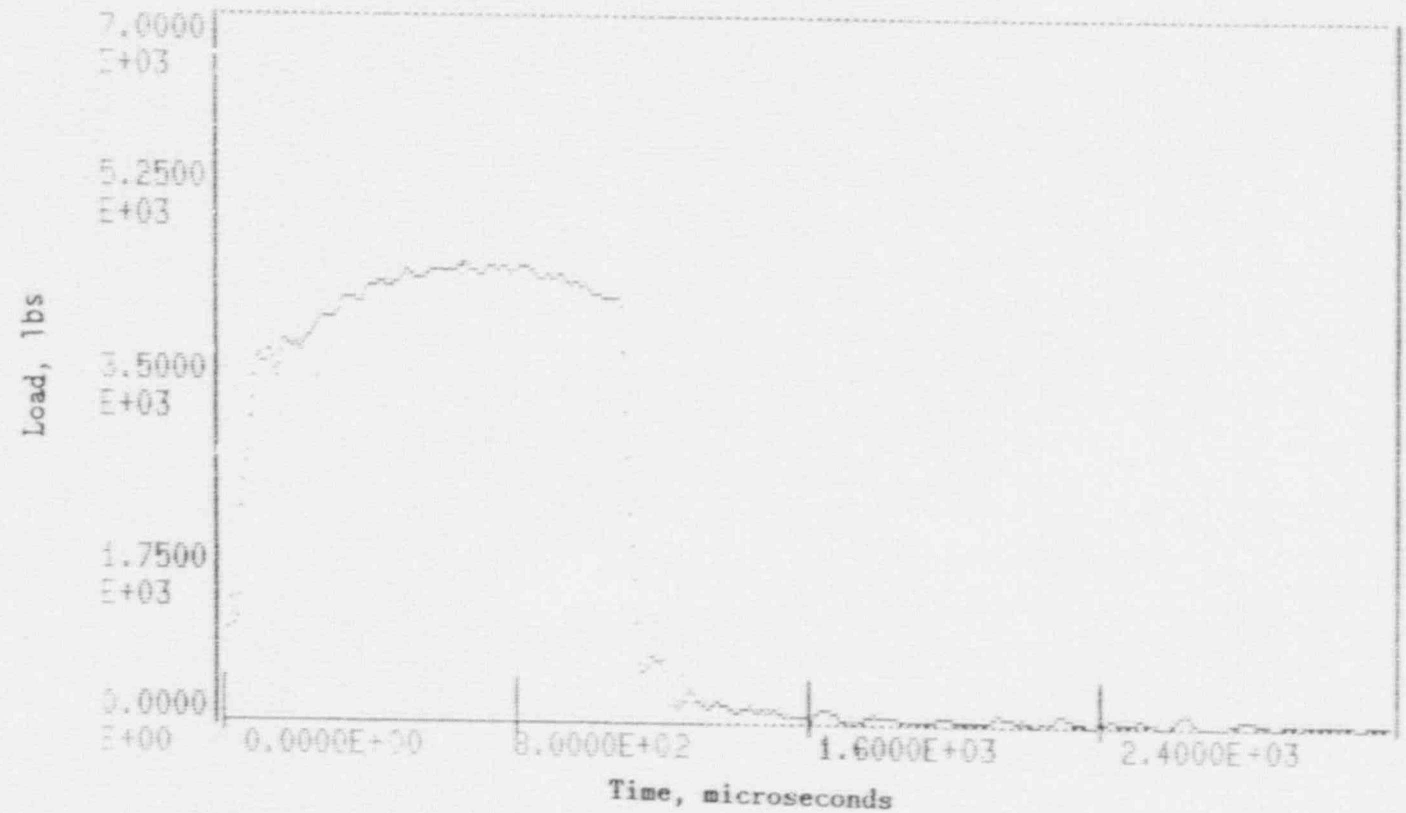

Figure A-52. Load-time record for Specimen FH7.

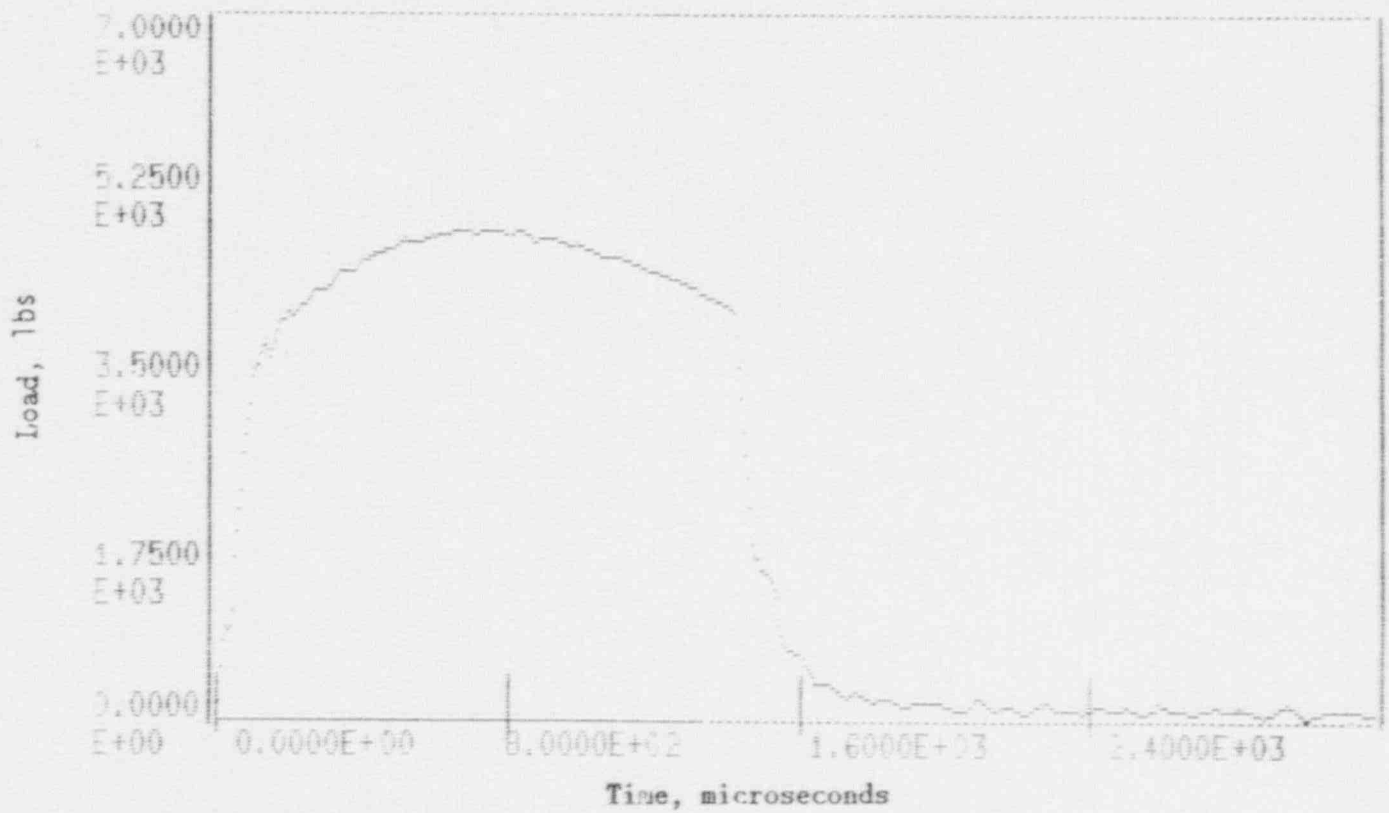

Figure A-53. Load-time record for Specimen FH9.

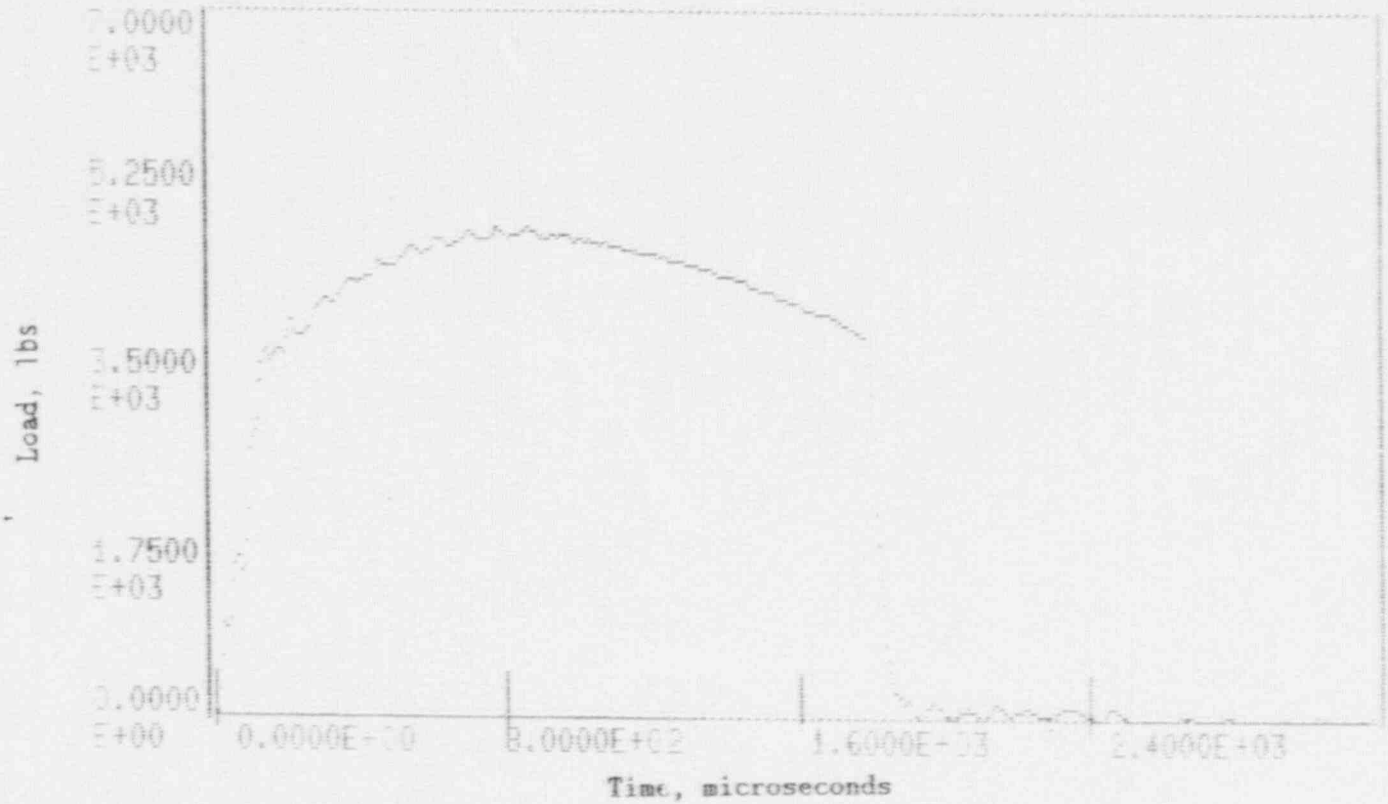

Figure A-54. Load-time record for Specimen FH11.

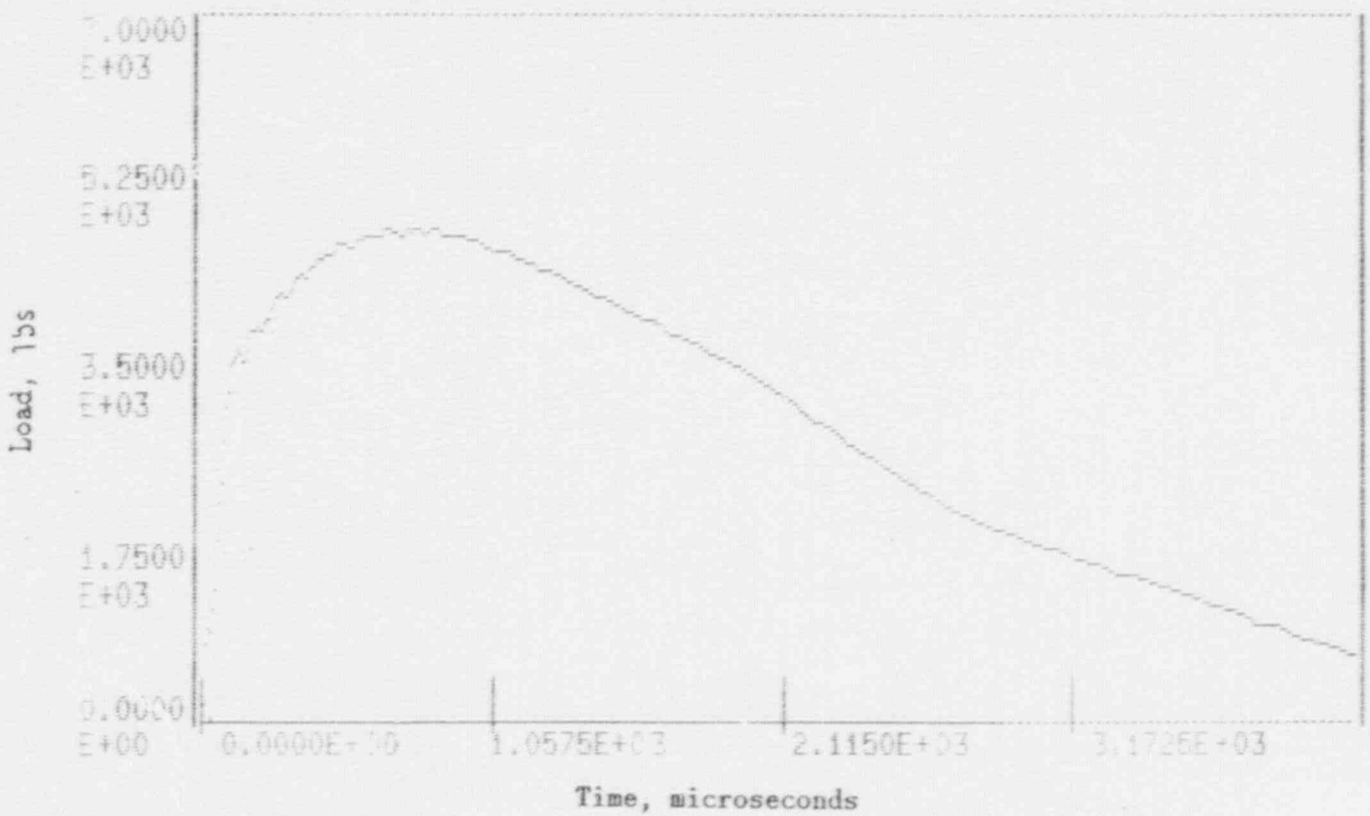

Figure A-55. Load-time record for Specimen FH14.

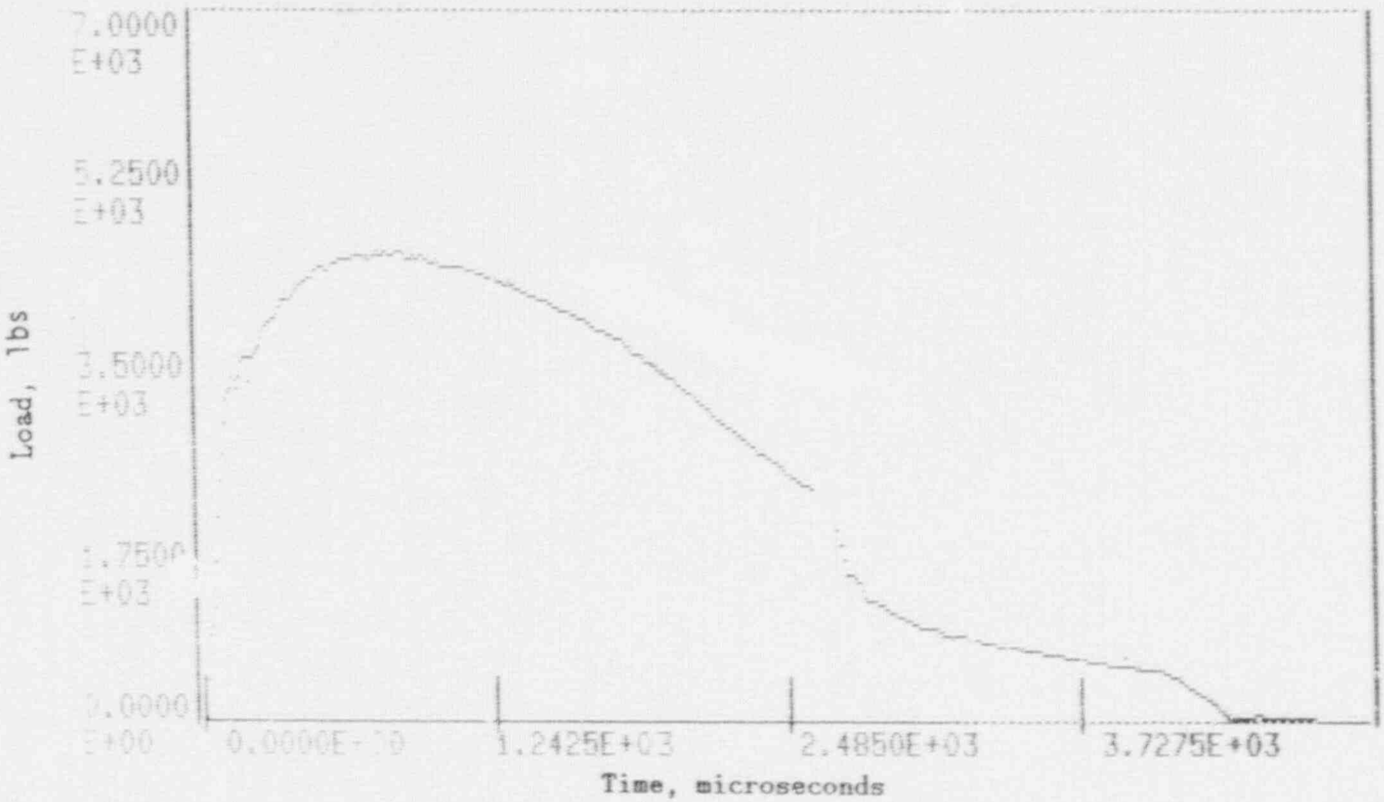

Figure A-56. Load-time record for Specimen FH12.

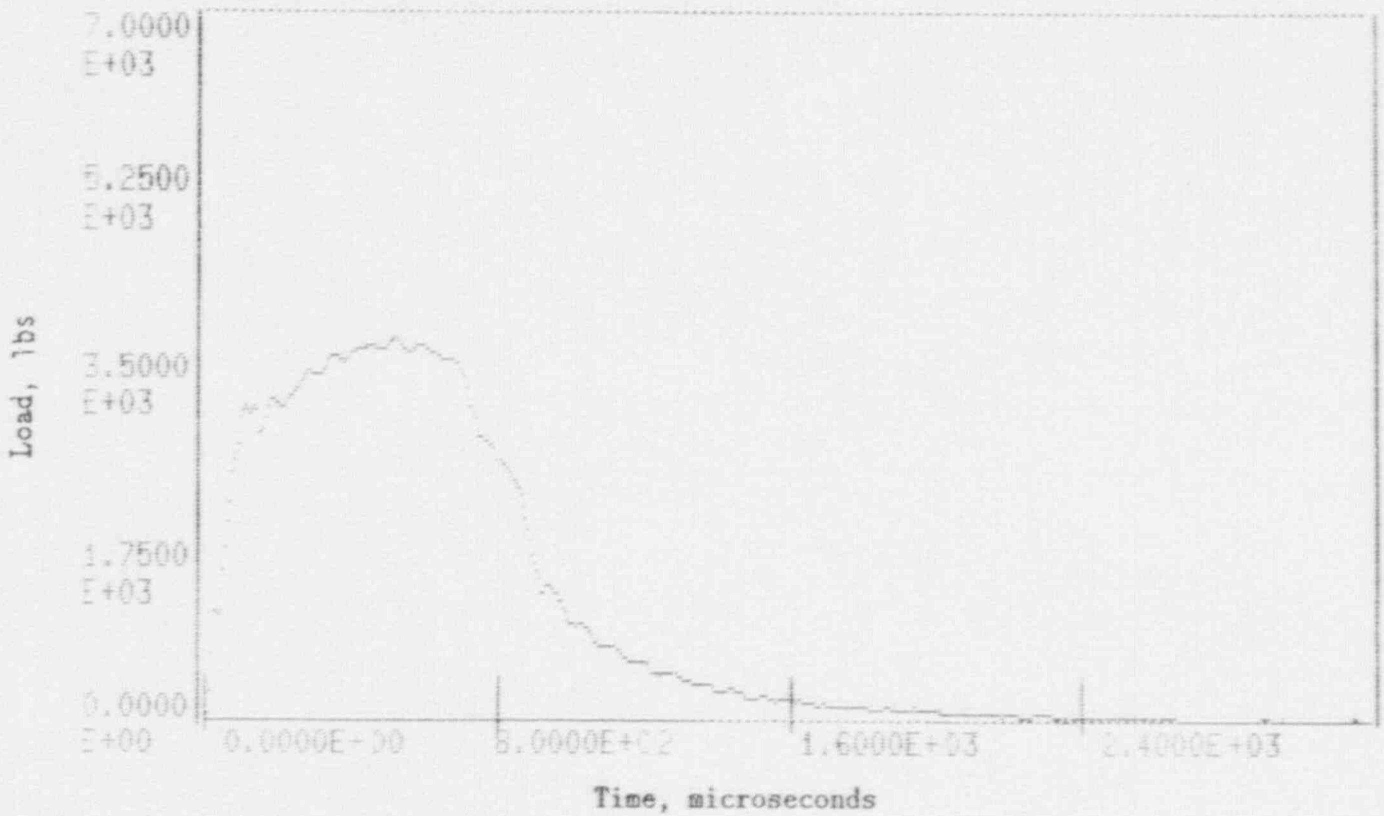

Figure A-57. Load-time record for Specimen FH10.

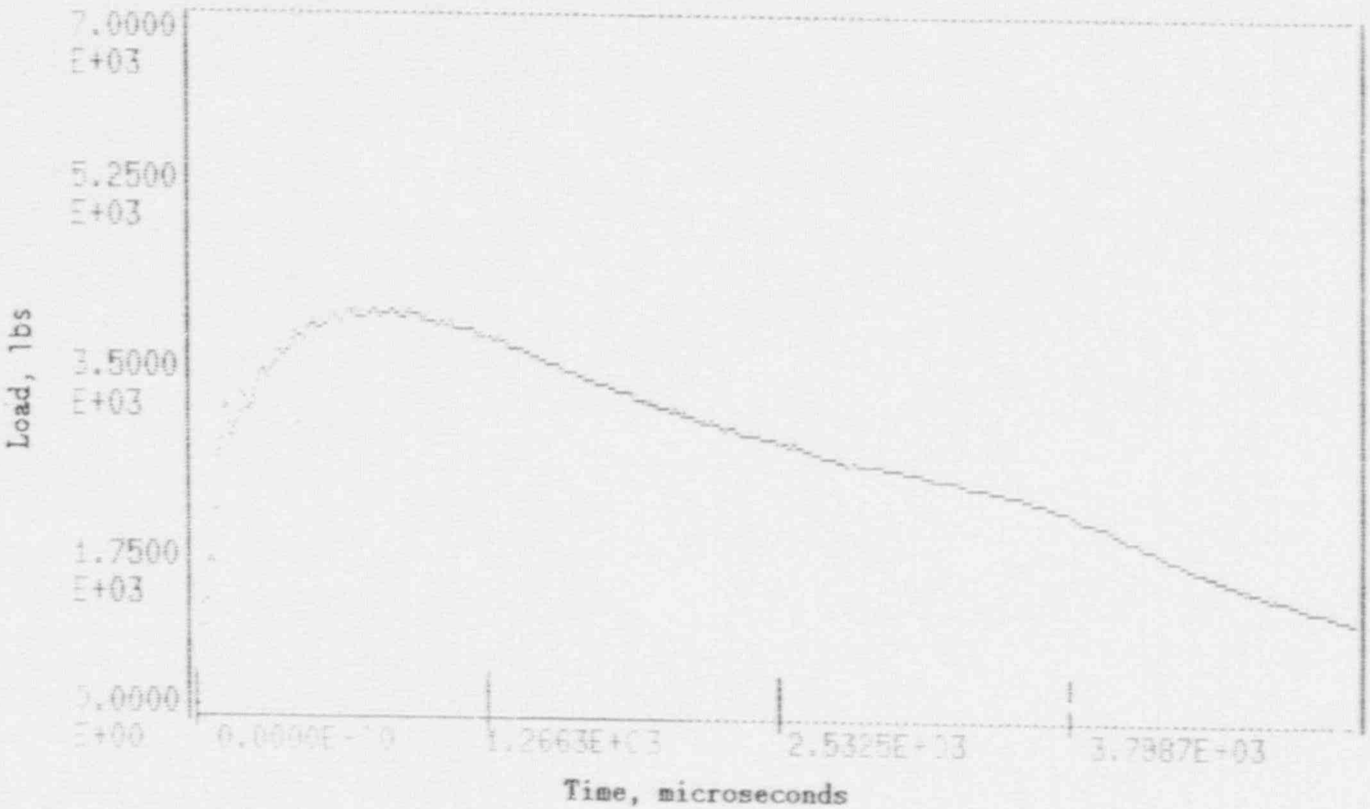

Figure A-58. Load-time record for Specimen FH13.

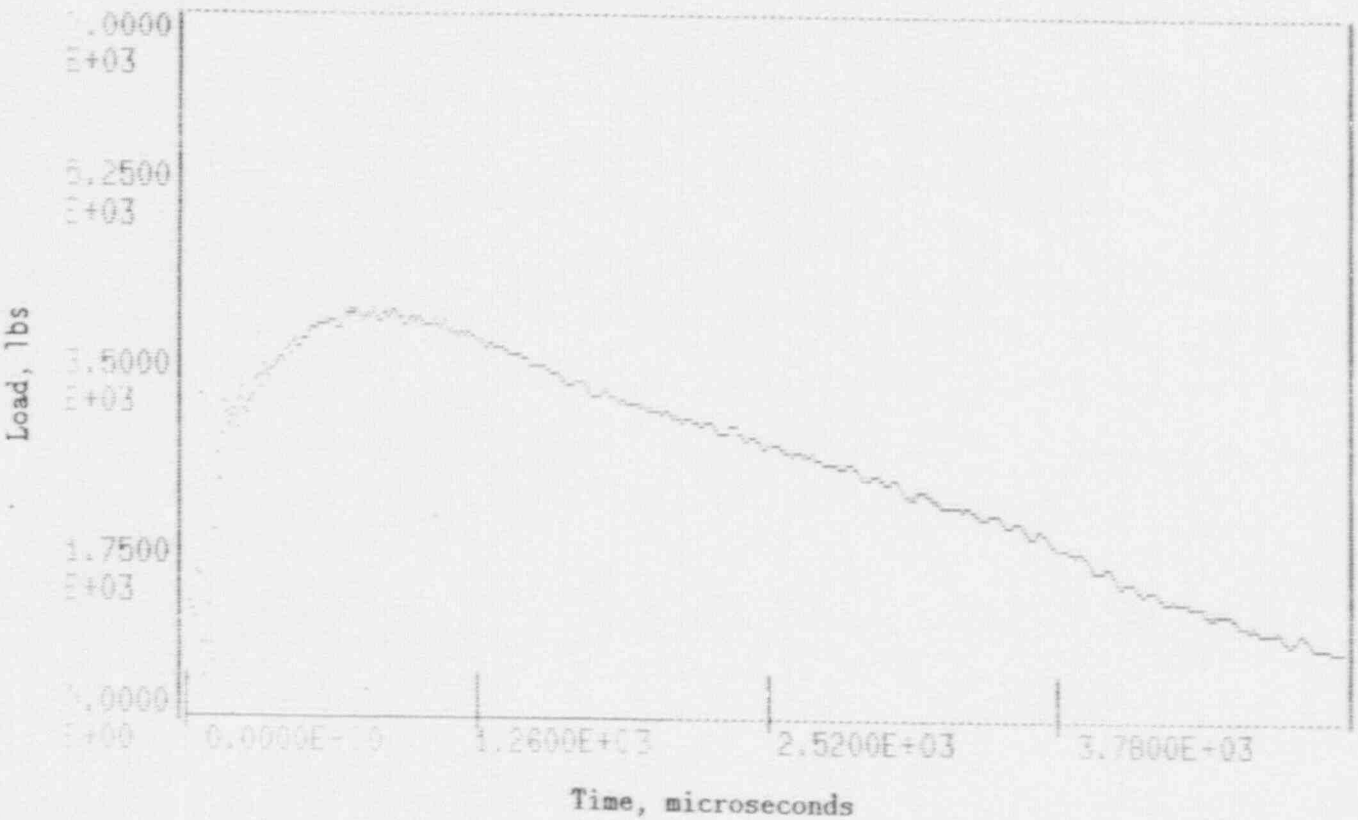

Figure A-59. Load-time record for Specimen FH5.

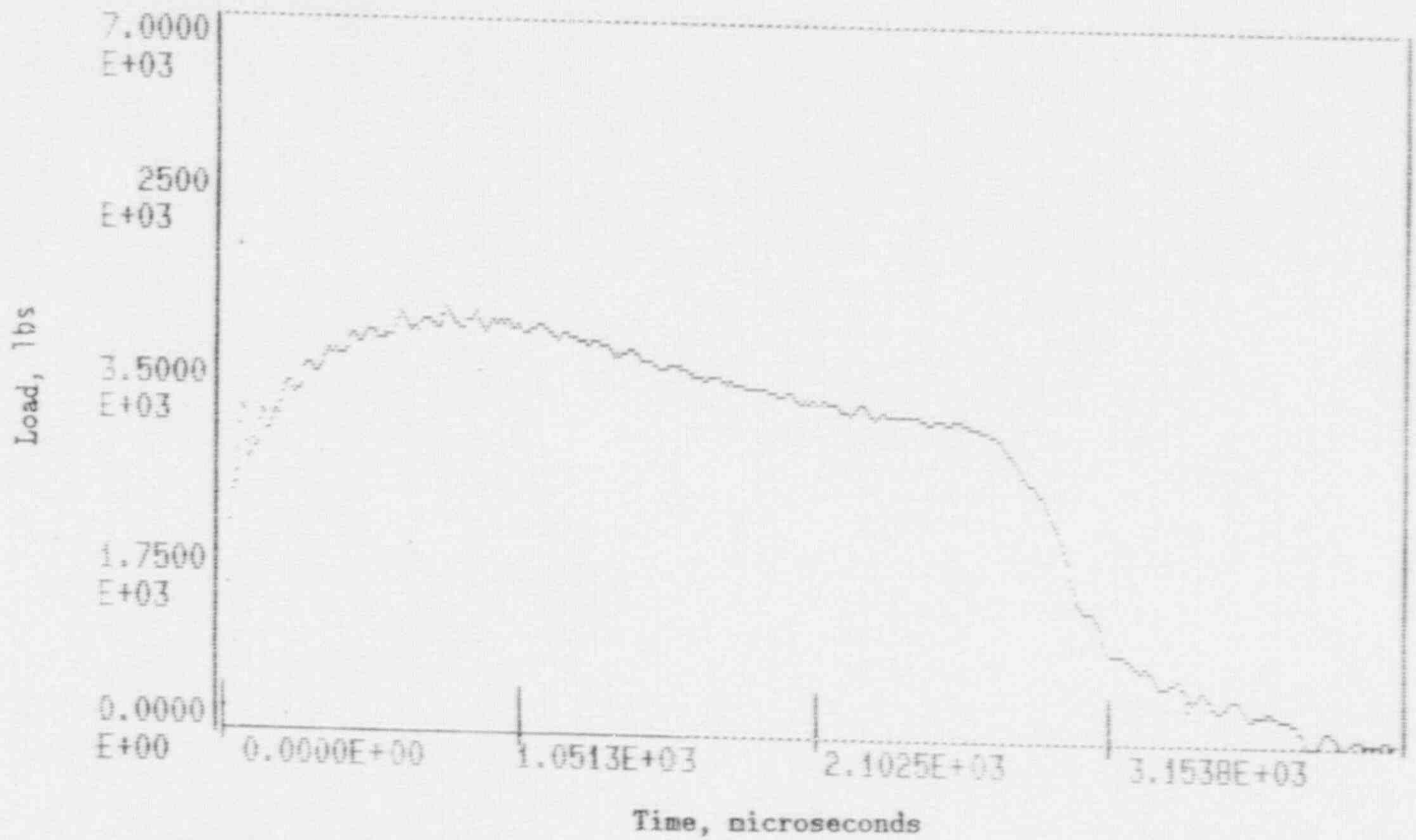

Figure A-60. Load-time record for Specimen FH1.

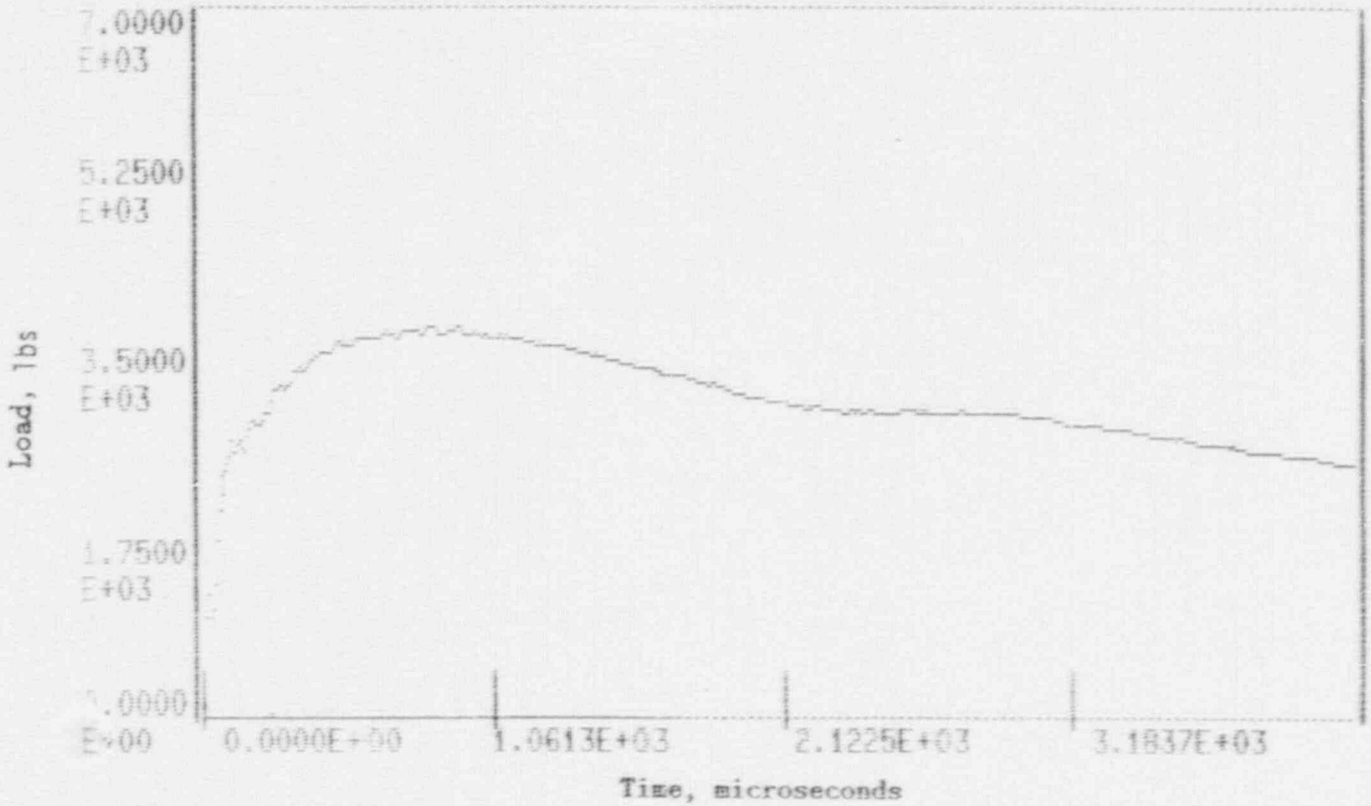

Figure A-61. Load-time record for Specimen FH2.